Fall 9-2016

Brain encoding of saltatory velocity-scaled somatosensory array in glabrous hand among neurotypical adults

Hyuntaek Oh
University of Nebraska - Lincoln, hyuntaek.oh@huskers.unl.edu

BRAIN ENCODING OF SALTATORY VELOCITY-SCALED SOMATOSENSORY ARRAY IN GLABROUS HAND AMONG NEUROTYPICAL ADULTS

by

Hyuntaek Oh

A DISSERTATION

Presented to the Faculty of

The Graduate College at the University of Nebraska

In Partial Fulfilment of Requirements

For the Degree of Doctor of Philosophy

Major: Biological Engineering

Under the Supervision of Professor Steven M. Barlow

Lincoln, Nebraska

September, 2016

BRAIN ENCODING OF SALTATORY VELOCITY-SCALED SOMATOSENSORY ARRAY IN GLABROUS HAND AMONG NEUROTYPICAL ADULTS

Hyuntaek Oh, Ph.D.

University of Nebraska, 2016

Advisor: Steven M. Barlow

Neurons in human somatosensory cortex are somatotopically organized, with sensation from the lower limbs mediated by neurons near the midline of the brain, whereas sensations from the upper body, hands and orofacial surfaces are mediated by neurons located more laterally in a sequential map. Neurons in Brodmann's area (BA) 3b are exquisitely sensitive to tactile stimulation of these skin surfaces. Moreover, the location, velocity and direction of tactile stimuli on the skin's surface are discriminable features of somatosensory processing, however their role in fine motor control and passive detection are poorly understood in health, and as a neurotherapeutic agent in sensorimotor rehabilitation. To better understand the representation and processing of dynamic saltatory tactile arrays in the human somatosensory cortex, high resolution functional magnetic resonance (fMRI) is utilized to delineate neural networks involved in processing these complex somatosensory events to the glabrous surface of the hand.

The principal goal of this dissertation is to map the relation between a dynamic saltatory pneumatic stimulus array delivered at 3 different velocities on the glabrous hand and the evoked blood-oxygen level-dependent (BOLD) brain response, hypothesized to involve a network consisting of primary and secondary somatosensory cortices (S1 and S2), insular cortex, posterior parietal cortex (PPC), and cerebellar nuclei. A random-balanced block design with fMRI will be used to record the BOLD response in healthy right-handed adults. Development of precise stimulus velocities, rapid rise-fall

transitions, salient amplitude, is expected to optimize the BOLD response.

ACKNOWLEDGMENTS

I would first like to thank my advisor, Dr. Steven Barlow, for his support, friendship and encouragement of me throughout the past four years. I have learned a tremendous amount from him and gave me more research experience than I ever thought I would have. I am deeply grateful for all the time and effort that he's invested in my education, research and future direction. Thank you Dr. Greg Bashford for his help with all transfer processes from Kansas to Nebraska and support throughout this project. I would also like to thank my dissertation committee members: Drs. Michael Hoffman and Yingying Wang for being on my committee that gave me valuable feedback on my dissertation.

I would like to thank the MRI technologists, Joanne Murray and Kerry Hartz, at the Center for Brain, Biology and Behavior for the opportunity to collect the functional imaging data for this project.

I would also like to thank the Communication Neuroscience Laboratories (CNL) members for their encouragement, friendship and support to preserve in the pursuit of my PhD degree. Especially, thank you to my old jayhawks, Austin Rosner, PhD and Rebecca Custead, PhD for being a supportive and genuine friend (we are now all PhDs!).

Lastly, thank you to my parents for supporting and encouraging me to persue this degree. I also would like to thank you to my parents-in-law for their kind help and generous suggestions through the last four years. Also to my wife, Youjin, and daughter, Lael, without whom I would never have finished, thank you.

GRANT INFORMATION

The author was partially supported by the Barkley Trust Foundation, Department of Special Education and Communication Disorders, at the University of Nebraska - Lincoln.

Table of Contents

List of Tables

List of Figures

List of Abbreviations

ACh	Acetycholine
AFNI	Analysis of Functional NeuroImages
ATP	Adenosine triphosphate
BA	Brodmanns cytoarchitechtonic map
BNC	Bayonet Neill-Concelman
BOLD	Blood-oxygen-level-dependent
CBF	Cerebral blood flow
CBV	Cerebral blood volume
CSF	Cerebro-spinal fluid
D1	Thumb
D2	Index finger
D3	Middle finger
DCML	Dorsal column-medial lemniscus
EEG	Electroencephalogram
EPI	Echo-planar imaging
FFX	Fixed-effects
FID	Free induction decay
fMRI	Functional magnetic resonance imaging
fNIRS	Functional near-infrared spectroscopy

FoV	Field of view
FUS	Focused Ultrasound
FWHM	Full-width at half-maximum
GABA	$\gamma-$ aminobutyric acid
GLM	General linear model
GLUT	Glutamate
GRE	Gradient echo
GM	Grey matter
HRF	Hemodynamic response functions
IC	Internal capsule
ID	Inside diameter
MEG	Magnetoencephalography
MFX	Mixed-effect
MNI	Montreal Neurological Institute
MPRAGE	Magnetization Prepared Rapid Acquisition Gradient Echo
MRI	Magnetic resonance imaging
OD	Outside diameter
p1	Distal phalanges
p2	Intermediate phalanges
p4	Metacarpals
PC	Pacinian corpuscle
PD	Proton density
PET	Positron emission tomography
PMC	Premotor cortex
PPC	Posterior parietal cortex
RA	Rapidly adapting

RF	Radiofrequency
RFX	Random-effects analysis
ROI	Region of interest
S1	Primary somatosensory
S2	Secondary somatosensory
SA I	Slowly adapting type I
SA II	Slowly adapting type II
SE	Spin echo
SNR	Signal-to-noise ratio
SPM	Statistical parametric mapping
TA	Acquisition time
TCD	Transcranial Doppler
TE	Echo time
tFUS	Transcranial focused ultrasound
TMS	Transcranial magnetic stimulation
TPMs	Tissue probability maps
TR	Repetition time
TTL	Transistor-Transistor Logic
VOI	Volume of interest
VPL	Ventral posterolateral
WM	White matter

Chapter 1

Introduction

Animal and human models of brain plasticity have shown that the development of functional motor tasks depend on the interplay between sensory input and motor output (Buonomano & Merzenich, 1998; Khaslavskaia et al., 2002). Among the many functions of the somatosensory system, processing information about the location, velocity, traverse length and direction of tactile stimuli on the body surface is presumed essential for the development and maintenance of fine motor control of the hand (Dreyer et al., 1978; Whitsel et al., 1986; Olausson & Norrsell, 1993). Improving our knowledge of velocity and directional encoding in this sensory domain will help formulate innovative neurotherapeutic strategies for the rehabilitation of brain-damaged patients to regain motor skills in the limbs (hand, foot) and orofacial (speech, gesture, swallowing) systems. Limited data exist on the cortical representation of moving touch stimulation on the glabrous skin of the digits in humans (Wienbruch et al., 2006; Huang & Sereno, 2007), and many studies involving sensorimotor tasks have been limited to neurotypical adults using electrical and/or transcranial magnetic stimulation (TMS) (Bertolasi et al., 1998; Hamdy et al., 1998; Ridding et al., 2000; Nitsche & Paulus, 2000).

The sensory flow of tactile information derived from mechanoreceptros in the glabrous skin of the hand is conveyed along the dorsal column-medial lemniscus and transmitted through the contralateral ventroposterolateral thalamus and primary

somatosensory (S1), whereas the secondary somatosensory cortex (S2) typically shows a bilaterally response to a unilateral somatosensory stimulus (Tommerdahl et al., 2006; T. Chen et al., 2008). Many neurons in the posterior parietal cortex (PPC) respond to both tactile and visual inputs (Rozzi et al., 2006; Karkhanis et al., 2014), with select sensorimotor transformation and output to the premotor cortex (PMC) (Xing et al., 2000). The cerebellum represents the "forward model" of the sensorimotor system that implements predictions of the sensory result from motor commands, and theses predictors can be used to improve a motor skill or activate sensorimotor plasticity (Blakemore et al., 1999; Blakemore & Sirigu, 2003). Several neuroimaging studies using fMRI and positron emission tomography (PET) have discovered that the cerebellum is involved in signaling the sensory consequence of movements resulting from continuous sensory feedback and the feed forward models are stored in the cerebellum (Blakemore et al., 2001; Kawato et al., 2003). Since the cerebellum plays and important role in predictive motor control and storing forward models (Bursztyn et al., 2006; Johansson & Flanagan, 2009), recent human studies highlight that the cerebellum has been shown to respond to the adaptation of motor cortex and functional recovery from stroke (Small et al., 2002; Tseng et al., 2007).

The hand and face have high peripheral innervation densities and cortical magnification resulting in acute sensitivity and a large number of receptive fields in the primary somatosensory cortex (S1) (Iggo, 2012). Many neuroimaging modalities such as 1.5 T fMRI, magnetoencephalography (MEG), or PET of the human brain do not provide enough spatial resolution to map individual fingers and their phalanges because the distances between individual digits and segments represented in S1 are only a few mm (Weibull et al., 2008). Thus, high resolution fMRI (small voxel size) combined with precisely controlled dynamic spatial tactile arrays is required to map the hand-finger somatotopy (Martuzzi et al., 2014; Schweisfurth et al., 2014) under

conditions where velocity and/or direction are dependent variables of interest. Because of the challenges inherent in the design of an MRI-compatible tactile stimulus array control system that is scalable for velocity and direction, few studies have implemented moving tactile stimulation using continuous moving brush, piezo-element vibration, and compressed air (Whitsel et al., 1978; Keyson & Houtsma, 1995; Olausson et al., 2002; Gleeson et al., 2010; Hlushchuk et al., 2015). Thus, in order to better understand the tactile velocity encoding networks in the human brain, the need exists for a programmable, multichannel tactile stimulus control system with easy, fast coupling to skin anywhere on the body that will permit scalable velocity control and fully compatible with MRI.

The principal aim of this study is to map the relation between saltatory pneumotactile stimulation at 3 velocities on the glabrous hand and the evoked hemodynamic BOLD response in cerebral somatosensory areas (S1, S2, PPC, insula), and cerebellum among a cohort of 20 neurotypical adults using high-resolution fMRI methods. Saltatory cutaneous stimulation in this study involves the presentation of pneumatic pulses which essentially "jump" from one TAC-Cell node to another node in the 5-channel array on the surface of the skin at traverse velocities ranging from slow (5cm/second), intermediate (25cm/second), to fast (65cm/second) on the glabrous surface of the hand involving D1 (thumb), D2 (index finger), and D3 (middle finger). The evoked BOLD signal will be recorded by placing the participant within the bore of a magnetic resonance imaging (MRI) scanner. Results of this study are expected to provide new information on the spatiotemporal features of saltatory tactile velocity encoding in cerebral and cerebellar somatosensory representations in neurotypical adults. Moreover, this work may inform future investigations whose goal is to develop new approaches to motor rehabilitation through somatosensory neurotherapeutics to improve sensorimotor function in individuals who have sustained cerebrovascular stroke

or traumatic brain injury. Other future applications may include multimodal studies using fMRI and electroencephalography (EEG), MEG, and functional near-infrared spectroscopy (fNIRS) methods. Although fMRI provides a high spatial resolution, the temporal resolution is limited (seconds) due to intrinsic properties of the hemodynamic response (Kim et al., 1997). The combination of fMRI and EEG/MEG would improve the both spatial and temporal resolution.

1.1 Specific Aims

Characterize the changes of BOLD response of the somatosensory areas with 3 different velocities of saltatory pneumotactile stimulation.

Hypothesis 1.

Hypothesis $\mathbf{H}_0$: There will be a significant difference pattern of BOLD response regarding to the main effect of velocity across the different areas of the cortical and subcortical somatosensory cortex.

Hypothesis $\mathbf{H}_A$: The alternative hypothesis suggests that there will be no significant difference pattern of BOLD response regarding to the main effect of velocity across the different areas of the cortical and subcortical somatosensory areas will not have different pattern of BOLD activation.

Hypothesis 2.

Hypothesis $\mathbf{H}_0$: There will be a significant difference pattern of BOLD response regarding to the individual velocities (5 cm/s, 25 cm/s, and 65 cm/s) among the cortical and subcortical somatosensory areas.

Hypothesis $\mathbf{H}_A$: The alternative hypothesis suggests that there will be no significant difference pattern of BOLD response regarding to the individual velocities (5 cm/s, 25 cm/s, and 65 cm/s) among the cortical and subcortical somatosensory areas.

The somatosensory areas to be imaged include the primary somatosensory (S1), secondary somatosensory (S2), and somatosensory related areas such as the posterior

parietal cortex (PPC), insula, and cerebellum. A group of neurotypical right-handed adults (14 male, 6 female, 19 to 30 years of age) were served as participants for this study. Different velocity of pneumotactile stimulation were delivered through 7 small plastic pneumatic TAC-Cells (6mm ID) placed on the glabrous skin of right hand, including p1, p2 (phalangeal) segments of D3, p1, p2, p4 segments of D2, and p4, p1 of D1 to map the changes of BOLD response using fMRI. The directional sequence of saltatory pneumotactile stimulation initiates at p1 of D2 and D3, jumps to both p2 of D2 and D3, then p4 of D2 and p4 of D1, and terminates at p1 of D1. We compared the spatial organization of brain BOLD responses to 3 different saltatory velocities, including 5, 25, and 65 cm/s. A randomized-balanced block design (each block equals 40 seconds) includes five different conditions: (1) 5 cm/s saltatory, (2) 25 cm/s saltatory, (3) 65 cm/s saltatory, simultaneous all TAC-Cells ON, and all TAC-Cells OFF. The duration of each condition is 20 seconds, followed by 20 seconds of rest. A region of interest (ROI) was assigned to S1, S2, and somatosensory association areas such as PPC, insular cortex, and the cerebellum. These regions were used to examine the differential pattern of BOLD response among the different areas of the cortical and subcortical somatosensory processing areas of the brain.

1.2 Primary and Secondary Somatosensory Representations

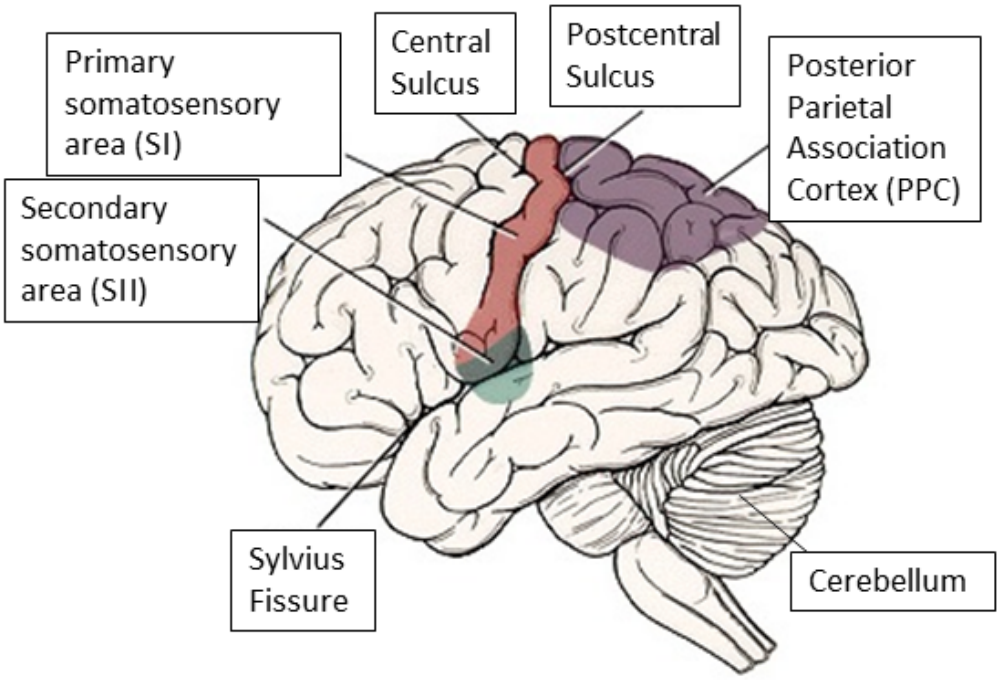

Figure 1.1: Major functional areas (adapted from `http://humanphysiology.tuars.com/program/section8/8ch5/s8ch5_25.htm`

1.2.1 Primary Somatosensory, S1

Primary somatosensory (S1) lies along the posterior bank of the central sulcus in the postcentral gyrus of the parietal lobe. Primary somatosensory cortex includes four areas corresponding to Brodmann's cytoarchitechtonic map (BA) 3a, 3b, 1 and 2 and generally organized in an anterior-posterior sequence (Brodmann, 1909). Connectivity within S1 is extensive with massive projections to layer 4 of S1 from the ipsilateral ventroposterolateral (VPL) nucleus of the thalamus for limb and trunk soma, and ventroposteromedial (VPm) for orofacial, pharynx, and laryngeal sensory surfaces. Outputs from S1 include axons to the precentral gyrus, S2, M1, posterior parietal

cortex, and thalamus (Aronoff et al., 2010). Fig. 1.1 displays the location of the S1. Area 3a occupies the depths of the central sulcus and followed by caudally by area 3b, 1, and 2 (Geyer et al., 1999). Area 1 lies near the apex of the postcentral gyrus and area 2 occupies the posterior crown of the postcentral gyrus (Powell & Mountcastle, 1959). BA 3b and BA 1 mainly receive cutaneous input from SA (slowly adapting) and RA-I (rapidly adapting type I) mechanoreceptive afferents in VPL, respectively. Proprioception information from muscle spindle afferents and Golgi tendon organs are mapped to area 3a, while area 2 integrates both cutaneous and muscle information (Kaas, 1993). Parylene-insulated tungsten microelectrodes with impedances of ≤ 2 MΩ were used to record single unit neural activity in the somatosensory cortex of monkeys (Xerri et al., 1996). In Xerri's study, adult owl and squirrel monkeys were trained to retrieve small banana-flavored food pellets which were placed on a modified board located in front of their cage, and monkeys were allowed to use their any digits of either hand in this task. Adult Long-Evans rats were raised in one of three different housing conditions to get familiar with poor, moderate or rich sensory experience. Their housing conditions were defined by differences in shape, size, and texture. For each successful pellet retrieval, the monkeys developed left-hand preference motor skills to acquire pellets using multiple-digit (most in index and middle finger) flexion-extension movements. The representations of the glabrous skin of the index and middle finger showed larger cortical areas than other digits of the monkeys in area 3b. Environmental enrichment experienced rats induced an enlargement of the glabrous skin surface representations as compared with moderate environmental conditions.

1.2.2 Secondary Somatosensory, S2

Secondary somatosensory (S2) is located in the upper bank of the lateral sulcus of the brain, also known as the lateral fissure of Sylvius in the parietal operculum.

BA 40 and BA 43 are parts of the secondary somatosensory which are located at the posterior end of the lateral fissure of Sylvius and the ventrolateral depth of the central sulcus, respectively. Associated functions of BA 40 are somatosensory spatial discrimination and the integration of tactile and proprioceptive information (Milner et al., 2007; Akatsuka et al., 2008). BA 43 is related to the responses to vibrotactile digit stimulation (Francis et al., 2000). The existence of S2 was first described by Adrian in cat (Adrian, 1940, 1941). The first report of the human secondary somatosensory (SII or S2) was given by Penfield during epilepsy surgery using electrical stimulation (Penfield & Jasper, 1954). Their results were subsequently verified using through a combination of cortical stimulation and measuring evoked potentials from the exposed brain of epilepsy patients (Woolsey et al., 1979).

In constrast to the contralateral response found in S1, S2 typically shows a bilaterally response to a unilateral somatosensory stimulus such thermal, tactile, and electrical stimuli (Casey et al., 2001; Hämäläinen et al., 2002; T. Chen et al., 2008). Although S2 typically shows a weaker response to somatosensory stimuli compared to S1, several fMRI studies have shown a somatotopic organization (Ruben et al., 2001; Del Gratta et al., 2002), and involved in higher order function and stimulus coding mechanisms such as tactile learning (Ridley & Ettlinger, 1976), attention (Burton et al., 1999), and shape perception (Hsiao, 2008). Somatosensory information is processed serially and in parallel from the VPL to S1 and onto S2 (Jones & Powell, 1969; Ploner et al., 1999). A MEG study using repetitive pneumotactile pulse train stimulation of the glabrous hand has shown that evoked activity in the S2, albeit inconsistent across subjects (A. Popescu et al., 2013).

1.2.3 Somatosensory association areas

The posterior parietal cortex (PPC) is known as a somatosensory association area and includes BA 5 and 7. The PPC is situated posterior to the S1 and anterior and superior to the occipital lobe. In early studies, PPC was thought to be most responsive to the passive visual and/or sensory stimulus but later revealed that PPC was involved in a higher-level somatosensory information processor including visual tactile multisensory integration, perception of movement, and control of eye movements (Andersen & Gnadt, 1989; Pasalar et al., 2010). For example, the PPC is not only involved in prompts to move the contralateral hand, arm, or foot with electrical stimulation but also is involved in cognitive functions (Desmurget et al., 2009; Constantinidis et al., 2013).

Many neurons in the PPC respond to tactile stimuli, visual inputs, attention, sensorimotor transformation and sends output to the premotor cortex (PMC) (Xing et al., 2000). The sensorimotor transformation is defined as the process which converts a sensory stimulus into a resultant motor plan or action (Pouget & Snyder, 2000). As the PPC neurons receive multiple sensory inputs, functional properties of PPC neurons are sensitive to changes in visual and tactile stimulation (Rozzi et al., 2006; Karkhanis et al., 2014). Because the PPC has both sensory and motor characteristics, several studies implicate this region of the parietal cortex in visually guided movements for control of hand position in eye coordinates (Buneo & Andersen, 2006). When the PPC is damaged, it can lead to loss of visual and motion perception (Lomber et al., 2006). Damage to the PPC also can produce a syndrome called apraxia in which patients show an impairment in generating the correct movement sequence, even though they understand the motor goal to perform the task (Rushworth et al., 1997).

The cerebellum lies in the posterior cranial fossa, subtentorial and posterior to

the pons, forming the roof of 4^{th} ventricle and underlying the temporal and occipital lobes of the cerebral hemisphere. There are three major fiber bundles which carry the input and output of the cerebellum. The superior cerebellar peduncle is the output from the cerebellum primarily containing all the efferents from the cerebellar nuclei. The massive middle cerebellar peduncles is the major source of afferent to the cerebellum. The inferior cerebellar peduncles includes both afferents from the medulla and the remaining cerebellar efferents. The cerebellum receives information for motor movement from the spinal cord and brainstem, and this information lets the cerebellum notify the movements that have been performed. The outputs from the cerebellum are conveyed to the cerebral motor cortex through the red nucleus and ventral lateral (VL) nucleus in the thalamus (Nolte, 2010). The cerebellum is involved in not only motor control but also cognitive functions such as emotional processing, attention, and language (Wolf et al., 2009). The cerebellum is likely considered as a "forward model" of the sensorimotor system that implements predictions of the sensory result from the motor commands, and the predictions can be used to improve a motor skill or activate sensorimotor plasticity (Blakemore et al., 1999; Blakemore & Sirigu, 2003). This proposed role of the cerebellum was supported by Jeuptner and Weiller using the results from PET studies (Jueptner & Weiller, 1998). The results suggested that the cerebellum is involved in sensory information processing which is monitoring and optimizing movements using sensory proprioceptive feedback information. The cerebellum also plays an important role in voluntary movements such as balance, coordination and posture (Thickbroom et al., 2003). Many symptoms of cerebellar disorders include the posterior lobe, anterior lobe and flocculonodular syndrome. The posterior lobe syndrome can disturb gait and the coordination of voluntary movements. The dysfunctions of anterior lobe and flocculonodular lobe contribute to lower limb dyscoordinations and gait impairment, respectively (Fredericks, 1996). Although the

cerebellum appears to be a relatively small part of the brain, it contains over 50% of the brain's neurons (Herculano-Houzel, 2009). Several neuroimaging studies using fMRI and PET have discovered the cerebellar response during natural movement like tapping a button with right index finger or the table with the tips of each fingers (Aoki et al., 2005; Stoodley et al., 2012).

1.3 Mechanoreceptors

Cutaneous mechanoreceptors come in a variety of morphologically-distinct sensory nerve endings that have unique adaptation profiles and are specialized to encode different stimulus features such as light touch, deep pressure, vibration, lateral strain, temperature and pain. Ectoderm and mesoderm gives rise to skin which is generally composed of epidermis, dermis and subcutaneous tissue.

There are four different types of skin: mucocutaneous, mucous membrane, glabrous, and hairy skin. Glabrous skin is free of hair follicles and is found on the palmar and plantar surfaces of the hand and foot, respectively, and the lip vermilion. Mucocutaneous skin is associated with the transition zones of the lips and anus. Mucous membranes line the inside of body orifices, aerodigestive and alimentary tract, and oral-nasal cavities. For all four types of skin, there are four types of Aβ mechanoreceptors found in glabrous skin, including Pacinian corpuscle, Meissner corpuscle, Merkel cell-neurite complex, and Ruffini endings. As shown in Fig.1.2, cutaneous mechanoreceptors are categorized by their rate of adaptation, best frequency, and receptive field size: RA (Rapidly Adapting), PC (Pacinian corpuscle), SA I (Slowly Adapting type I) and SA II (Slowly Adapting type II) (Johansson & Vallbo, 1979; Berne et al., 2008).

Rapidly adapting fibers (RA, or Fast Adapting) are associated with Meissner receptors and Pacinian corpuscles, and slowly adapting fibers (SA) are associated

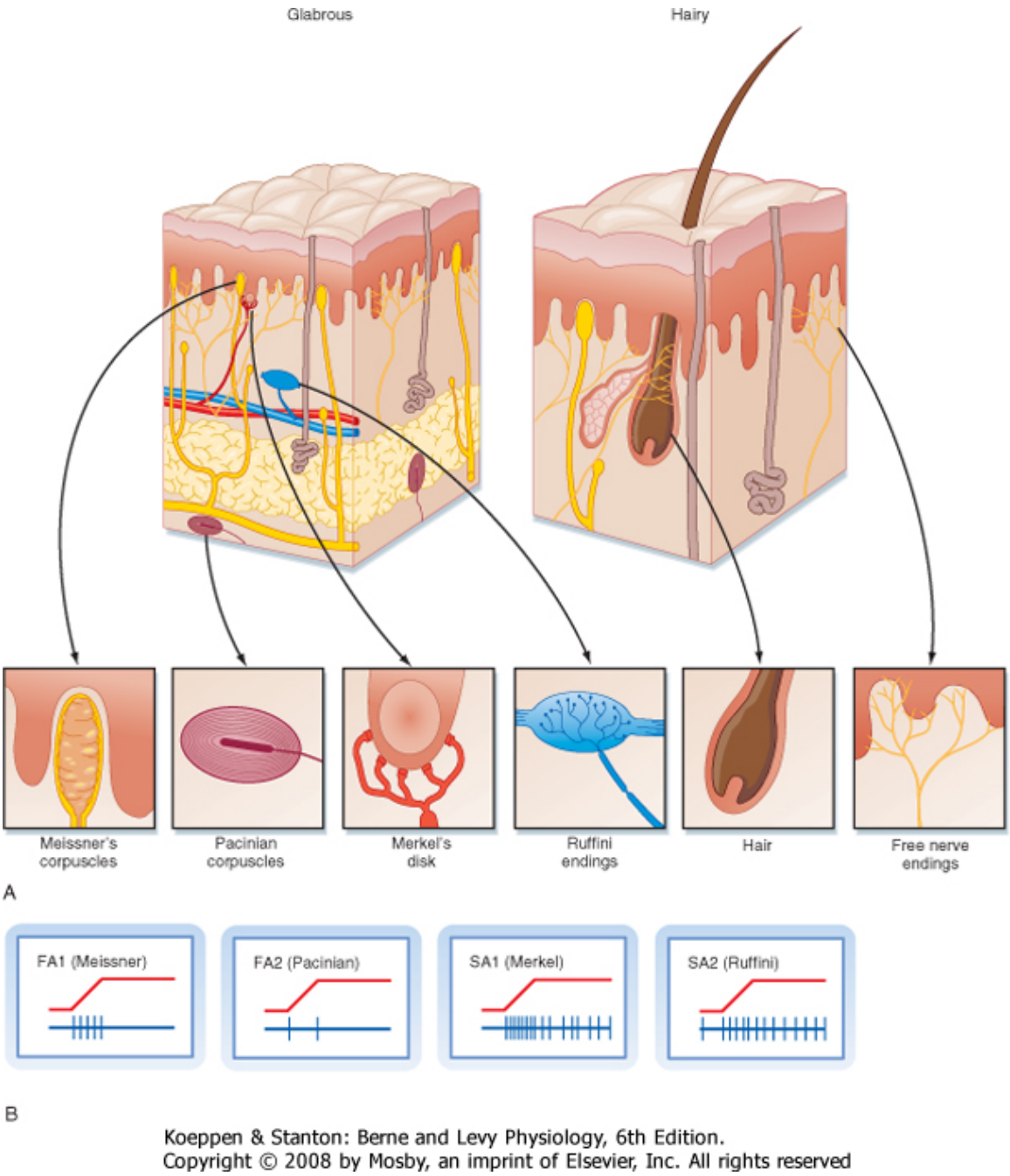

Figure 1.2: Aβ cutaneous mechanoreceptors (Berne et al., 2008)

with Merkel and Ruffini mechanoreceptors. The SA receptors produce constant train activity as long as mechanical stain is applied, whereas RA receptors are triggered at the onset or sometimes the offset of mechanical stimulation. RA and SA receptors

are further separated into Type I and Type II receptors based on spatial properties. Both RA I and SA I mechanoreceptors located near the skin's surface manifest small receptive fields ($\sim$ 1-3 mm diameter). Type II mechanoreceptors for rapidly and slowly adapting units (PC and SA II) are located deeper in the skin and associated with relatively large receptive fields ($\sim$ 10-20 mm diameter) (Johansson, 1978). The Pacinian corpuscle (PC) is an RA II mechanoreceptor which is well suited to transduce and encode vibration and pressure with a best frequency of approximately 250 Hz (Biswas et al., 2015; Scheibert et al., 2009). The Meissner corpuscle is an RA I which is sensitive to light touch and is most concentrated in the glabrous lips and hand (Cauna & Ross, 1960). The Merkel cell-neurite complex is an SA I unit and effectively transduces light touch (Maricich et al., 2009). The Ruffini ending or Ruffini corpuscle is an SA II which is exquisitely sensitive to skin stretch and directional strain (Hamann & Iggo, 1988). The human face, including the perioral region, lacks muscle spindles but is endowed with a pseudo-Ruffini corpuscle mechanoreceptor which has been hypothesized to play a proprioceptive role in orofacial kinematics (Barlow, 1987; Nordin & Hagbarth, 1989).

Mechanoreceptor	Adaptation Profiles	Best Frequency (Hz)	Receptive Field diameter (mm)
Meissner corpuscle	Fast-adapting, type I (FA I)	≤ 50	1 - 2
Pacinian corpuscle	Fast-adapting, type II (FA II)	250	≥ 8
Merkel cell neurite complex	Slow-adapting, type I (SA I)	5 - 15	2 - 8
Ruffini ending	Slow-adapting, type II (SA II)	0 - 10	2 - 3

Table 1.1: Aβ cutaneous mechanoreceptors (Barlow & Rosner, 2015)

1.4 Neuroanatomy of the hand

Maps of the human body surface on the cerebral cortex was discovered by Penfield nearly 80 years ago (Penfield et al., 1937; Penfield & Rasmussen, 1950). The primary and secondary somatosensory cortices include multiple representations or maps of the

body surface. The somatotopic representation of body parts from ventral to dorsal and medial to lateral are shown in Fig.1.3a (Goldstein & Thomson, 2007). The hand and face parts are represented by a disproportionately large area of S1, consistent with their involvement in sensation and fine motor control. Several fMRI studies used tactile and electrical stimulation to map the somatotopic representation of the body surface in the primary somatosensory cortex (Nii et al., 1996; Maldjian et al., 1999). Body parts such as hand and face have high innervation densities resulting in overall better sensitivity. Therefore, the somatotopic mapping of the hand and face is represented by a large number of receptive fields in the primary somatosensory cortex (Iggo, 2012). Although the somatotopic representation of the hand shows the largest areas in S1, neuroimaging modalities, e.g., fMRI, MEG or PET, may not provide enough spatial resolution to map individual fingers because the distances between different fingers and orofacial tissues represented on the somatotopic mapping of S1 are only a few mm (Weibull et al., 2008). This is why the high resolution fMRI (small voxel size) combined with precisely controlled tactile stimulation is required to map the hand/finger somatotopy (Martuzzi et al., 2014; Schweisfurth et al., 2014). Different velocities or direction of tactile stimulus can be used to control the stimulus but these parameters have not been investigated for the encoding of the somatosensory cortex. Because it is difficult to design a tactile stimulus control system that is scalable for velocity and direction, few studies have implemented moving tactile stimulation. In addition, a dynamic tactile array must be compatible with the MRI or MEG environment to record the brain response without introducing stimulus artifacts. Failure of any of these factors interrupts the somatosensory mapping of moving tactile stimulus to reliably map the somatosensory cortices.

Fig.1.3b shows the two principal pathways from the glabrous skin of the hand to the primary somatosensory cortex. The somatosensory information processed by Aβ

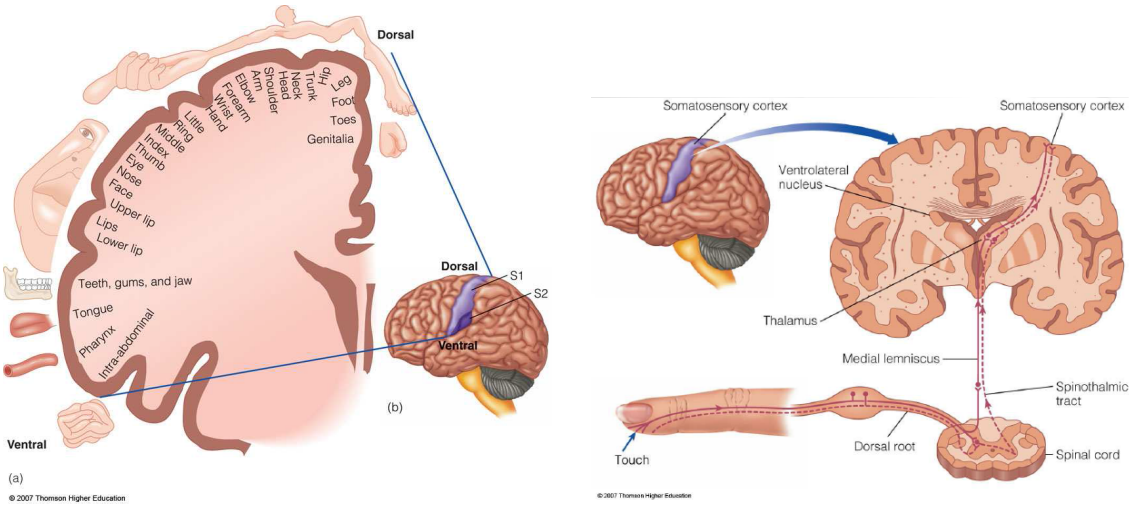

(a) A map of the body surface (b) Pathways from skin to cortex

Figure 1.3: Hand neuroanatomy (Goldstein & Thomson, 2007)

mechanoreceptors originating in the glabrous hand travels in bundles of myelinated nerve fibers to the spinal cord and along different pathways based on information types. There are two major pathways in the spinal cord: Dorsal column-medial lemniscus (DCML) and the spinothalamic tract. The spinothalamic pathway primarily consists of small fibers that carry temperature and pain information (Price, 2000). The DCML pathway includes large myelinated afferent fibers (Aβ) that convey tactile information such as vibration, pressure, discriminative touch and proprioceptive information (Coulter, 1974). The first, and second-order neurons form this pathway. The cell bodies of first-order neurons are located in the dorsal root ganglia at all spinal levels. Sensory information travels from the skin and extends into the dorsal column of the spinal cord. These first-order primary afferent neurons ascend ipsilaterally to the spinomedullary junction where they synapse with second-order neurons within the somatotopically organized nucleus gracilis (from somatic tissues below T6, lower trunk, hips and lower limbs) and nucleus cuneatus (from somatic tissues above T6, upper trunk and upper limbs). From there, second-order neurons cross midline (decussate) to

form the medial lemniscus (ML). Axons of the ML ascend through the brainstem and project to the ventroposterolateral (VPL) nucleus of the thalamus. Third-order neurons originating in the VPL course through the internal capsule as thalamocortical afferents, the majority of which project to layer 4 of the primary somatosensory cortex within the postcentral gyrus. Hence, somatosensory information derived from the glabrous skin of the hand is ultimately transmitted to the contralateral S1 representation (Tommerdahl et al., 2006).

1.5 Moving tactile stimulation

Moving tactile stimulation on the glabrous skin, known as 'surface parallel stimulation', evoked activity among cortical and subcortical somatosensory representations (Whitsel et al., 1986). In the previous human psychophysical studies, it has been revealed that the optimal range of stimulus velocity for human and non-human are between 3 and 25 cm/s, and 5 and 50 cm/s, respectively (Dreyer et al., 1978; Whitsel et al., 1978, 1986). Fig. 1.4 shows how mean firing rate of S1 neuron for moving tactile stimulus (brush motion) varies with different velocities.

These optimal range of stimulus were applied to map the BOLD responses in primary somatosensory and posterior insular cortex using soft brush stroking in recent fMRI studies (Björnsdotter & Olausson, 2011; Ackerley et al., 2014). Outside this range, even subjects were able to recognize the moving tactile stimulus over 50 cm/s, the perceptual sensitivity of stimulus became unreliable because increasing velocities led to changes in perceived stimulation location, direction and distance. On the contrary, at slow velocities below 3 cm/s, the cerebral cortical neurons receives the moving tactile stimulation as discrete stimulus rather than the motion track. This is why velocities, including speed and direction, of moving tactile stimulation across the skin are sensitive factors in designing perceptual experiment with human subjects

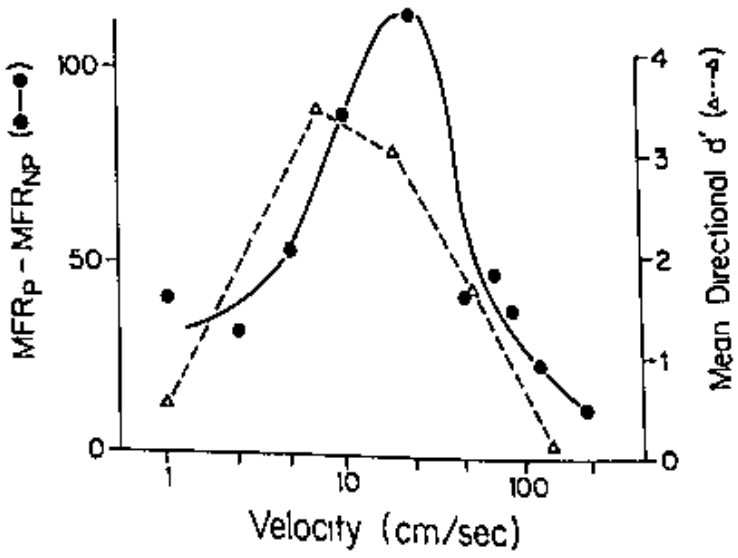

Figure 1.4: Comparison of the velocity dependence of cutaneous directional sensitivity in humans (△) and single S1 neurons (•) (Whitsel et al., 1986)

(Pei & Bensmaia, 2014; Dallmann et al., 2015).

1.6 Methods to Map Somatosensory Cortex in vivo

The first mapping of human primary somatosensory was pioneered by neurosurgeon Wilder Penfield using electrical cortical stimulation in pre- and postcentral gyri during surgical intervention for epilepsy (Penfield et al., 1937). More recently, noninvasive imaging modalities, e.g., fMRI or MEG, have been used to map tactile representations in S1 (Nakamura et al., 1998; Stippich et al., 1999; Kurth et al., 2000). Recent studies using high-field strength 7T fMRI have generated detailed somatotopic maps of individual fingers (from D1 to D5) within the postcentral gyrus representations for BAs 3b, 1, and 2 using tactile stimuli (Sanchez-Panchuelo et al., 2010; Martuzzi et al., 2014). The Martuzzi study showed that the thumb has a considerably

larger representation than other fingers in human BAs 1, and 2. Positron emission tomography (PET) is another imaging modality that has been successfully applied to detect cerebral blood flow changes to functionally map human somatosensory cortex (Fox et al., 1987). The PET detects gamma ray emissions from radioactively labeled molecules (tracers) that are injected into the bloodstream (Nasrallah & Dubroff, 2013). Because PET provides the molecular specificity with high sensitivity and is sensitive to glucose metabolism changes in the tissues of the brain, a hybrid PET-MRI imaging technology has been developed to not only measure metabolic activity in the brain but also provide high resolution anatomical brain imaging (Z. Cho et al., 2007, 2008). A transcranial focused ultrasound (tFUS) was recently accepted for noninvasive neuromodulation methods for focally modulating the SI response of human brain (Legon et al., 2014). Unlike high intensity, continuous ultrasound (UR), tFUS uses low energy ultrasound waves passing through the skin and skull, and can be highly focused with accuracy in the brain area to trigger neural activity (Panczykowski et al., 2014; Bystritsky & Korb, 2015). This highly targeted neuroimaging modality delivers highly-focused acoustic energy to the biological tissue through the use of the transducer, the acoustic lens, or the phased array focused ultrasound (FUS) elements such as piezo-composite material (Daum & Hynynen, 1999; Hynynen et al., 2004; W. Lee et al., 2015). Legon et al applied a single element tFUS transducer with 0.5-MHz pulsed wave to record acoustic pressure fields emitted from the tFUS transducer. The author targeted left S1 by transmitting tFUS pulsed wave into cortex to evoke neural activity and the acoustic field distribution of the evoked activity in the brain was mapped on 3D simulation whole-head structural magnetic resonance images. Because tFUS provides highly-focused acoustic energy to evoke human brain activity, tFUS was recently combined with magnetic resonance thermometry to heat and damage the ventral intermediate region for the clinical treatment of essential tremor in awake

patients (Elias et al., 2013).

1.7 Functional Magnetic Resonance Imaging

Magnetic resonance imaging (MRI) is the most common medical imaging modality for diagnosis of not only brain but also human body. Functional MRI (fMRI) is a powerful technique to measure brain response by detecting activity-dependent changes in cerebral blood flow (Matthews & Jezzard, 2004). The change in cerebral blood flow (CBF) can be measured by BOLD responses which are related to changes in oxyhemoglobin and deoxyhemoglobin in a locally defined area (Ogawa et al., 1990; Kwong et al., 1992). Tactile, auditory, visual, motor, and cognitive processes evoke activity among complex networks of neurons, which is associated with an increased demand for oxygen and increased cerebral blood flow to match metabolic demands (Kim & Uğurbil, 1997; Uludağ et al., 2004). Because a peak of BOLD response occurs about 4-6 seconds following activation, temporal resolution is the major limitation of fMRI, in spite of relatively high spatial resolution (millimeters) (Glover, 2011).

Over the last two decades, fMRI has evolved to feature higher magnetic field strengths and improved image acquisition sequences to map focal brain responses induced by different stimulus types such as tactile, auditory, and visual representation (Kurth et al., 1998; Francis et al., 2000; Foxe et al., 2002; DeYoe et al., 1996). Functional MRI can also be implemented and combined with EEG (electroencephalogram) and fNIRS (functional near-infrared spectroscopy) to improve both spatial and temporal resolution (Portas et al., 2000; Steinbrink et al., 2006).

1.7.1 Principles of MRI

Atomic nuclei containing an odd number of protons possess characteristic properties such as spin and precession. Precession produces a magnetic moment because

the nuclei has a charged particle. Fig. 1.5a shows a proton with a magnetic moment created by the precession. These nuclei (hydrogen [H] is used in MRI) are aligned

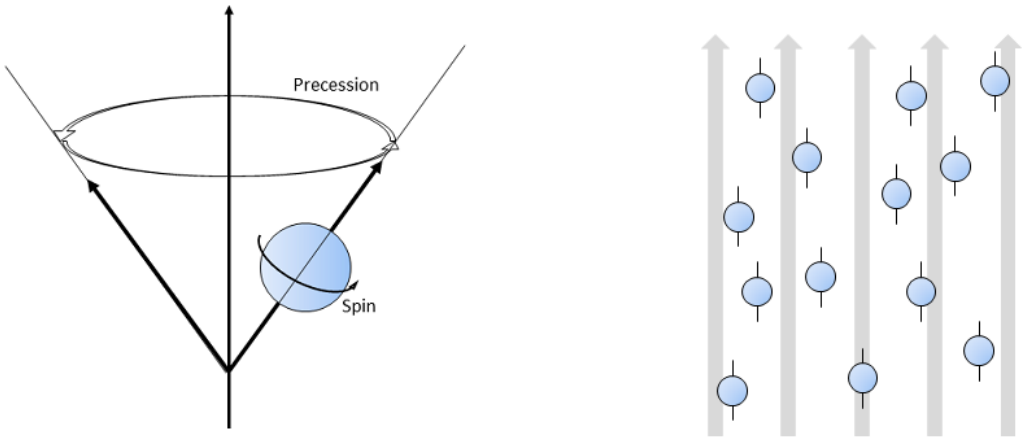

(a) Spin and Procession (b) Nuclei aligned with the magnetic field

Figure 1.5: Nuclei and magnetic field

randomly if there is no external magnetic field. When the [H] nuclei in a human body or head are placed in a strong magnetic field, the nuclei are aligned parallel to the direction of the magnetic field. Fig. 1.5b represents the nuclei aligned with the magnetic field. The alignment of nuclei with a magnetic field yields the precession of nuclei around the magnetic field which oscillates like a gyroscope. This is known as the Larmor or precessional frequency which can represented using equation 1.1.

$$\omega = \gamma B \tag{1.1}$$

where ω is the angular or Larmor frequency, γ is the gyromagnetic ratio which is constant and B is the strength of the applied magnetic field in Tesla. The gyromagnetic ratio of hydrogen is 42.58 MHz/Tesla.

The human body or head must be located in a uniform magnetic field, B = 1.5T or 3.0T, to achieve an MR image. As a result, hydrogen nuclei in the human body or head align parallel to the magnetic field, B, and generate a net magnetic momentum,

M. A radiofrequency (RF) pulse is transmitted to the nuclei perpendicular to the magnetic field, B. When the RF pulse matches the Larmor frequency of the precessing protons, the nuclei tilt away from the uniform magnetic field direction. If the RF pulse is removed, the hydrogen nuclei realign themselves in parallel to the magnetic field which is known as relaxation. Free induction decay (FID) response signal occurs during relaxation since the nuclei lost their energy due to release from the RF pulse (Haase et al., 1986). In fMRI, a 20 or 32 channel head coil is used to detect the FID response signal to produce 3D grey-scale MR images.

1.7.2 T1 and T2 weighted image

Signals in MR images are determined by three basic parameters: 1) proton density of the tissue, 2) longitudinal relaxation time (T1), and 3) transverse relaxation time (T2). First, hydrogen proton density is the concentration of protons in the target tissue. As proton density is homogeneous for most soft tissues in the human body, the proton density weighted image is useful for imaging the extremities, such as ankle, shoulder or knee (Tokuda et al., 2014). Proton weighted images are also used to compare between the fat and fluid. A long repetition time TR (2000 - 5000 ms) and short echo time TE (10 - 20 ms) sequence mainly produces proton density weighted to minimize the effects of T1 and T2.

When the RF pulse applied to the nuclei is turned off, the protons revert back to their initial states and this process is known as relaxation. The relaxation time differs from one tissue to another and the difference in the relaxation times is used to categorize tissue types. The T1 refers to the process of how quickly a net magnetization returns to its initial states parallel to the magnetic field and be ready for the next excitation. The net magnetization is known as the averaged angular momentum from all spins in the subject (Melzack & Katz, 2007). The T2 is approximately 63%

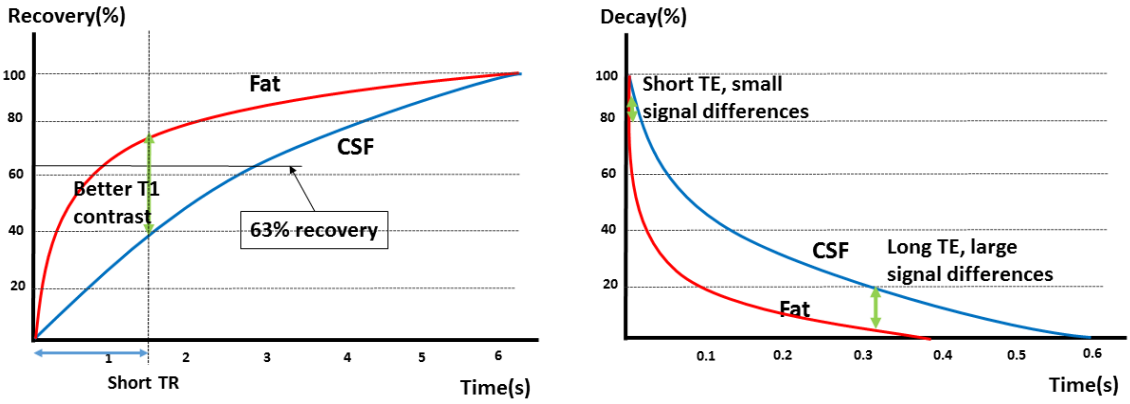

(a) T1 curves (b) T2 curves

Figure 1.6: T1 and T2 curves

recovery of the net magnetization. The T2 is the progressive dephasing or decaying of the transverse factors of magnetization and the time required for the transverse magnetization to decay approximately 37% of its initial intensity (Mugler III, 2006). Fig.1.6 shows the T1 and T2 curves, respectively.

Compared to the proton density weighted images, T1 and T2 vary according to tissue types and they are useful to distinguish various tissue types. A short TR (300 - 600 ms) and short TE (10 - 15 ms) sequence is called T1-weighted, and a long TR (2000 - 6000 ms) and long TE (100 - 150 ms) is T2-weighted. From the Larmor equation, the frequency of hydrogen nuclei in CSF is higher than in fat. This is why hydrogen atoms in fatty tissues return to their initial state faster along the longitudinal axis than in CSF. Because the 63% recovery time of fat ($\simeq$ 240 ms) is faster than CSF ($\simeq$ 3000 ms), the fat appears bright on T1-weighted image while the CSF seems dark. In contrast, the CSF and the fat present bright and dark on T2-weighted image, respectively, as the 37% decay time of fat ($\simeq$ 80 ms) is shorter than CSF ($\simeq$ 200 ms). Fig.1.7 shows the T1- and T2- weighted images (Almeida et al., 2012).

There are two main factors that affect transverse relaxation: 1) intrinsic, and 2)

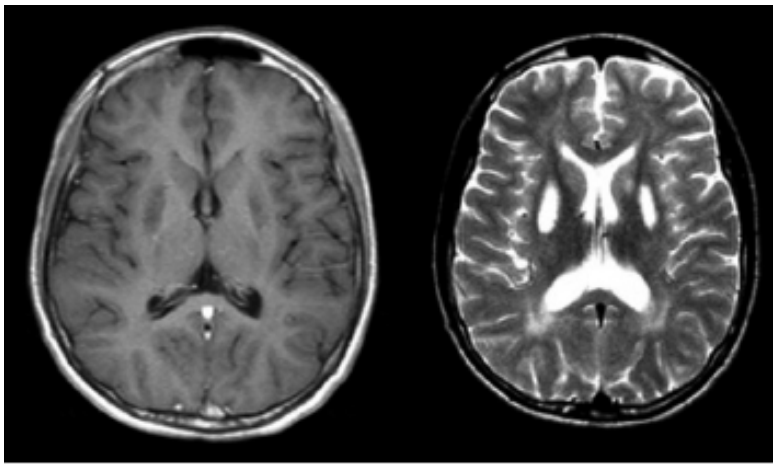

Figure 1.7: T1- and T2- weighted axial brain images (Almeida et al., 2012)

extrinsic. The intrinsic factor is spin-spin interaction caused from different Larmor frequencies of spins. The extrinsic factor indicates magnetic field inhomogeneity within voxel due to imperfections of the scanner magnet construction. These two factors can be combined to form T2* (or T2-star) which is the nomenclature used in fMRI.

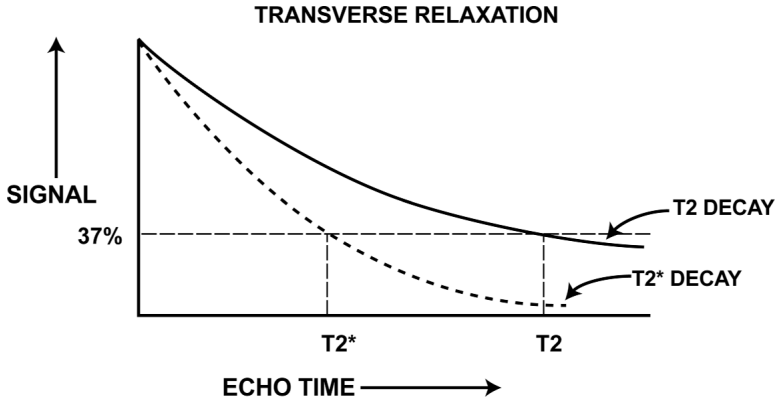

Figure 1.8: T2 versus T2* (Chavhan et al., 2009)

Fig.1.8 represents T2 and T2* decay transverse relaxation curves (Chavhan et al., 2009). As shown, the T2* decay drops its signal intensity more rapidly than T2 because T2* decay has greater magnitude than T2 in tissue. The difference in signal loss between T2* and T2 decay is caused by magnetic field inhomogeneity.

1.7.3 Echo-Planar Imaging (EPI)

Echo-planar imaging (EPI) sequence was first described by Mansfield nearly 40 years ago (Mansfield, 1977). Compared to an hour of lying inside the MRI scanner before, EPI sequence makes it possible to acquire MR images within a few minutes thereby minimizing the artifacts associated with movement. EPI acquires multiple echoes of different phase steps after a single RF excitation (Poustchi-Amin et al., 2001). The spin echo (SE) sequence and the gradient echo (GRE) sequence are two main characteristics of the EPI sequence.

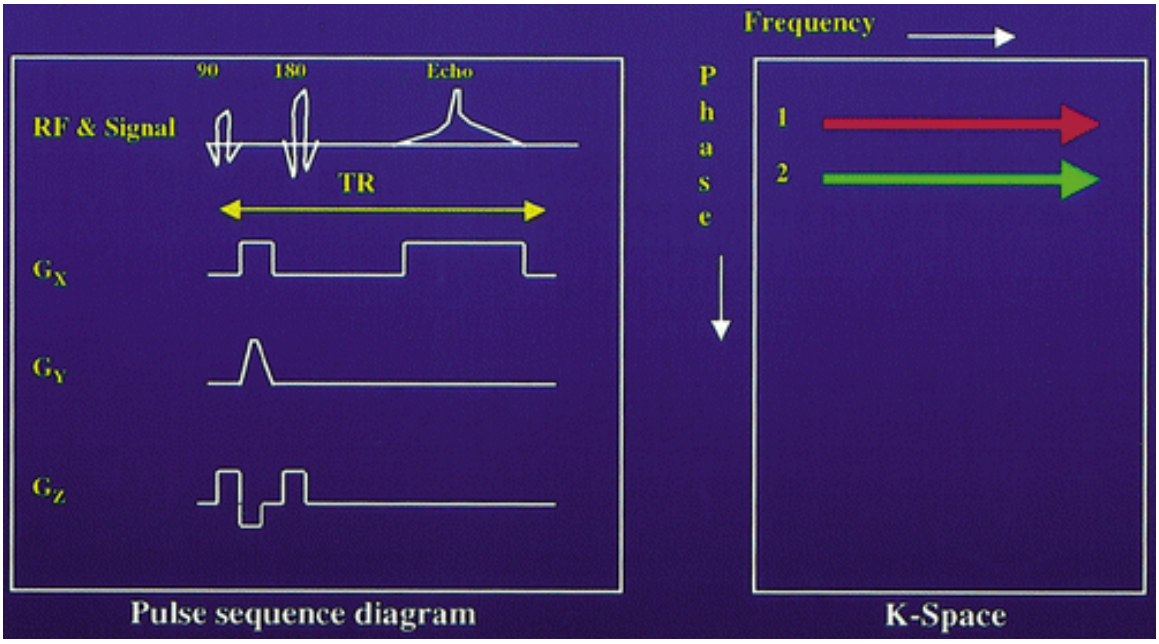

Figure 1.9: Conventional SE imaging (Poustchi-Amin et al., 2001)

Fig.1.9 shows conventional spin echo imaging where G_x is the frequency-encoding gradient, G_y is the phase-encoding gradient and G_z is the section-selection gradient (Poustchi-Amin et al., 2001). K-space refers a data matrix containing raw MRI data. In MRI physics, k-space is the 2D or 3D Fourier transform of the MR image measured. The SE sequences initiate with 90° and 180° RF (radio frequency) pulses, followed

by an echo. The time between each sequence is known as the repetition time (TR). The echo time (TE) is the interval between the middle of first 90° RF pulse and the peak of the spin echo which is shown as the echo in fig.1.9. During each TR period, one line of MR imaging data is obtained and k-space is filled with the multiple TR periods. The total imaging acquisition time (TA) is same as the product of the TR and the phase encoding step numbers.

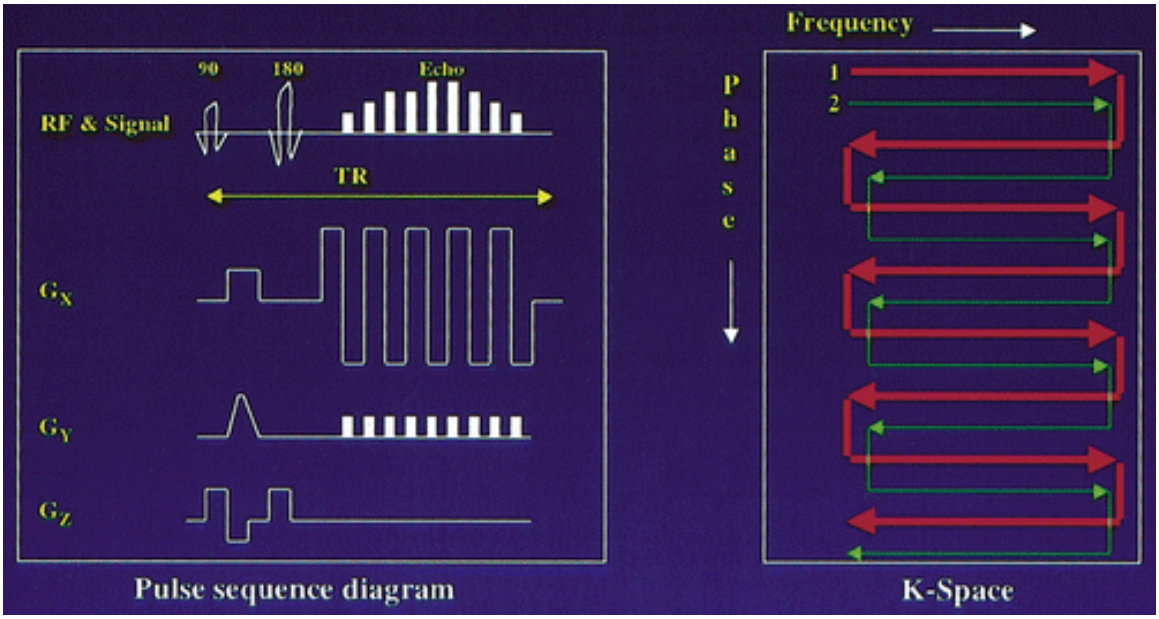

Figure 1.10: Echo-planar imaging (Poustchi-Amin et al., 2001)

The pulse sequence and k-space for Echo-planar imaging is shown in Fig.1.10 (Poustchi-Amin et al., 2001). The SE sequence initiates with 90° and 180° RF (radio frequency) pulses similar to conventional SE sequence. G_x, the frequency-encoding gradient, fluctuates from positive to negative after 180° RF pulses, creating a train of gradient echo (GRE). GRE is acquired with each oscillation and result is shown as a "zig-zag" traversal of k-space. This "zig-zag" traversal of k-space is accomplished by rapid modulation of the frequency-encoding gradient. The echo planar sequence may accept all gradient echoes or combined with a spin echo. Whereas TA of SE is

the multiplication of the TR and the number of phase encoding step numbers, TA of single-shot EPI is equal to one TR. EPI provides sufficient temporal resolution (2-3 seconds) to detect the hemodynamic response to neural activities as required in functional or diffusion imaging studies (Narsude et al., 2015).

1.7.4 Neural activity

The adult human brain consists of approximately 86 billion neurons, with approximately 16 billion neurons in neocortex and 49 billion neurons in the cerebellum (Herculano-Houzel, 2009). These neurons form an adaptive and immensely complex network to generate movement, sense, predict, make decisions, formulate language and speech, and emote.

Neurons represent the only type of cell which exhibits a resting membrane potential and is irritable. Neurons in mammals feature a semipermeable phospholipid bilayer membrane organized around a nucleus with complex cytoplasmic extensions known as dendrites and axons. Dendrites are always unmyelinated and subject to the properties of electrotonic spread of current/voltage gradients, whereas most axons in the central nervous system rely on a fatty sheath (myelin) to ensure high velocity nerve conduction (salutatory) to a postsynaptic target in the form of another neuron. If the neuron is part of the peripheral motor nervous system, action potentials may be directed to synaptic terminals to activate muscle cells or glands in somatic tissues of the body for movement and excretory function, respectively. The cell membrane of the axon includes voltage-gated Na+ and K+ channels, among others, which are involved in the generation and propagation of the action potential. The action potential is produced by integrated opening and closing of voltage-gated ion channels. External sensory events (i.e., touch, electrical current, vision, auditory, olfactory, gustatory, etc.) result in local generator potentials, and if these stimulus events are large enough

in amplitude or include summation, it then becomes possible to induce the nerve cell to generate an obligatory signal known as an action potential (Cooper, 2008). For many neurons, the resting membrane potential hovers around -70 mV (inside neuron relative to outside the cell) and the threshold point of the membrane potential is usually above -55 mV. When an inbound stimulus causes the membrane potential to pass in a positive direction above this threshold, then a very rapid and obligatory phase of depolarization occurs to $\sim \pm$ 40 mV followed by re-polarization of the neuron towards its resting membrane potential. During the rapid initial phase of depolarization ($\sim$ 1-2 ms), Na+ channels open allowing this ion to move into the neuron. At the peak voltage, Na+ channels close and K+ channels open which directly results in movement of K+ ions out of the neuron into extracellular space which is correlated to membrane repolarization, typically manifest as an undershoot to -90 mV which is known as the refractory period. The refractory period is associated with an ATP-driven Na+/K+ pump which serves to restore ionic concentrations to their resting membrane levels. The refractory period may last for several milliseconds and it is during this period where the neuron is limited in generating a new action potential. In essence, a neurons maximal firing rate is largely determined by the depth and duration of the refractory period. Once the action potential arrives the terminal bouton of the axon, Ca^{++} voltage sensitive channels open allowing an influx of this ion into the terminal thereby mobilizing vesicles containing neurotransmitters (i.e., glutamate (GLUT), γ-aminobutyric acid (GABA), acetycholine (ACh)) to fuse with the presynaptic membrane and undergo exocytosis to release the neurotransmitters into the 20 nm synaptic cleft, and diffuse to activate the postsynaptic neuronal membrane. In mammals, the interconnection between an axon terminal and the postsynaptic dendritic or soma target is called a chemical synapse.

Electrical signaling by neurons is a continuous process in the brain and therefore

requires oxygen and adenosine triphosphate (ATP) to power this mechanism. Thus, large numbers of specialized organelles known as mitochondria are common to synaptic terminals and the soma of neurons to meet the metabolic demands associated with electrical signaling (action potentials). Thus, an increase in neural activity causes an increase in oxygen consumption and ATP which leads a change of ratio between the oxyhemoglobin and deoxyhemoglobin in the blood flow (Heeger & Ress, 2002). This process creates a BOLD contrast for fMRI.

1.7.5 BOLD-contrast imaging

Neurovascular coupling is the relationship between neural activity and changes in cerebral blood flow (CBF) (Girouard & Iadecola, 2006). The living brain has a continuous need for oxygen and glucose which is required to maintain adequate CBF. Release of neurotransmitters associated with sensory stimulation, motor and cognitive activity are followed by the production of vasoactive chemical agents including K+, nitric oxide (NO), and carbon dioxide (CO_2) which effect changes in the cerebral blood volume (Raichle & Mintun, 2006). This neurovascular coupling process facilitates the changing ratio between oxyhemoglobin and deoxyhemoglobin, particularly in areas of the brain where neural activity is high.

The concept of BOLD-contrast imaging was introduced by Seiji Ogawa in 1990, and the first human study with BOLD-contrast imaging was performed by Kenneth Kwong in 1992 (Ogawa et al., 1990; Kwong et al., 1992). The BOLD represents the ratio of oxyhemoglobin and deoxyhemoglobin in the blood. Hemoglobin (Hb) in blood cells exists in two distinct states and each state has different magnetic moment properties. Oxyhemoglobin and deoxyhemoglobin have diamagnetic and paramagnetic properties, respectively (Pauling & Coryell, 1936). The BOLD image takes advantage of the change from diamagnetic oxyhemoglobin to paramagnetic deoxyhemoglobin

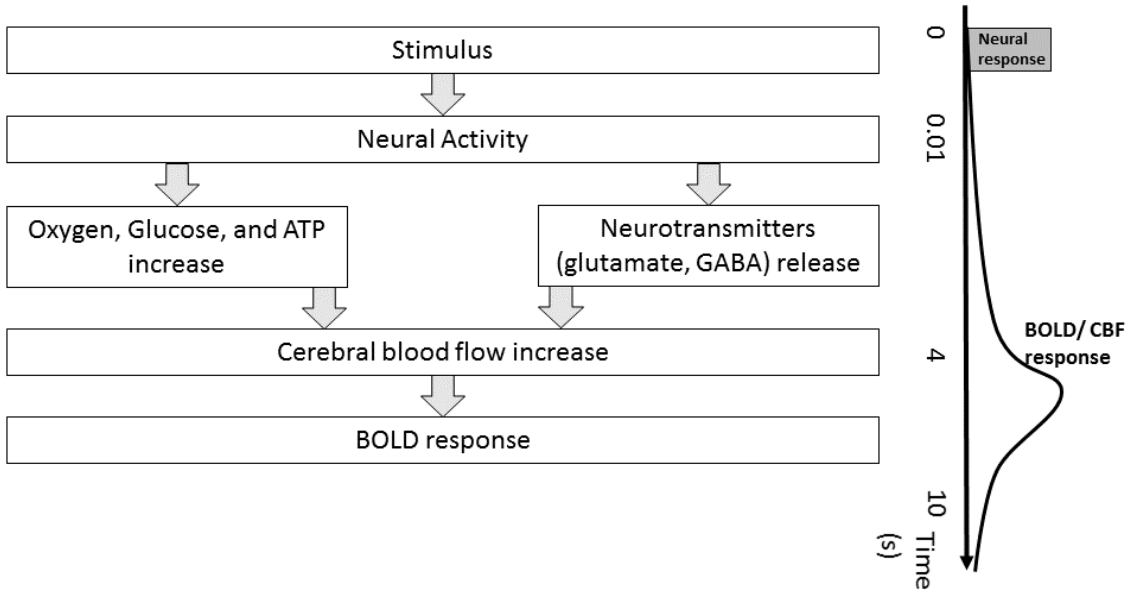

Figure 1.11: Neurovascular coupling

which results in a decreased MR signal (Hare et al., 1998). As local concentration levels of the paramagnetic deoxyhemoglobin decreases during neural activity, the MR signal increases.

The hemodynamic response function (HRF) is the change in the MR signal triggered by neural activity. As stimulus-evoked neural activation increases in a specific part of the brain, there is increased demand for O_2 and ATP. When O_2 is extracted from the blood, the Hb becomes deoxyhemoglobin which has paramagnetic properties. The paramagnetic properties are termed the magnetic susceptibility effect which leads signal loss on MRI (K. Cho et al., 2005). Since oxyhemoglobin has diamagnetic properties and does not create the same signal loss, oxygen changes in the blood can be detected with the signal changes (Ogawa et al., 1990). The blood requires oxygen demand due to an overcompensation of deoxyhemoglobin and the balance between oxyhemoglobin and deoxyhemoglobin. Although the MRI signal would be expected to decrease due to an increase of the level of deoxyhemoglobin, there is a much larger

increment in cerebral blood flow which brings more oxyhemoglobin (Silva et al., 2000). The oxygen demand results in an increase in the BOLD signal which peaks around 5 seconds following the initial stimulus, and then HDR level falls back to baseline upon stimulus cessation (Malonek & Grinvald, 1996; Miezin et al., 2000). The HRF often goes below the baseline upon stimulus cessation. This phenomenon, known as the refractory period or post-stimulus undershoot, is due to an increase in local blood volume (J. Chen & Pike, 2009).

Figure 1.12 shows the post-stimulus undershoot following 30 seconds of visual stimulation (Lu et al., 2004). Plot panel (A) shows the changes in BOLD, CBV, and CBF pooled among all activated voxels, and plot panel (B) shows the changes when focusing attention only on the subset of voxels activated in BOLD, CBV, and CBF.

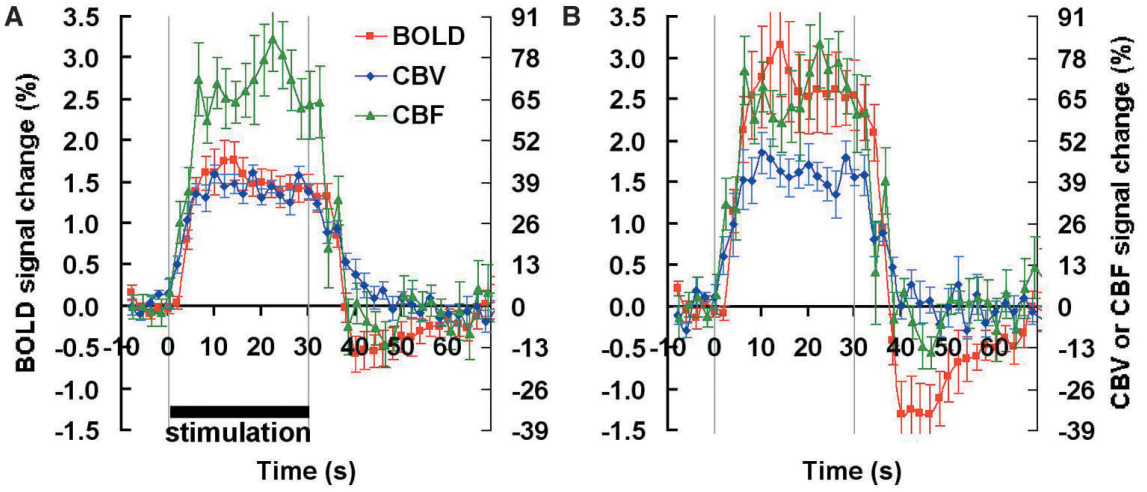

Figure 1.12: BOLD, cerebral blood volume (CBV), and cerebral blood flow (CBF) (Lu et al., 2004)

1.7.6 fMRI experimental design

There are independent variables which can be adjusted by the researcher: stimulus modality (auditory, tactile, visual, etc.), stimulus timing, response mode (pushing button, eyeblink, verbal, none, etc.), participant instructions, etc. Dependent variables are the response outcomes or physiological data derived from fMRI such as the BOLD response. Most fMRI experimental designs consist of two basic types of conditions which include active and control conditions. Active conditions are most often associated with the stimulation period (i.e., hand movement, tactile stimulation, etc.) and the control condition is without stimulation. Because the BOLD-contrast imaging measures relative oxygen changes (i.e., not absolute), the control condition is required for comparison or contrast with the experimental condition(s).

There are two guiding concepts for fMRI experimental design, known as the 'block' and 'event-related' designs. Advantages of event-related design are the response to a single stimulus which eliminates predictability of repeated stimuli, good temporal hemodynamic response function (HRF), and various stimulus events which can be performed randomly in one run. The main drawback is low statistical strength due to small BOLD changes and more complicated experimental design (Friston et al., 1998, 1999). Another major downside of event-related design is that the signal-to-noise ratio (SNR) is lower than block design (Dale & Buckner, 1997; Kay et al., 2008). In contrast, the fMRI block design affords higher statistical power and it is relatively simple to construct. In addition, the block design minimizes task-switching and randomization which makes it easier for the research participant (Chee et al., 2003). Disadvantages of block design include expectation and adaptation due to stimulus repetition within-block. The repetition of the stimulus may lead to possible BOLD signal decrease which makes study of slow changes in neural activity using BOLD complicated (Logothetis,

2008; Hernandez-Garcia & Jahanian, 2014). Second, BOLD response timing is not as easy to derive within a block compared to an event-related design. Third, since the block design usually represents relatively long periods for each block, controlling a specific task could be challenging. For example, resting conditions may not be truly resting states if a participant is not engaged in resting. Finally, each block length should be precisely considered to create the block design. When there is a short interval between active and rest blocks, BOLD effect size could be decreased because of the post-stimulus undershoot (van Zijl et al., 2012). A combination of even-related and block designs are often used to overcome the limitations of each design. Given the advantages and disadvantages of each experimental design, it is important to select independent and dependent variables carefully because the combination model is a more complex design. In addition, it is essential for researchers to create the most appropriate design in order to advance the experimental paradigm and optimize the BOLD response result. Fig. 1.13 (A), (B), and (C) represent block, event-related, and mixed design, respectively (Amaro & Barker, 2006).

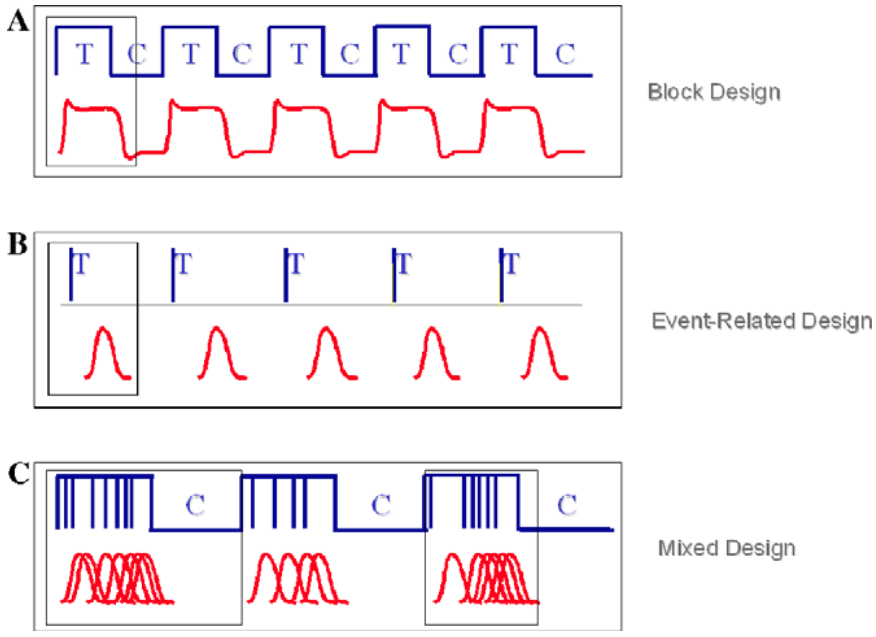

Figure 1.13: Block, event-related, and mixed design (Amaro & Barker, 2006)

1.7.7 fMRI Data Analysis: SPM

SPM (Statistical parametric mapping, The Wellcome Trust Centre for Neuroimaging, London, UK) is a statistical tool created by Karl J. Friston for analysis of brain responses recorded during a functional experiment using fMRI, MEG, or EEG. Fig. 1.14 shows a schematic representation of the preprocessing steps and general linear model (GLM) method for fMRI data analysis (Friston et al., 2007). SPM is freeware written using MATLAB and offers extensive toolboxes (e.g., xjView (`http://www.alivelearn.net/xjview`) - anatomy description of particular brain area) for detailed fMRI data analysis was created and continues to be supported by many SPM users worldwide.

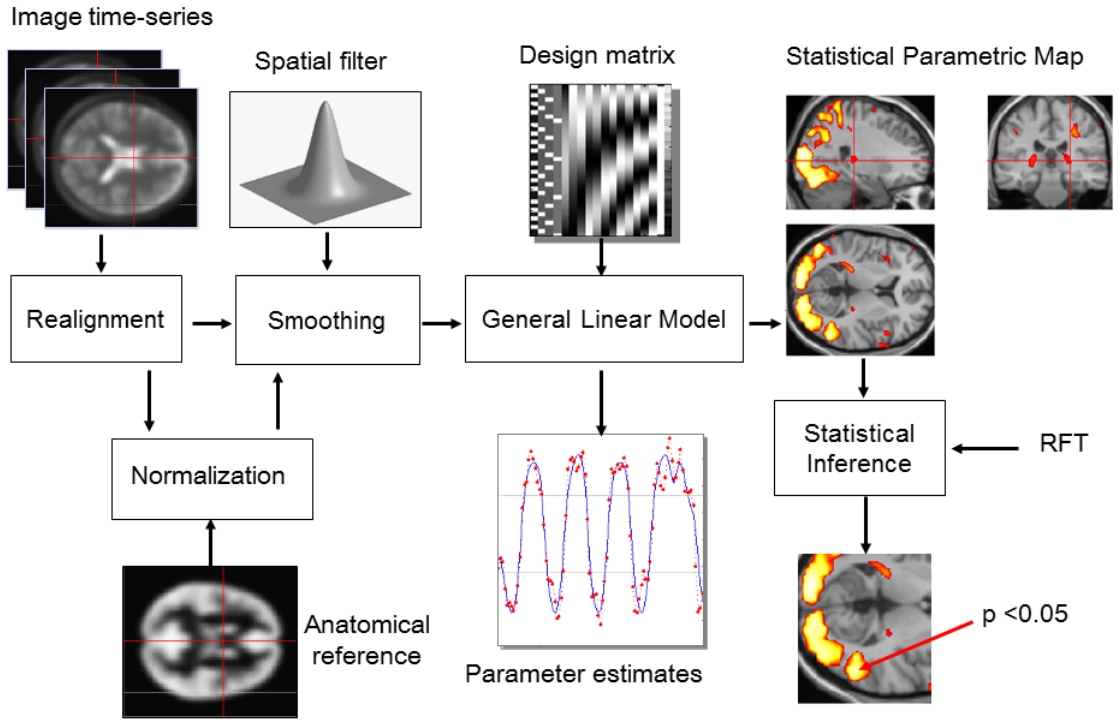

Figure 1.14: Schematic representation of data analysis using SPM (Friston et al., 2007)

1.7.7.1 Preprocessing

Before analysis of fMRI BOLD data can proceed, several preprocessing steps are required to adjust the data for head movement artifacts, and normalize and smooth the fMRI dataset. The first preprocessing step is **realignment** which registers all functional images to the first functional image of the first session. Three translational axes (x, y, and z translation) and 3 rotations (pitch, roll and yaw) are used to realign all functional images. Performing realignment will create a mean image from all functional images which can be used to match or co-register functional images to an anatomical image. Realignment also generates text and pdf file. The text files include the estimated translations in mm of dimension, and the estimated rotations in radians (rad), and a resultant ***.pdf** file presents a plot based on these parametric estimates. Co-registration is the next step to align the anatomical image to the mean functional image created by the realignment process. After the co-registration is completed, the anatomical and mean functional image are displayed as a source and reference image, respectively. The **segmentation** processing step occurs next and is designed to separate brain tissues based on their composition. Segmentation is based on a modified Gaussian mixture model (Ashburner & Friston, 2000). Healthy human brain can be classified into three major tissue types: gray matter (GM), white matter (WM), and cerebrospinal fluid (CSF). Segmentation is a tool that allows the investigator to extract GM, WM and CSF from the anatomical image. SPM offers the prior probability maps derived from a large number of subjects provided by BrainWeb (Cocosco et al., 1997). The initial segmentation image can be combined with prior probability maps using Bayesian rule. Fig. 1.15 shows the results from applying the segmentation method to the BrainWeb data (Ashburner & Friston, 2005). The first column displays the tissue probability maps (TPMs) for GM and WM. The first row

of second, third, and fourth column show T1, T2, and PD (proton density) images. Below these first row cells are the extracted images of the GM (row 2) and WM (row 3) segmentation results.

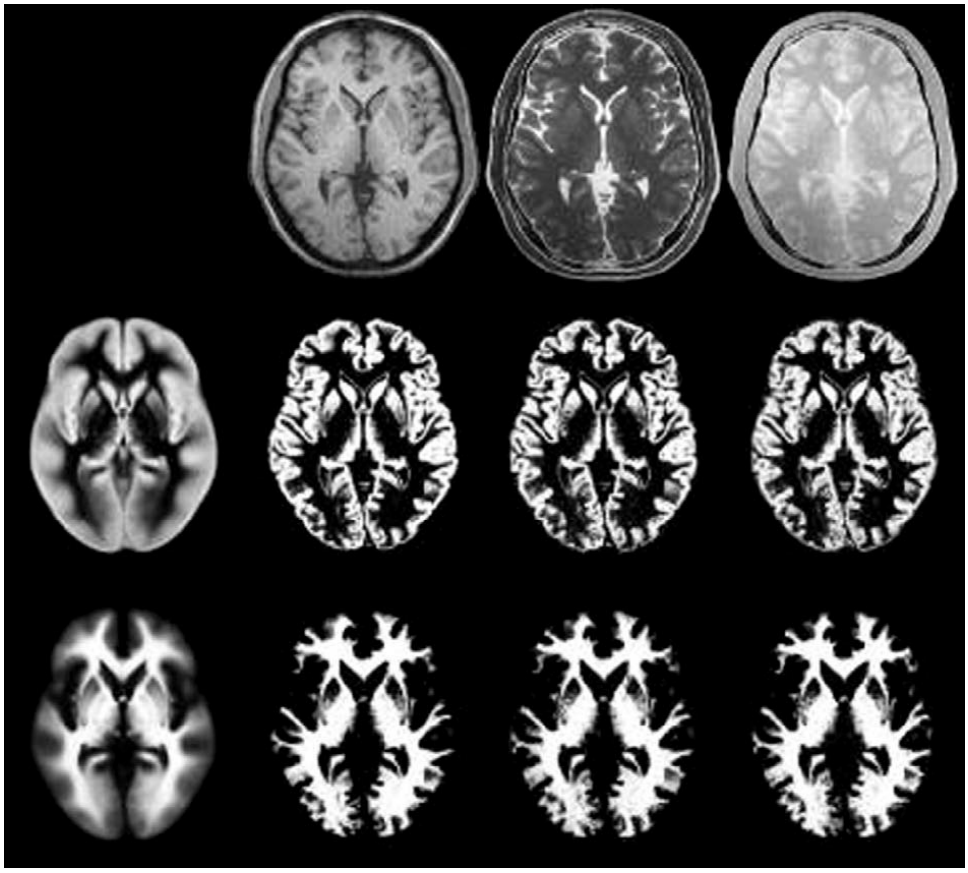

Figure 1.15: Segmentation results (Ashburner & Friston, 2005)

Spatial normalization is the step that normalizes both the functional and anatomical images to the MNI (Montreal Neurological Institute) structural template. Because different people have different brain size and shape, the normalization process is needed to adjust overall size and orientation into the standard template. The first standard coordinate system, known as Talairach coordinate space, was developed by neurosurgeon and psychiatrist Jean Talairach and was based on single post-mortem dissection of a human brain (Talairach & Szikla, 1967; Talairach & Tournoux, 1988).

More recently, alternative standard templates such as MNI coordinate system, based on 305 human brains, have widely replaced the Talairach template (Evans et al., 1993). As such, SPM provides MNI standard space for the spatial normalization process. Fig.1.16 shows Talairach and MNI coordinate systems. Talairach coordinates use the standard brain space with the same dimensions that were published in 1988 and its primary axis corresponds to the anterior commissure - posterior commissure line (AC-PC line) which is also used as a referent in neurosurgical planning (Laird et al., 2010). In contrast, the MNI templates differ considerably from the Talairach coordinates because the MNI coordinates are represented by differences in reference frames (position and orientation) and larger brain dimensions (x = 142 mm, y = 180 mm, z = 134 mm) than the Talairach coordinates (x = 136 mm, y = 172 mm, z = 118 mm) (Laird et al., 2010). Several neuroimaging analysis software programs such as Analysis of Functional NeuroImages (AFNI) accept the Talairach database and AFNI provides a tool to convert from the Talairach to MNI coordinates, whereas the MNI templates are implemented in SPM (Lancaster et al., 2007).

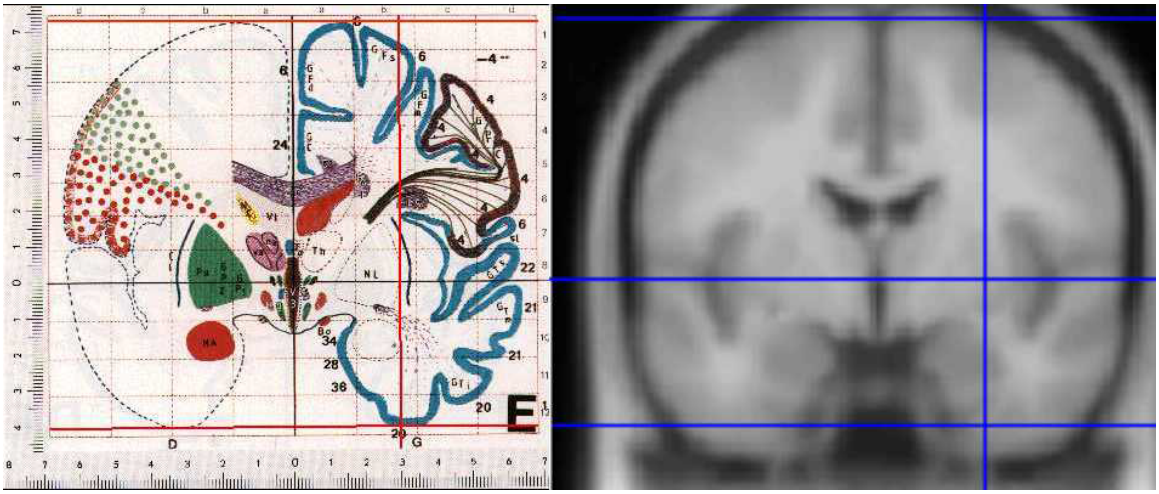

Figure 1.16: Talairach and MNI space

The final step is **smoothing** via a blurring kernel to all realigned and normalized

functional images. The goal of smoothing is to improve the signal-to-noise ratio (SNR) and increase sensitivity of BOLD signals (Jo et al., 2007). By the central limit theorem, smoothing makes data more normally distributed. Smoothing is implemented by convolution with a 3D Gaussian kernel specified full-width at half-maximum (FWHM) in *mm*. The size of the kernel can be calculated by following equation 1.2.

$$\text{FWHM (mm)} \geq 3 \times \text{voxel size (mm)} \tag{1.2}$$

For example, when a voxel size of functional images is 2.5 x 2.5 x 2.5 mm, the 8 x 8 x 8 mm kernel size is an appropriate selection for smoothing.

1.7.7.2 General Linear Model (GLM)

An application of the GLM uses a multiple regression approach to enhance hypothesis testing with SPM (Friston et al., 1994). The GLM allows for correlations between the design matrix with weighted parameters and an error term. The GLM for observed data can be written in matrix form using equation 1.3:

$$\mathrm{Y} = \mathrm{X}\beta + e \tag{1.3}$$

where Y is the BOLD signal for a given voxel, X is a combination of predictors which is the design matrix, β is a set of weighted parameters, and e is an error term. The GLM assumes the error term is independent and identically distributed [$e \sim \mathrm{N}(0, \sigma^2)$]. Results of the GLM can be used for estimates of the true value of parameters, β.

In this study, the GLM was applied to a block design including 320 volumes of fMRI images among 5 different stimulus conditions. There are 3 different saltatory pneumocutaneous velocities (5cm/s, 25cm/s, and 65cm/s), one condition without stimulation, and one condition in which all TAC-Cells in the array are activated simultaneously. The voxel time course, the value of parameters, error terms, and

predictors of this block design can be represented using equation 1.4.

$$\begin{pmatrix} y_1 \\ y_2 \\ \vdots \\ y_{100} \\ \vdots \\ y_{320} \end{pmatrix} = \begin{pmatrix} 1 & 0 & 0 & 0 & 0 \\ 1 & 0 & 0 & 0 & 0 \\ 1 & 0 & 0 & 0 & 0 \\ \vdots & \vdots & \vdots & \vdots & \vdots \\ 0 & 0 & 0 & 0 & 1 \\ 0 & 0 & 0 & 0 & 1 \end{pmatrix} \begin{pmatrix} \beta_1 \\ \beta_2 \\ \beta_3 \\ \beta_4 \\ \beta_5 \end{pmatrix} + \begin{pmatrix} e_1 \\ e_2 \\ \vdots \\ e_{100} \\ \vdots \\ e_{320} \end{pmatrix} \tag{1.4}$$

where $\beta_1, \cdots, \beta_5$ corresponds to the 5 different conditions. In practice, we assume the data Y are mean corrected which indicates there is no error term. The normal equation is applied to calculate least squares estimates of β (Scheffe, 1999).

$$\mathrm{X^T X}\beta = \mathrm{X^T Y} \tag{1.5}$$

$\mathrm{X^T X}$ term can be inverted if X is of full rank and the equation 1.5 can be adjusted as follows.

$$\beta = (\mathrm{X^T X})^{-1}\mathrm{X^T Y} \tag{1.6}$$

To get the final results from GLM, the null hypothesis can be simply described as $\mathrm{C^T}\beta = 0$, where C is the scalar product of contrast vector. This contrast vector can be calculated with the following t-test equation 1.7.

$$\mathrm{t} = \frac{\mathrm{C^T}\hat{\beta}}{\sqrt{\mathrm{Var}(\mathrm{C^T}\hat{\beta})}} \tag{1.7}$$

The denominator of equation 1.7 is described as the standard error of $C^T\hat{\beta}$ which is derived from noise variations. For example, if we want to see the BOLD signal difference between the 5 cm/s velocity of tactile stimulation and resting condition, a contrast vector C^T = [1 0 0 -1 0] can be used.

1.7.7.3 Region of Interest

A region of interest (ROI) analysis in functional neuroimaging indicates a select cluster or subset of voxels in a brain region to explore the fundamental BOLD response behind a whole-brain voxel-wise analysis (Poldrack, 2007). The main reason to draw a ROI on neuroimaging data is to elicit data for a specific region from a corresponding functional dataset. Because functional images generally have poor resolution to detect anatomic boundaries compared to a high-resolution anatomical scan, the ROI is drawn based on the anatomical landmarks (Nieto-Castanon et al., 2003). The ROI is used to investigate the statistical analysis of brain response across subjects (Ng et al., 2006). The ROI is used to characterize the HRF among voxels from a homogeneous area in MRI brain image which is difficult to define in other functional imaging modalities such as positron emission tomography (PET) (Devlin et al., 2000). The ROI analysis can be done by creating a sphere with a selected radius. Creating the sphere defines voxels within a functional volume image which are of interest. SPM allows specification of the ROI analysis in three dimension, also known as a volume of interest (VOI). The ROI analysis in SPM offers the options of creating a sphere with a radius or box dimensions in *mm*. The ROI analysis in SPM also can be processed using several toolboxes such as MarsBar or xjView (Brett et al., 2002).

Chapter 2

Methods

2.1 Participants

Participants include twenty neurotypical, right-handed subjects (14 females, 6 males) aged 18-30 (mean age = 22.3 ± 2.47 years). Participants for this study were recruited by posted advertisement at UNL East Campus (Union, Barkley Memorial Center, Chase Hall, etc.) and City Campus (Union, CB3 (Center for Brain Biology and Behavior)). Participants provide informed written consent in accordance with UNL Human Subjects Protocol #14515. Prospective participants who have sustained traumatic injury to the hand or neurological disease resulting in sensorimotor impairment affecting hand movements were excluded for this study. Each subject participated in a single 90-minute session at CB3. This session includes informed consent, pneumotactile TAC-Cell application to the right hand, one anatomic MRI image acquisition (MPRAGE; 7 minutes) and three fMRI acquisitions for BOLD (13.3 minutes each).

No.	Male/Female	Age
7	Female	29
8	Male	23
11	Female	23
14	Female	22
15	Female	22
16	Female	22
20	Female	24
22	Female	23
25	Female	22
27	Female	21
29	Female	21
30	Female	21
33	Female	20
34	Female	28
41	Male	20
42	Male	21
46	Male	22
47	Male	19
48	Female	23
50	Male	20
		22.3 ± 2.47

Table 2.1: Participants

2.2 Somatosensory pneumatic stimulus control

Over the past 30 years, the Barlow laboratory has pioneered the development and application of several direct-coupled linear servo motors and pneumatic mechanical stimulus generation control systems for use in humans across the lifespan (Barlow et al., 2008; Venkatesan et al., 2010; M. Popescu et al., 2010; A. Popescu et al., 2013). One of these stimulus control systems, known as the NTrainer System (Innara Health, Inc., Olathe KS, USA) was FDA-approved in 2008 and is a single-channel pneumatic tactile stimulator used widely in neonatal intensive care units in the US to stimulate mechanoreceptor units in the soft tissues of mouth in premature infants to promote sucking and feeding. Pneumatic stimulators are safe, non-invasive, achieve normal 'physiologic' recruitment order of primary mechanosensitive afferent neurons, and avoid the potential risks associated with direct-current stimulation methods. Over the past decade, the Barlow laboratory has been closely involved with the development of a multichannel pneumatic tactile array featuring scalable pulse generation with rapid rise/fall times ($\simeq$ 10ms), and constructed from non-ferrous materials making this mode of stimulation compatible with MEG and MRI scanners. Channeling the pneumatic pulse waveforms to the skin was achieved using specially machined TAC-Cell probes (Venkatesan et al., 2010). The TAC-Cell is essentially a small capsule, which can be placed on virtually any skin surface of the body, including the glabrous hand and face. The first TAC-Cells were relatively large (19.3mm ID) and machined from Delrin® acetal thermoplastic. A custom non-commutated servo-motor (H2W Technologies, Inc., NCM 08-25-100-2LB) coupled to a custom Airpel® glass cylinder (Airpot Corporation, 2K4444P series) operating under position feedback (Biocommunication Electronics, LLC, model 511 servo-controller) constituted the pneumatic amplifier to control the timing and amplitude of pulsed tactile inputs to the hand and face. More recently,

the TAC-Cell has been miniaturized (OD = 15mm, ID = 6mm). Fig.2.1 shows a TAC-Cell in 3 views as placed on the face and glabrous index finger in fig.2.1 (b) and (c), respectively (Venkatesan et al., 2014).

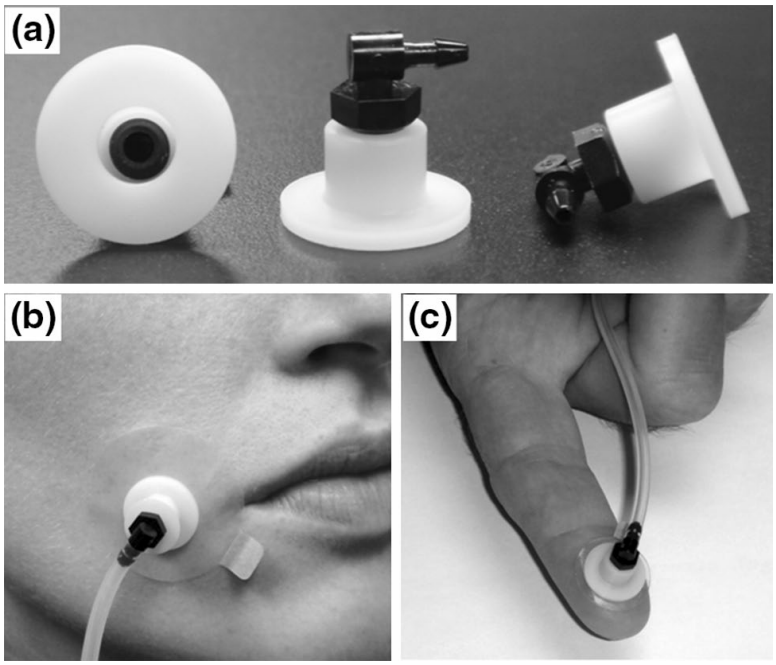

Figure 2.1: TAC-Cell (Venkatesan et al., 2014)

A new multichannel array has been developed around this concept, known as the Galileo Somatosensory^{TM} system developed by Epic Medical Concepts & Innovations© (Mission KS, USA). The Galileo Somatosensory^{TM} is an 8-channel pneumatic tactile stimulation system that has found wide application in the neurosciences for the study of animal and human somatosensory physiology. Fig.2.2 shows the Galileo Somatosensory^{TM} pneumatic evoked response tactile stimulation system. The pneumatic stimulator probes are made from thermoplastic homopolymer, use tiny volumes of air to stimulate the surface of the skin, and are ideally suited for use not only in fMRI but also MEG, fNIRS, TCD (transcranial Doppler), and EEG recording environments. The length of the 3/32" ID pneumatic lines is 18' which is used to connect between the Galileo Somatosensory^{TM} pneumatic controller and integrated

Figure 2.2: Galileo Somatosensory ^{TM} pneumatic stimulus system

dual-cylinder pump motor located outside the shielded MRI scanner suite room and the test participant who lies comfortably in the bore of the MRI scanner whose glabrous hand is configured with a spatial array of TAC-Cells.

Fig.2.3 shows a front panel of the Galileo Somatosensory^{TM}. The BNC inputs allow the researcher to integrate with other hardware or software such as the fMRI sync pulse sources or external function generator. The USB port can be used in combination with the included software to deliver a programmed event-related or block design stimulus sequence. The pressure modulated pneumatic stimulus can be measured/adjusted with a pressure sense port connected to an external referent pressure sensor for precise calibration. The positive and negative pressure adjust knobs can be used to increase the amplitude of the pressure waveform and increase/decrease the minimum negative pressure (vacuum) setting, respectively. Each channel of the

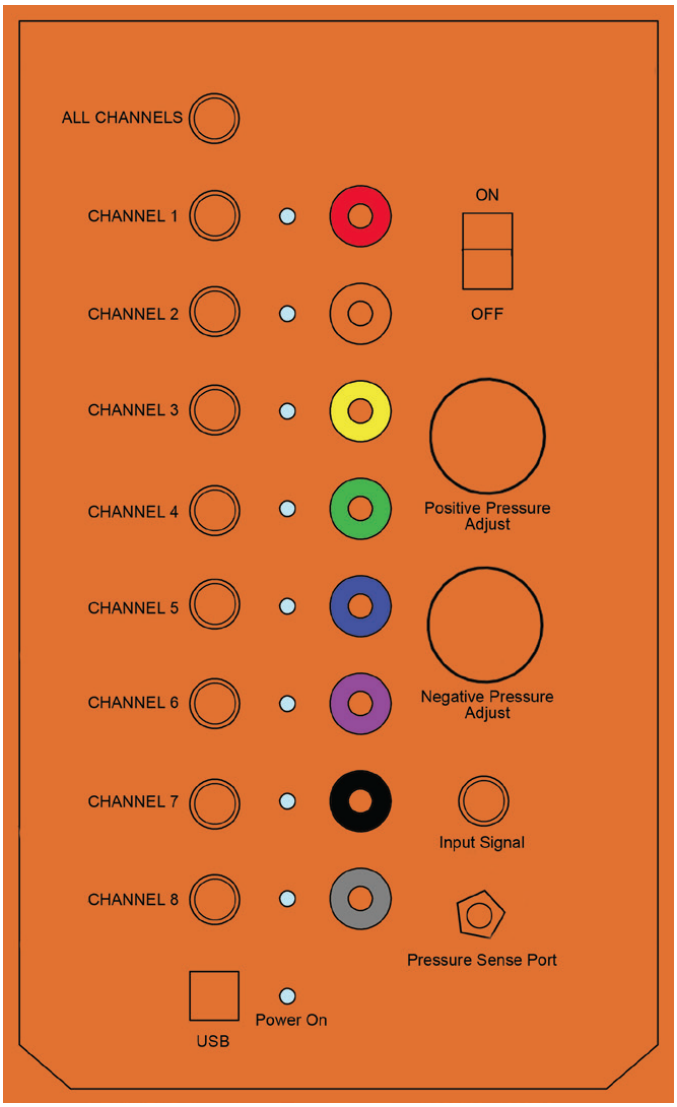

Figure 2.3: Galileo front panel

array has a corresponding TTL output port which can be used to drive external devices or monitored on a digital oscilloscope for pulse train timing and integrity. LED indicators show individual pneumatic channel activation in real time.

Fig. 2.4 displays the current version of the Galileo Somatosensory^{TM} software GUI. The Galileo Somatosensory^{TM} tactile array can be programmed using the included software to control pulse duration and timing, stimulus block design, data output file format, and number of active channels. The control of any given pneumatic stimulus

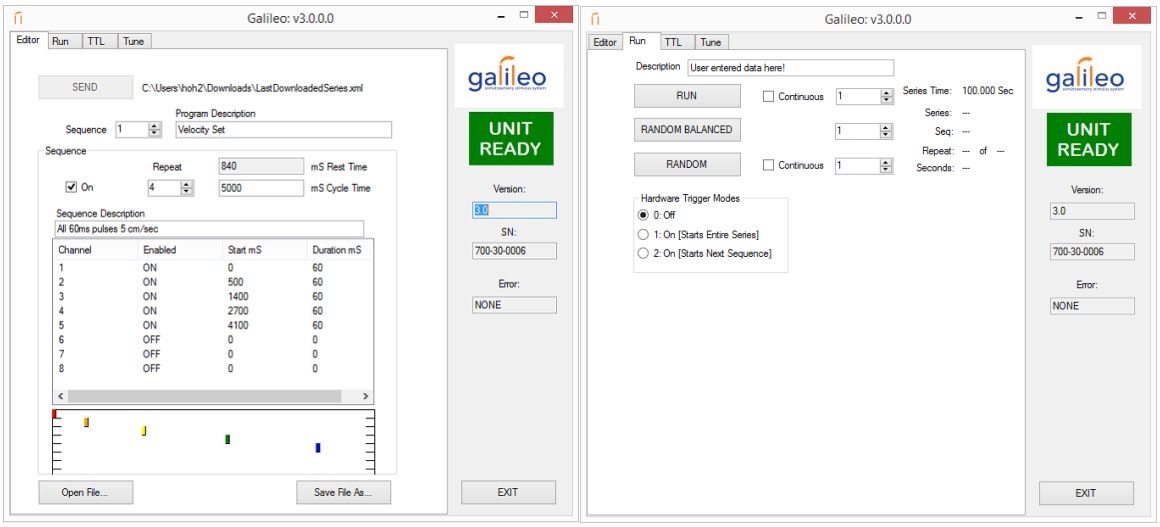

(a) Galileo^{TM} software editor (b) Galileo^{TM} software run

Figure 2.4: Galileo^{TM} software

sequence can be customized by writing an ***.xml** script file (see appendix A). Cycle, rest, start and duration time are adjustable at millisecond resolution in the script file. The included software provides counterbalanced and random modes for stimulus presentation with a desired number of cycle and optional hardware trigger modes.

2.3 MRI suite setting

The MRI suite at the Center for Brain-Biology-Behavior at UNL's East Stadium consists of a control room, shielded 3T Siemens Skyra scanner, equipment room, and MRI mock simulation suite. The MRI scanning room is isolated for both acoustic and vibration reasons and has radio-frequency and MU-metal for electromagnetic shielding. A chiller and helium compressor is located in the equipment room along with humidity and temperature controllers.

Fig.2.5 shows the MRI suite layout, including the MRI console computer, a trigger box (Net Amp 400) connected to the Siemens MRI, and a visual presentation control computer running E-prime 2.0 software (Psychology Software Tools, Inc.,

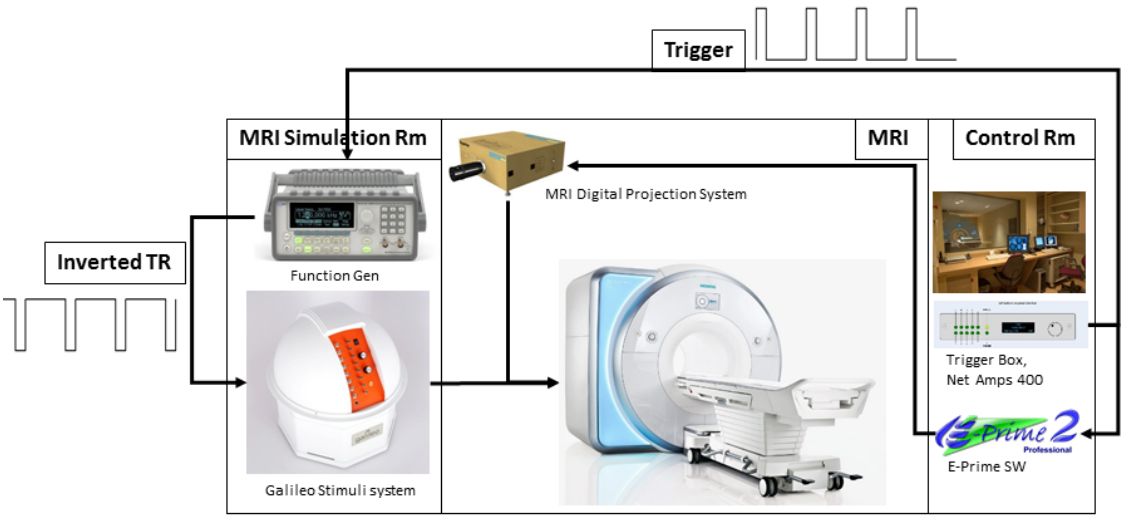

Figure 2.5: MRI suite layout

Sharpsburg, PA, USA). The MRI simulation room is located behind the scanning room opposite the rear of the magnet bore. The Galileo Somatosensory^{TM} stimulus control system, Berkeley Nucleonics programmable function generator, personal computer (WIN8.1), and an APC UPS 1500W battery backup system are located in the simulator suite near the waveguide proximal to the headward bore of the MRI scanner prior to an experimental session (Fig.2.5). Eight 18' pneumatic lines (3/32" ID) are run through the copper waveguide and permit connection between Galileo Somatosensory^{TM} pneumatic stimulus outputs and the TAC-Cells configured on the glabrous hand of the research participant. The 3.0T Skyra Siemens MRI, MRI digital projection system, and pneumatic terminal fittings and TAC-Cells are located in the scanner room.

The MRI scanner generates a series of TTL pulses (50ms pulse width, 0-5 V) corresponding to the volume repetition time (TR) during BOLD image acquisition. For the current study, the first TR pulse serves as the only control signal needed to the start the Galileo stimulus generation control system. The TR signal for each

block is used to control ePrime for synchronized visual stimulus presentation which is displayed on an MRI-compatible LCD projection system using a mirror positioned above the RF headcoil in the scanner bore in easy view of the participant.

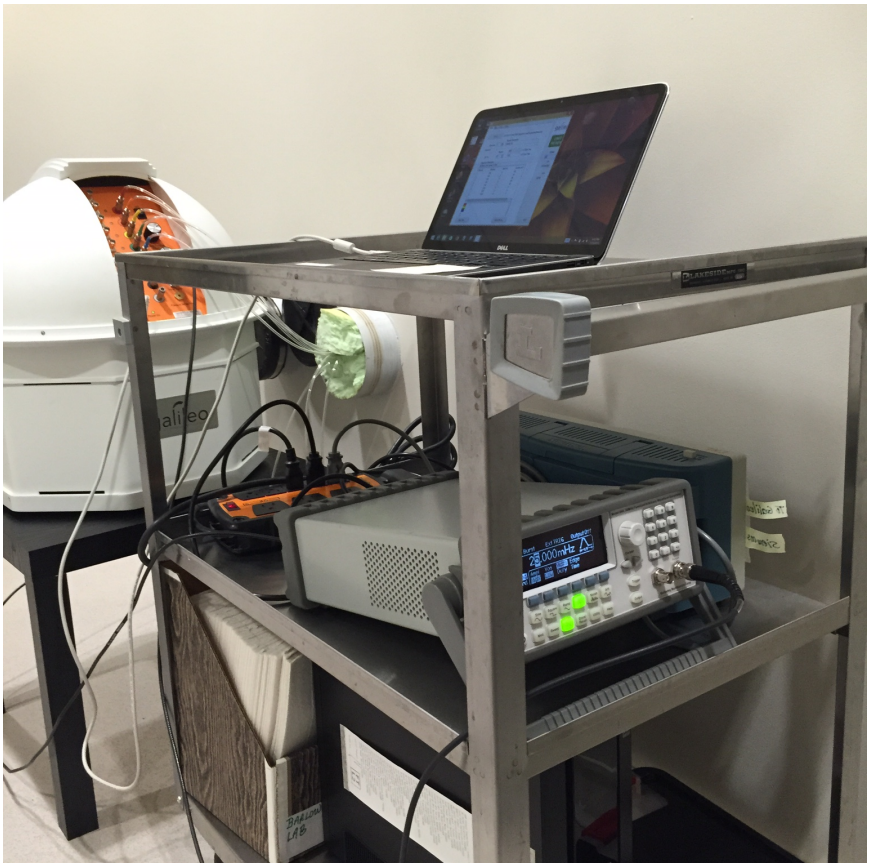

Figure 2.6: Galileo Somatosensory^{TM} stimulation control system located near the waveguide in the MRI simulation room

Note the polyethylene pneumatic lines (5 channels are active for this study) connected to the Galileo which pass through the copper waveguide. The Net Amps 400 amplifier module sends the trigger pulse (TR) from the control room to MRI simulation room through a 75' BNC cable, and connected to the Berkeley Nucleonics function generator. Because the Galileo Somatosensory^{TM} system initiates the tactile stimulation using inverted TTL logic pulses, the function generator is programmed to invert the source TTL pulse from the scanner (from 0-5 V to 5-0V). The frequency

and width setting of the function generator were 25mHz and 50ms, respectively. The inverted mode is applied to the function generator such that the 50ms inverted TTL pulse is generated every 40 seconds for 20 cycles. An output port in the function generator connects to the Galileo input with the BNC cable that makes Galileo trigger tactile stimulus. A Dell XPS13WIN 8.1 laptop connected via USB to the Galileo Somatosensory^{TM} stimulator runs the Galileo GUI control software.

2.4 fMRI data acquisition

The MRI Safety Screening form issued by CB3 will be reviewed with the participant by the investigator and MRI technician. It will need to be signed, initialed and dated before that participants involvement in the study can continue. The participant will be asked to change into scrubs and attach ECG leads to their upper torso. Directions on this will be posted within each changing room. After changing, the participant will be guided through metal detecting pillars and scanned by the MRI technician with a hand wand to double check for metallic items that may have been forgotten. The participant will be instructed to lie quietly on the bed of the MRI scanner and refrain from movement (no talking, no hand movement) during the anatomical brain scan and periods of pneumatic stimulation in order to minimize MRI image distortion. The participant will be given instructions regarding the research procedures that s/he will perform. If the participants glasses are not deemed to be MRI safe, it is the investigator or authorized research personnel members responsibility to help the participant find the correct lens from the MRI safe lens set. Earplugs will be provided to the participant and inserted either by the participant or the MRI technician. The participant will be required to remain in the bore of the scanner for approximately one hour to complete the fMRI protocol. This amount of time is typical for fMRI experiments.

A brain structural MRI scan and 3 functional images (BOLD) will be recorded at 3.0 T (Skyra, Siemens Medical Solutions, Erlangen, Germany) using a 32-channel head coil. Structural T1-weighted 3-dimensional image of the participant's brain (MPRAGE, Magnetization-Prepared Rapid Gradient-Echo) will be acquired at the beginning of the session [repetition time (TR) = 2400 ms, echo time (TE) = 3.37 ms, voxel size = 1 x 1 x 1 mm, flip angle = 7°, number of slices = 192, acquisition matrix = 256 x 256, field of view (FoV) = 256 x 256 mm^2, total acquisition time (TA) = 5:35 minutes].

Following the MPRAGE anatomical scan, three sessions of functional images will be recorded using a T2*-weighted EPI (Echo Planar Imaging) sequence [repetition time (TR) = 2500 ms, echo time (TE) = 30 ms, voxel size = 2.5 x 2.5 x 2.5 mm, flip angle = 83°, number of slices = 320, acquisition matrix = 88 x 88, field of view (FoV) = 220 x 220 mm^2, Phase partial Fourier factor = 7/8, total acquisition time (TA) = 13:53]. The Ernst angle was calculated for selecting the optimal flip angle (Ernst & Anderson, 1966).

$$a = \arccos(\exp(-\mathrm{TR}/\mathrm{T1})) \tag{2.1}$$

where T1 is the relaxation time of tissues in MRI, and TR is the repetition time between excitation pulse sequences. The average T1 relaxation time at 3.0 T is about 1100 ms (Wansapura et al., 1999). The Ernst angle was computed to be 83° when TR is 2500 ms. A 1 minute break is given between BOLD sessions.

Participant vigilance. Visual countdown presentation to maintain the participant's vigilance will be performed using E-prime 2.0 software (Psychology Software Tools, Inc., Sharpsburg, PA, USA). This visual presentation will be projected onto a screen behind (headward) the scanner bore. The participant will view the presentation

on a mirror which is attached to the 32-channel head coil. The visual countdown presentation will include a declining sequence of numbers (20:1) which corresponds to the number of remaining stimulus blocks in the BOLD session. As an added incentive, a special character ($$ dollar sign) is randomly inserted instead of a number. At the conclusion of each BOLD run, participants will be asked how many dollar signs they saw. The number and special letters on the presentation will be shown only for 0.5 second to minimize a primary visual cortex response.

2.5 Tactile stimulus paradigm

Seven small plastic pneumatic TAC-Cells (6mm ID) will be placed on the palm of the right hand along the length of index and middle finger using tincture of Benzoin (10% concentration to increase adhesion) followed by the application of double adhesive tape collars. A Galileo^{TM} Somatosensory tactile array is programmed to deliver punctate (60 ms duration, 9 ms rise/fall) pneumotactile sequence through TAC-Cells placed on the glabrous skin of the right hand, including p1, p2 segments of D3 (middle finger), p1, p2, p4 segments of D2 (index finger), and p4, p1 of D1 (thumb). Morphometric dimensions between p1 and p2 in D2 (Length 1), p2 and p4 in D2 (Length 2), p4 in D2 and p4 in D1 (Length 3), and p4 and p1 in D1 (Length 4) will be measured for each participant to adjust for variations in hand size to create accurate tactile traverse velocities. Programmed time delays between individual TAC-Cells results in a saltatory velocity sequence traversing the tips of D1, D2 through the basal phalyngeal segments to the distal phalaynx of the thumb. Figs.2.7a and 2.7b represent stimulated digit areas and TAC-Cell placement on the participant's hand, respectively. Different colors in the fig.2.7a shows channels 1 to 5 of the Galileo^{TM}. The silicon tubing in fig.2.7b was bifurcated at its terminal for channels 1 and 2 to deliver a pneumotactile stimulus on the p1 and p2 segments of the index and middle

finger. Fig. 2.8 shows the pressure wave of 5 cm/s, 25 cm/s, 65 cm/s, and All-ON conditions, and the No-stimulus (All-OFF) condition is not shown which is baseline of this study. Rice-filled hand-warmers placed within mitten gloves were fit to all participant's right hand to maintain normothermia of limb extremities during testing in the MRI scanner suite (Verrillo & Bolanowski, 1986).

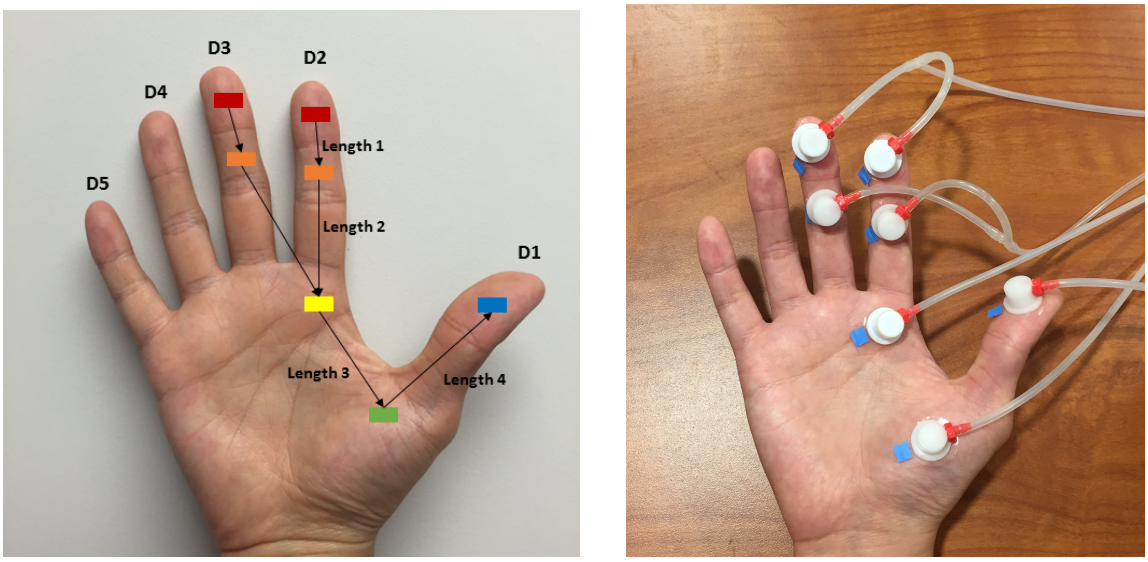

(a) Stimulated areas (b) TAC Cells location

Figure 2.7: Galileo Somatosensory^{TM} tactile stimulation. p1 in D2 and D3= red, p2 in D2 and D3= orange, p4 in D2 and D3= yellow, p4 in D1 = green, p1 in D1 = blue

It is through this array of pneumatically charged TAC-Cells that the participant experienced repeated trains of saltatory pulsed pneumotactile stimulation ranging from very slow (5 cm/second) to very fast (65 cm/second) traverse speeds on the glabrous surface of the hand. Participants typically perceive these pulsed stimulus as moving taps on the surface of their skin.

A randomized-balanced block design (40 sec duration/block) included the following 5 conditions: Saltatory velocities @ 5, 25, and 65 cm/sec, simultaneous TAC-Cells ON, and all cells OFF. Fig.2.9 shows the random-balanced block design for this study. There are three sessions during the fMRI BOLD response acquisition and each session

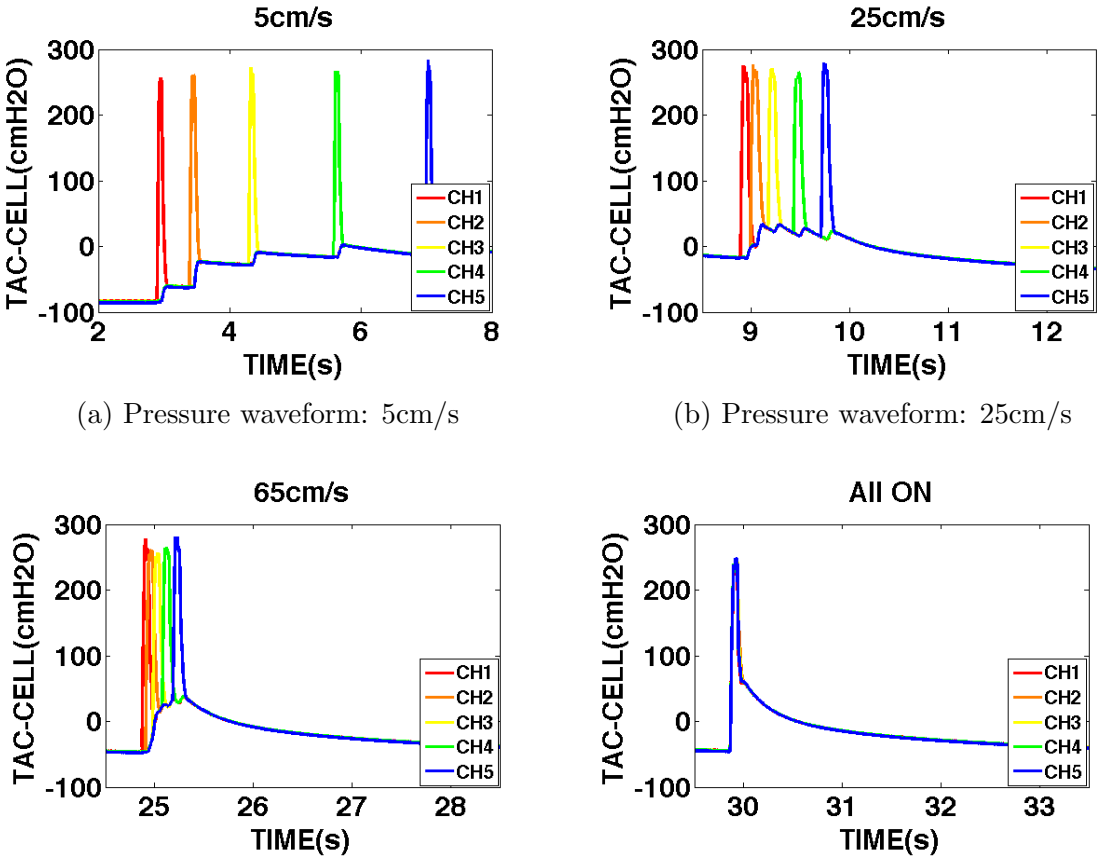

(a) Pressure waveform: 5cm/s

(b) Pressure waveform: 25cm/s

(c) Pressure waveform: 65cm/s

(d) Pressure waveform: All ON

Figure 2.8: Stimulus velocity pressure waveform

includes 4 cycles of the 5 stimulus conditions. Thus, a total of 20 conditions in each session are counter-balanced and randomized. The duration of the stimulus event for each condition is 20 seconds (8 volumes, TR = 2500 ms), followed by 20 seconds of rest. The tactile stimulus is continuously delivered from p1 of D2 and D3 to p1 of D1, passing through both p2 of D2 and D3, p4 of D2 and p4 of D1. Total measurement time of one session is 13:20 min (320 volumes). Therefore, 3 BOLD acquisitions of total 960 volumes of fMRI data per participant will be collected.

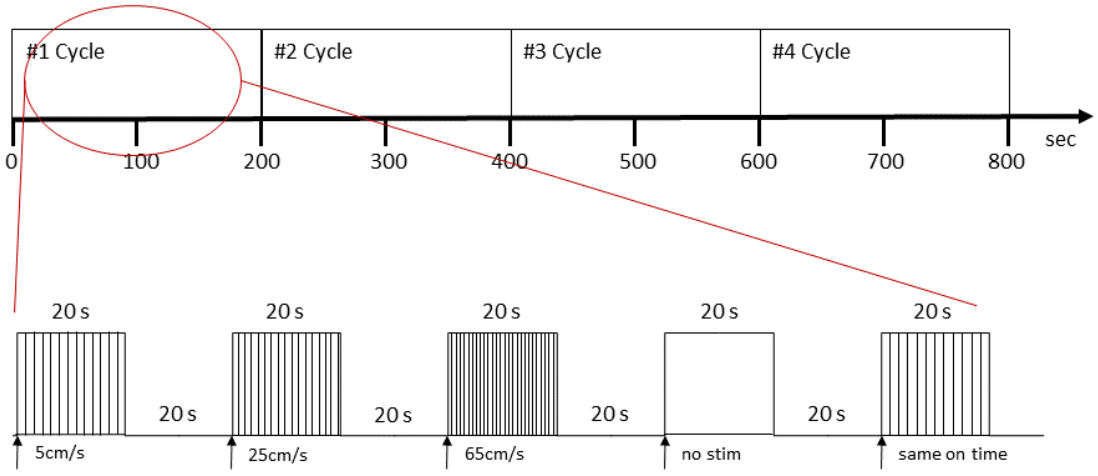

Figure 2.9: Random-balanced block design

2.6 fMRI data pre-processing

Pre-processing and statistical analysis of MPRAGE and functional images were performed using SPM. The 3 sessions of functional MRI volumes were realigned to the first volume in the each session. The 960 motion corrected functional images and one mean functional image were created after realignment. The estimated time series of three translational axes (x, y, and z translation) and three rotations (pitch, roll and yaw) were also saved as a text file after correction for movement. This text file was used as a motion correction after pre-processing. The mean functional and structural images were used as the reference and source image for the co-registration process, respectively. The segmentation in SPM is based on a Gaussian mixture model, which represents the intensity distribution of the image (Ashburner & Friston, 2000). Six different tissue probability maps (TPMs) are used as prior information; grey matter, white matter, CSF, bone, soft tissue and air/background. Deformation field created in the segmentation section was used to normalize the functional images. The normalization in SPM adjust overall size and orientation of the functional and anatomical images to the MNI template. All the realigned and normalized functional images are finally smoothed by convolution with an isotropic Gaussian kernel (full-width-at-half-maximum (FWHM) = 8 mm). The purpose of the smoothing is to improve of the signal to noise ratio (SNR) which increases sensitivity.

2.7 fMRI data analysis

The GLM model was applied for both single-subject and group data analysis of BOLD responses from different velocities of tactile stimulus. 1^{st}-level SPM contrast models are a data-driven statistical analysis method for each subject (Mumford & Nichols, 2009). Results from 1^{st}-level models are saved as spm.mat file format and

three result files are created for each participant. Three BOLD result files for each subject are then combined using "Mixed Effects" (MFX) analysis before entering into 2^{nd}-level group effects analysis adopting one-sample t-test (Friston et al., 2005; Pujol et al., 2009).

2.7.1 1^{st}-level model specification

1^{st}-level model specification is an appropriate method for single data analysis. A design matrix, as shown in fig.2.10, for the statistical analysis is generated with onsets and durations of stimulus block derived from Galileo Somatosensory^{TM} stimulus output log file. Design matrix is a dark-light color map and a part of GLM which is essential for data analysis.

In the design matrix, columns and rows indicate different conditions of stimulus (regressors) and the filenames from scans, respectively. The first 5 regressors from the left represent hypothesized contributors that are 5cm/s, 25cm/s, 65cm/s, no stimulus block, and all on stimulus. Next 6 regressors show the estimated time series of 3 translational axes and 3 rotations. Black which is close to 0 shows when the regressors are at its smallest value. White is near 1 and illustrates when the regressors are at its largest value. Grey implies intermediate value. A contrast which specifies effects of interests displays the design matrix and lists designated contrasts. A contrast vector is a length of interested regressors which are 5 different stimulus conditions so it has a 1 by 5 matrix in this study. For example, fig.2.11a is a representation of the 5cm/s contrast that has a vector C^T = [1 0 0 0 0]. Additionally, one sided main effects for 5cm/s condition can be determined by subtracting the no stimulus block contrast (e.g. C^T = [1 0 0 -1 0]. see fig.2.11b). SPM writes an spm.mat file with design matrix and the map of t-values of whole-brain.

Resulting t-maps from each BOLD session are then carried forward to the MFX

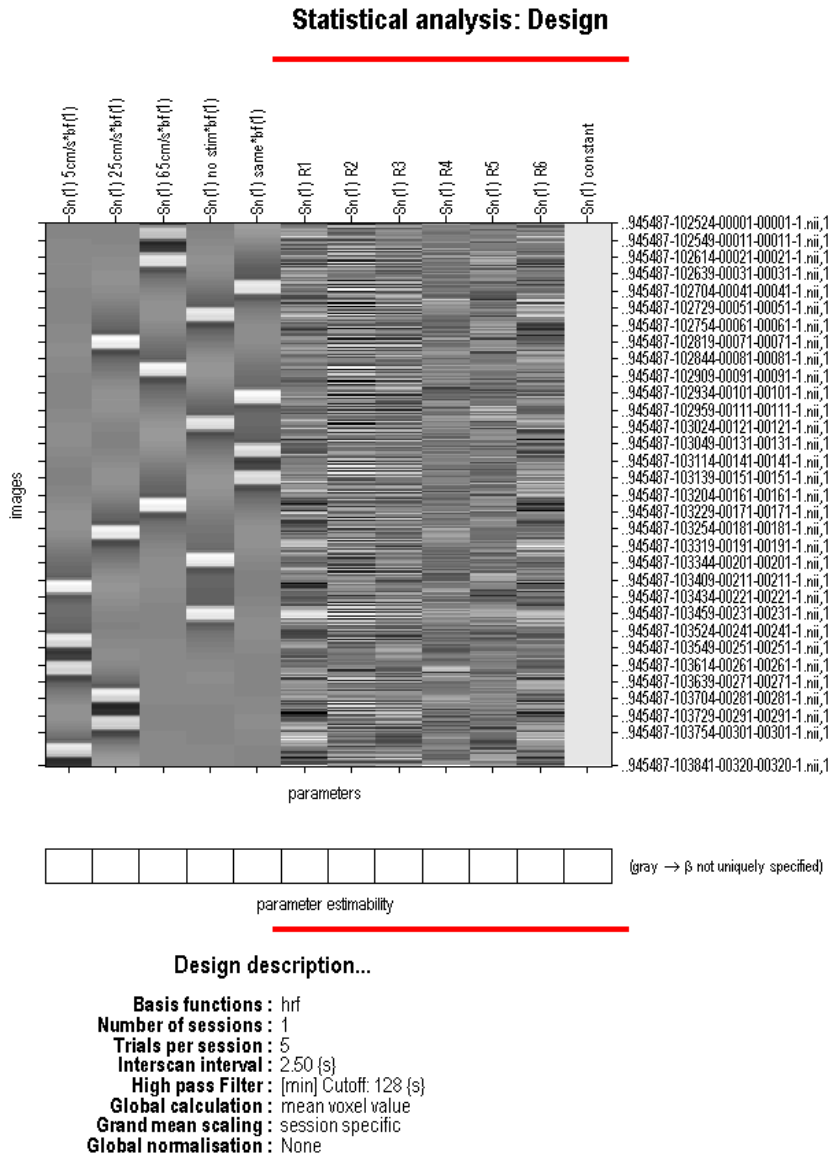

Figure 2.10: Design matrix

analysis to combine the 3 BOLD results within a subject (Friston et al., 2005). Fixed-effects (FFX) and random-effects (RFX) analysis are part of the MFX analysis and a preprocess of 2^{nd}-level model specification. While FFX analysis assumes that variables are fixed, RFX analysis assumes that variables are randomly drawn from a large population. Hence, results from RFX analysis lead to interferences on the general

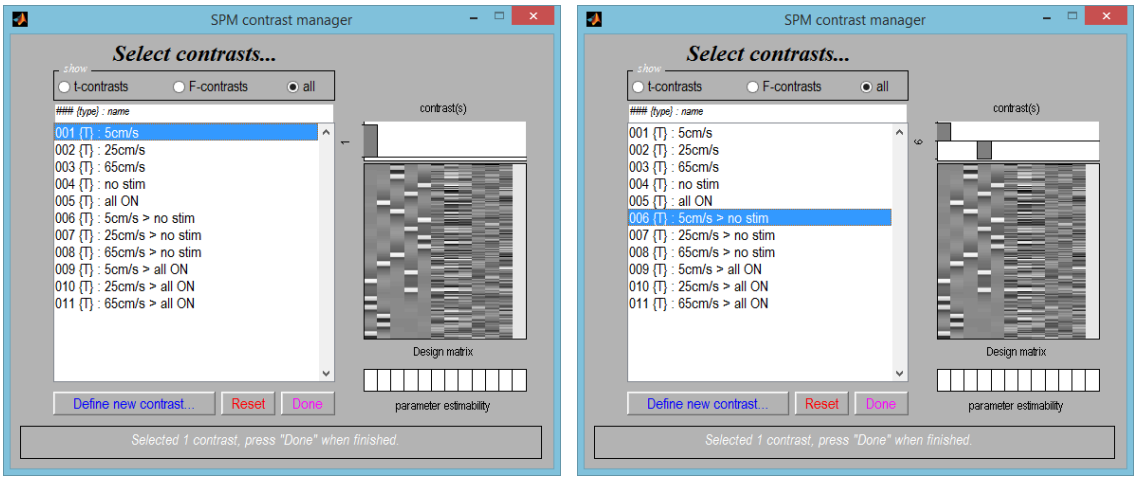

(a) 5cm/s contrast (b) One sided main effect of 5cm/s contrast

Figure 2.11: SPM contrast manager

populations from which the subjects were drawn. Generally, FFX and RFX analysis are used to compare the group effect to the within-subject and between-subject, respectively. FFX is required to create contrast across all 3 BOLD sessions from each subject performing one sample t-test. Fig.2.12 shows a FFX design matrix from 3 BOLD sessions of one participant including the motion correction. One sided main effects for 5cm/s condition can be represented by the following vector [1 0 0 -1 0 0 0 0 0 0 0 1 0 0 -1 0 0 0 0 0 0 0 1 0 0 -1 0 0 0 0 0 0 0 0].

An F-contrast is required to determine the main effect of velocity conditions. The result from the F-contrasts shows how the different stimulus velocities change brain response and where the stimulus affects the brain area. Fig.2.13 is a contrast representation of the FFX analysis in a single subject. The results from FFX analysis generate 12 contrast result files including the main effect of velocity (F-contrast). These results are combined in one-sample t-test to compute between subject contrasts at the 2^{nd}-level analysis.

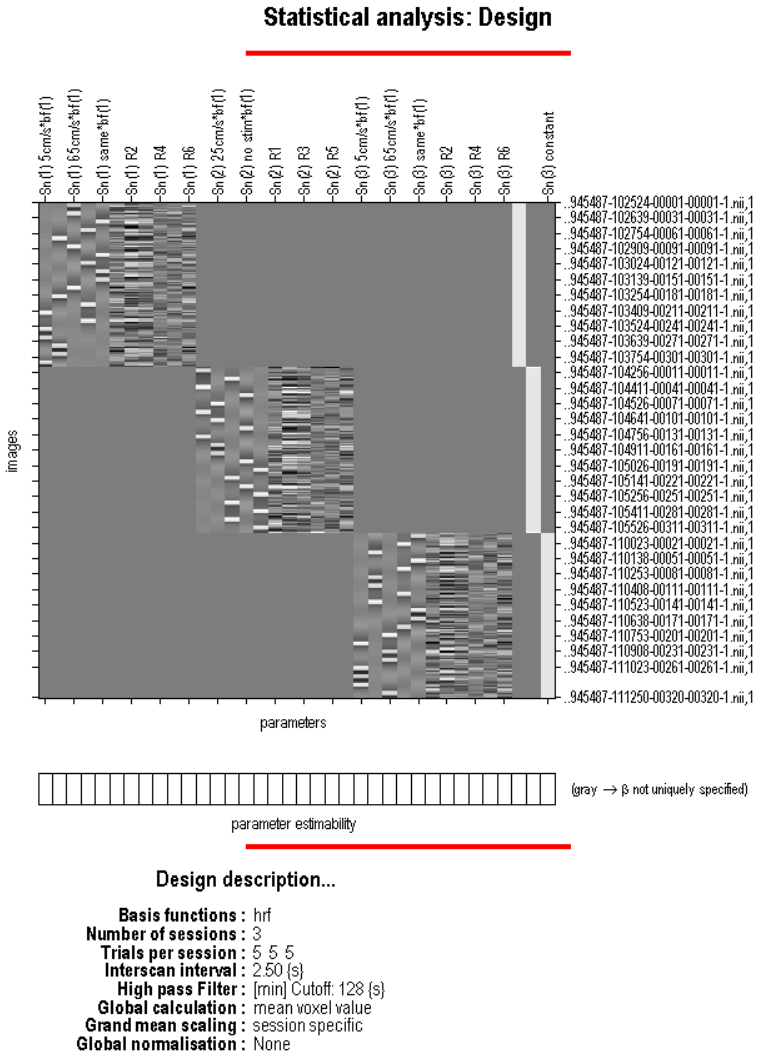

Figure 2.12: Fixed-effects design matrix

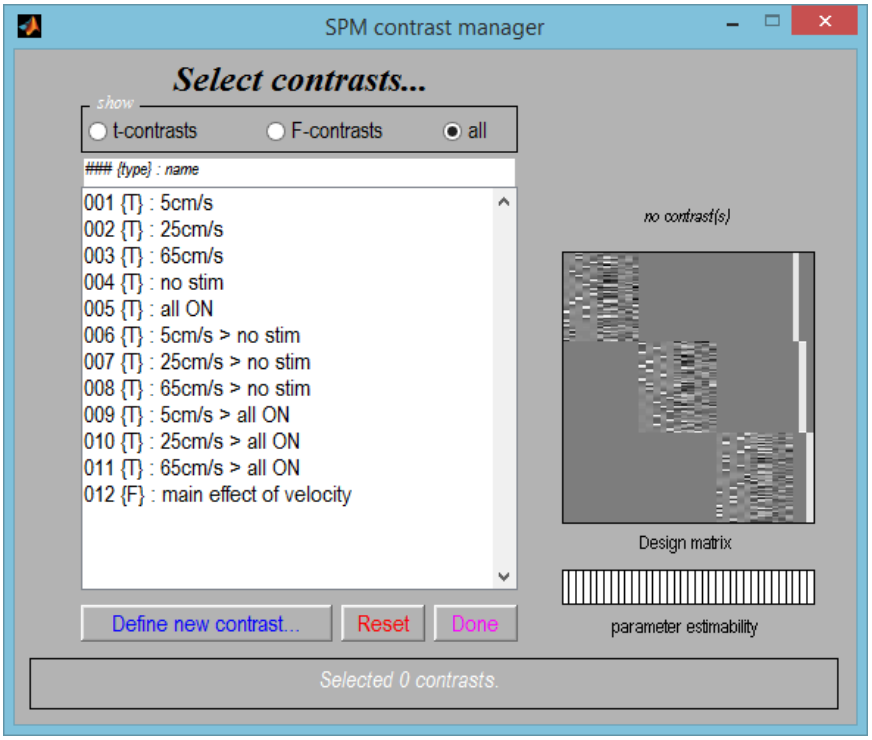

Figure 2.13: Contrast manager of FFX analysis

2.7.2 Group analysis

Second-level analysis or group analysis is used to see how often the stimulus effects observed in each subject are manifested across a group. Fig.2.14 shows the schematic of 2nd-level analysis. The contrast results from each subject enter into the 2nd-level analysis to access the group analysis. Y-axis in the 2nd-level analysis design matrix indicates the number of the subject.

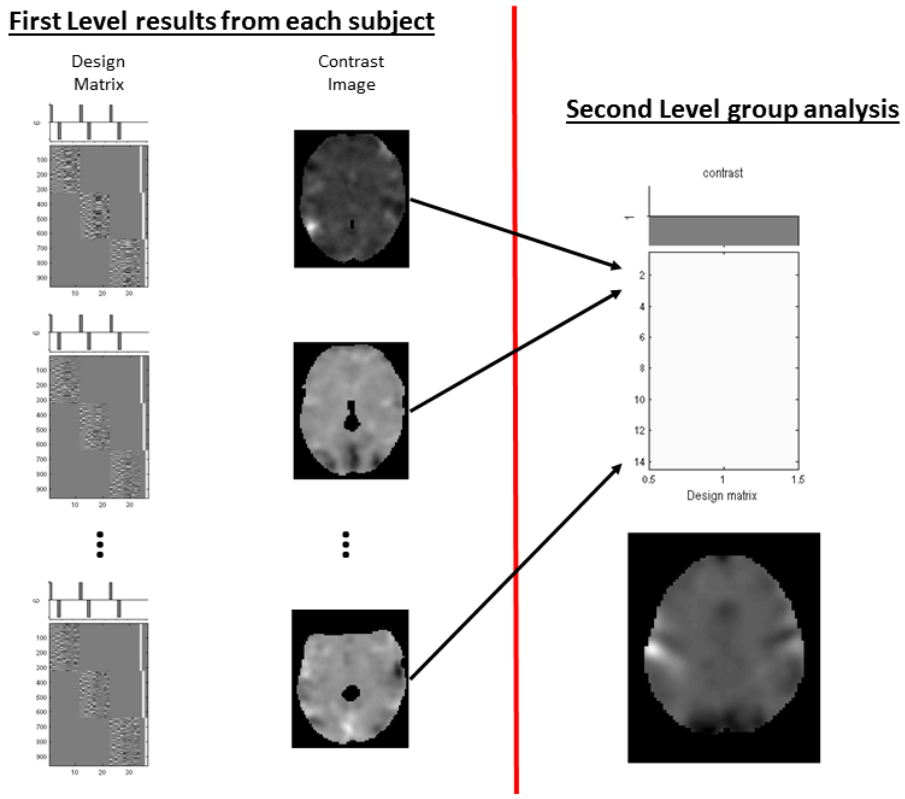

Figure 2.14: 2nd-level analysis

SPM provides multiple design types for 2nd-level analysis such as one sample t-test, one way ANOVA, and multiple regression. The group analysis of one sided main effects for 5cm/s, 25cm/s and 65cm/s accepts the one sample t-test which can compute within-subject contrast results from 1^{st}-level analysis. One way ANOVA analysis can be implemented to achieve the group main effect of various velocity

stimulus. The t-contrast results from each subject are used in the one way ANOVA analysis. Fig.2.15 represents the one way ANOVA analysis for the group main effect. Fig.2.15a and 2.15b display the design matrix and contrast vector, respectively. The contrast vector of the group main effect is followed by [1 -1 0; 0 1 -1].

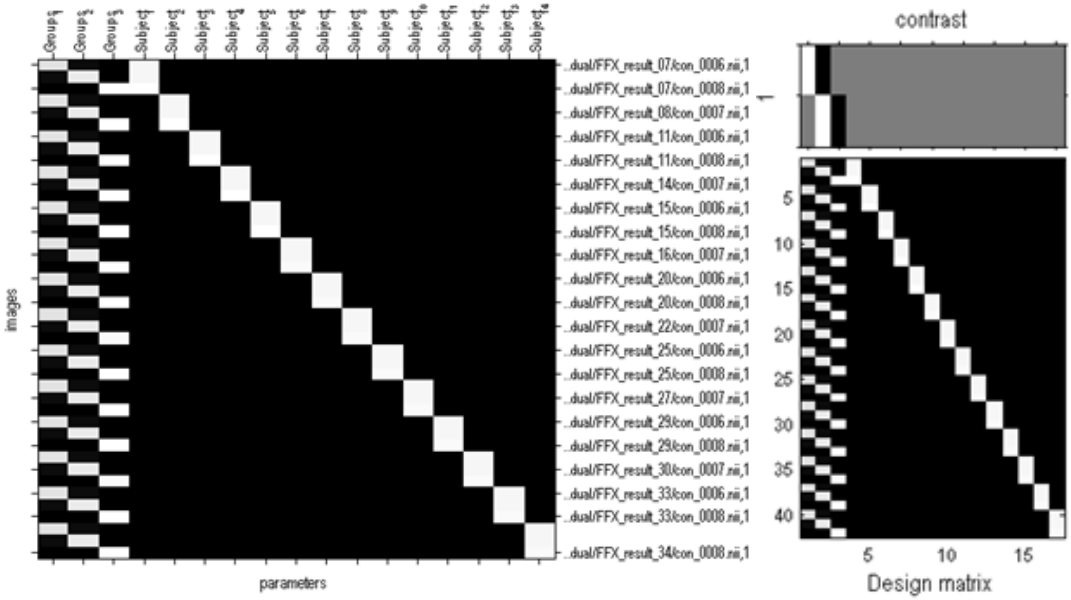

(a) One way ANOVA design matrix (b) Contrast

Figure 2.15: One way ANOVA analysis for group main effect

Chapter 3

Results

The seven TAC-Cells, configured to D1, D2, and D3 of the glabrous right hand and driven by 5 independently programmed pneumatic channels to create 3 saltatory velocities were highly effective in evoking the BOLD responses in the human somatosensory network. Three BOLD sessions from nineteen subjects and two BOLD sessions from one subject were used in fMRI data analysis due to movement artifact and/or poor BOLD responses. Each subject provided informed written consent in accordance with the university institutional review board approval.

3.1 fMRI Results: Single subject (first-level analysis)

The first-level result from each single subject was acquired by combining 3 BOLD sessions with the exception of one subject who had 2 BOLD sessions. Fig.3.1 shows the BOLD response from single subject in coronal view. The significant level was set to $P_{unc} < .0001$ for the five stimulus conditions (5cm/s, 25cm/s, 65cm/s, All-OFF (No stimulus), and All-ON).

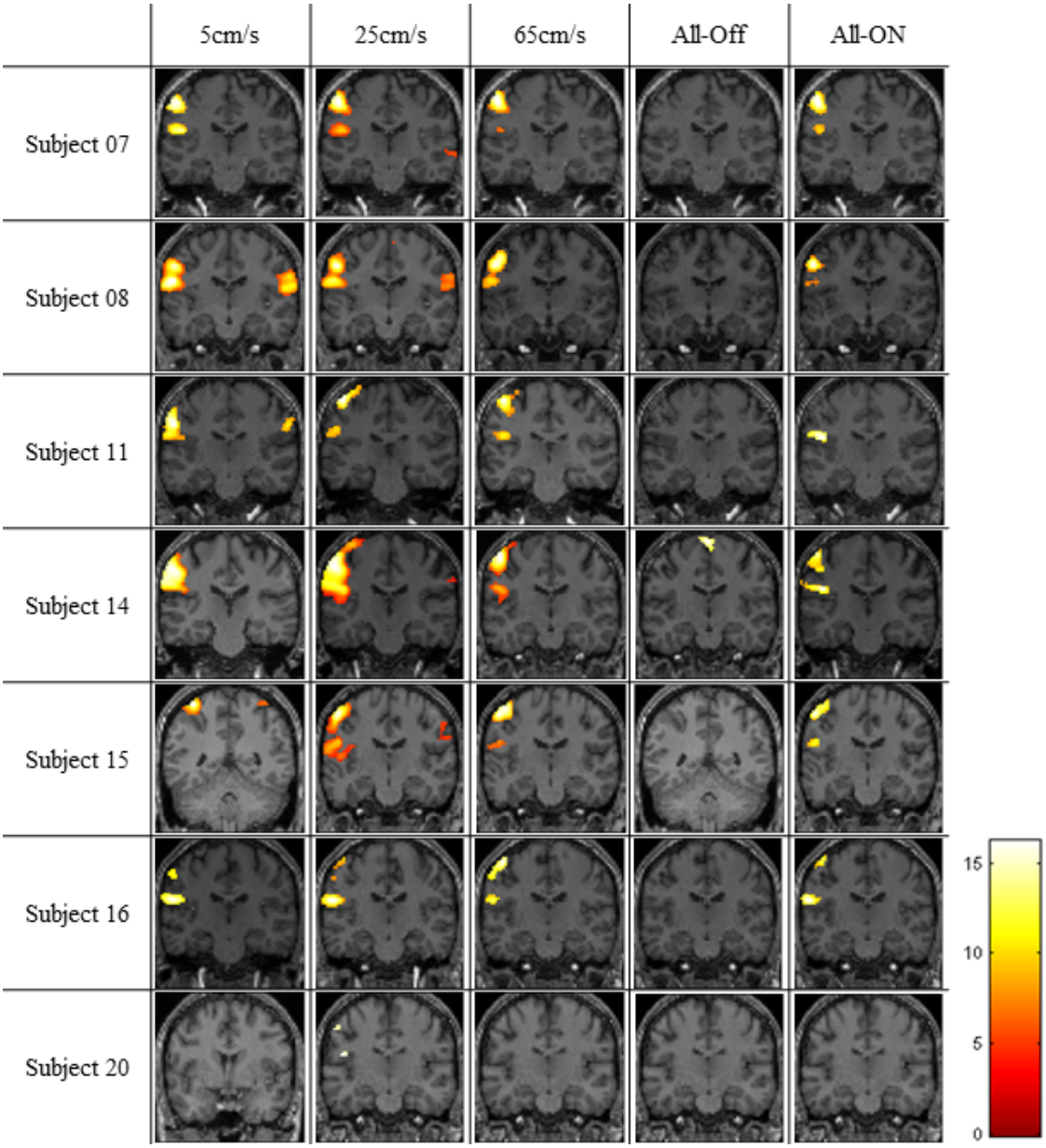
5cm/s
25cm/s
65cm/s
All-Off
All-ON
Subject 07
Subject 08
Subject 11
Subject 14
Subject 15
Subject 16
Subject 20
15
10
5
0

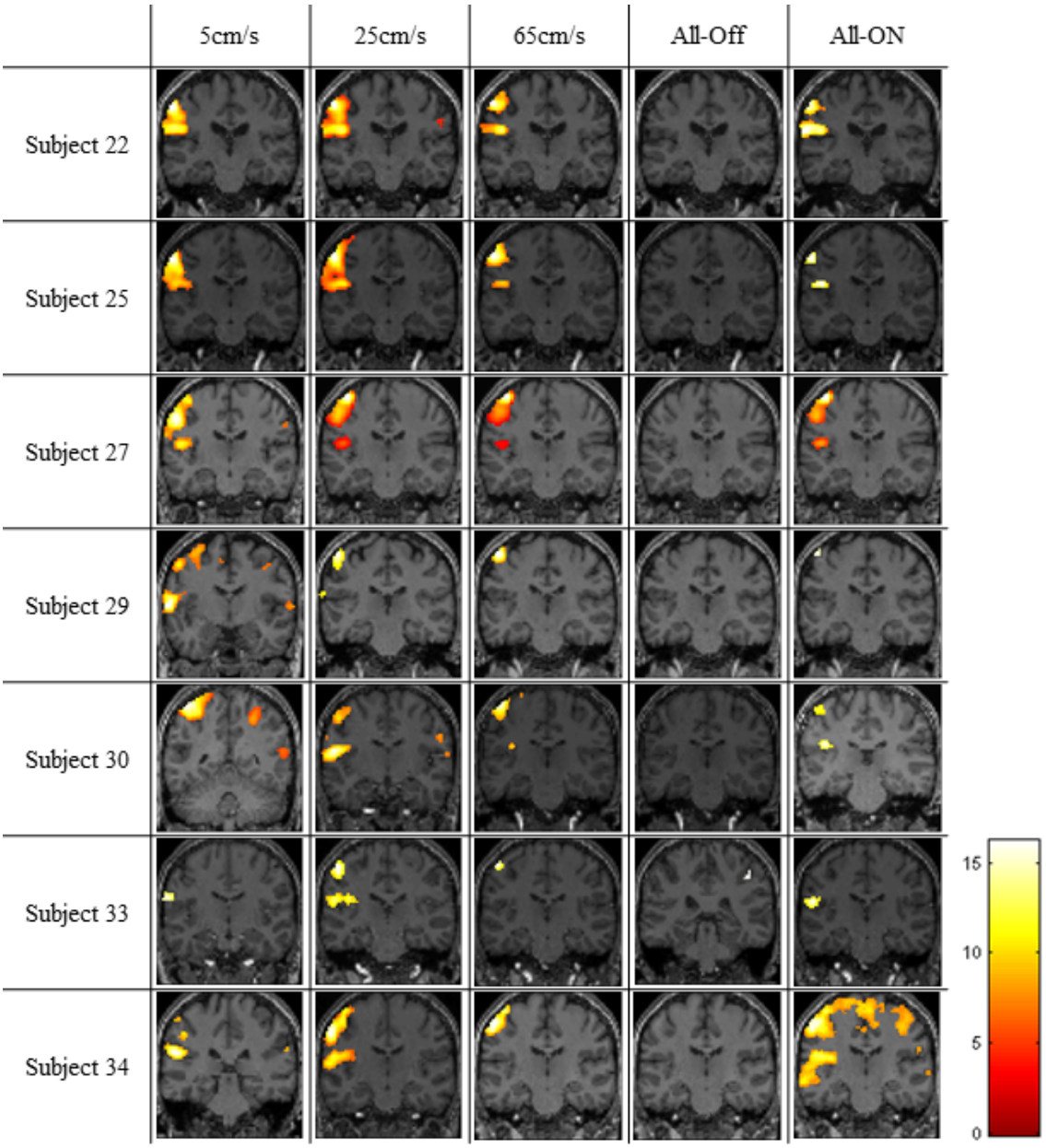
5cm/s
25cm/s
65cm/s
All-Off
All-ON
Subject 22
Subject 25
Subject 27
Subject 29
Subject 30
Subject 33
Subject 34
15
10
5
0

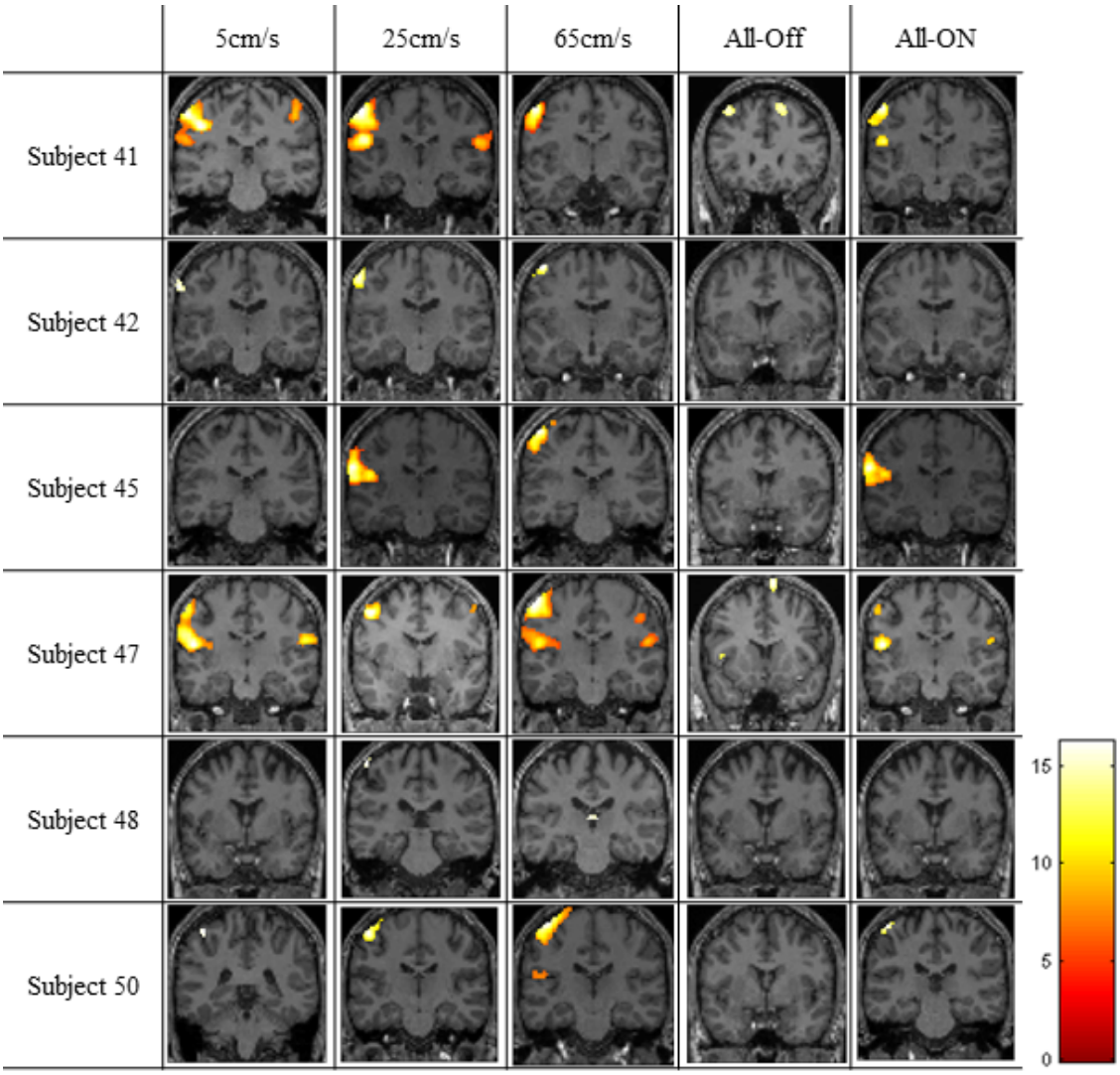

Figure 3.1: Single subject BOLD response by different stimulus conditions

A dominant contralateral response among the velocity conditions was consistently found in the majority of single subject BOLD activations (19 out of 20 subjects). Significant BOLD responses were localized to the sensorimotor cortex which includes the postcentral gyrus (S1, S2), primary motor cortex, premotor cortex (M1), posterior insula and deep cerebellum. For the 25cm/s stimulus condition, BOLD responses were found in the insula in 13 out of 20 subjects. The spatial extent of the evoked BOLD response was dependent on saltatory tactile velocity with the largest response apparent at 25cm/s. A contralateral insular BOLD response was found in ten, twelve, and six of the subjects at 5cm/s, 25cm/s, and 65cm/s, respectively. Table 3.2 shows the peak t-value and MNI coordinates of single subjects for the different stimulus conditions. All regions were selected by inserting peak MNI coordinates in xjView and Anatomy Toolbox v2.2b (`http://www.alivelearn.net/xjview`) (Eickhoff et al., 2005, 2006, 2007).

	MNI Coordinates				
5cm/s	x	y	z	t-value	Region
Subject 07	-55	-22	50	7.46	L BA1
Subject 08	-60	-17	25	12.23	L Postcentral Gyrus
Subject 11	-57	-20	35	8.35	L Postcentral Gyrus
Subject 14	-57	-25	43	11.08	L Supramarginal Gyrus
Subject 15	-37	-50	65	10.91	L Superior Parietal Lobule
Subject 16	-60	-22	23	6.34	L Postcentral Gyrus
Subject 20					
Subject 22	-60	-22	45	10.78	L Inferior Parietal Lobule
Subject 25	-60	-20	45	11.75	L Inferior Parietal Lobule
Subject 27	-57	-17	40	9.96	L BA1
Subject 29	-65	-7	5	9.83	L Superior Temporal Gyrus
Subject 30	-45	-50	63	12	L Middle Temporal Gyrus
Subject 33	-67	-15	23	5.51	L Postcentral Gyrus
Subject 34	-55	-32	20	7.74	L Insula
Subject 41	-47	-27	38	10.06	L BA2
Subject 42	-62	-20	48	6.45	L BA3
Subject 45	-65	-20	28	9.70	L BA1
Subject 47	-52	-17	15	9.17	L BA43
Subject 48					
Subject 50	-42	-40	58	3.99	L BA2

	MNI Coordinates				
25cm/s	x	y	z	t-value	Region
Subject 07	-52	-22	50	13.04	L BA1
Subject 08	-55	-17	40	11.68	L BA1
Subject 11	-50	-27	63	7.97	L BA1
Subject 14	-57	-22	50	16.2	L BA1
Subject 15	-55	-17	53	13.77	L BA3
Subject 16	-60	-20	20	8.38	L Postcentral Gyrus
Subject 20	-50	-17	20	4.41	L Postcentral Gyrus
Subject 22	-57	-20	50	14.91	L BA1
Subject 25	-57	-20	48	13.84	L BA1
Subject 27	-42	-20	65	21.74	L BA6
Subject 29	-55	-25	60	6.22	L BA6
Subject 30	-57	-12	15	9.14	L Postcentral Gyrus
Subject 33	-52	-25	53	6.82	L BA2
Subject 34	-60	-17	40	10.2	L BA6
Subject 41	-57	-22	50	11.64	L BA1
Subject 42	-60	-20	50	5.85	L BA3
Subject 45	-65	-20	25	12.21	L Postcentral Gyrus
Subject 47	-50	-5	48	8.10	L Precentral Gyrus
Subject 48	-52	-30	63	4.40	L BA2
Subject 50	-50	-20	58	6.43	L BA1

	MNI Coordinates				
65cm/s	x	y	z	t-value	Region
Subject 07	-55	-22	53	10.23	L BA1
Subject 08	-55	-15	43	9.28	L BA1
Subject 11	-47	-25	60	8.76	L BA1
Subject 14	-52	-17	58	13.37	L Postcentral Gyrus
Subject 15	-55	-17	53	9.32	L BA1
Subject 16	-47	-17	60	6.45	L Postcentral Gyrus
Subject 20					
Subject 22	-57	-20	50	10.81	L BA1
Subject 25	-57	-20	50	10.39	L BA1
Subject 27	-42	-20	65	25.36	L BA6
Subject 29	-52	-22	60	8.93	L BA3
Subject 30	-50	-22	63	8.56	L Postcentral Gyrus
Subject 33	-52	-22	58	5.9	L BA1
Subject 34	-57	-20	55	5.35	L BA3
Subject 41	-55	-12	53	13.78	L Postcentral Gyrus
Subject 42	-47	-15	60	5.53	L Precentral Gyrus
Subject 45	-50	-27	60	9.33	L BA1
Subject 47	-55	-20	55	11.13	L BA1
Subject 48	6	-25	8	4.22	R Thalamus
Subject 50	-45	-22	68	9.53	L Precentral Gyrus

	MNI Coordinates				
All-ON	x	y	z	t-value	Region
Subject 07	-52	-22	53	10.23	L BA1
Subject 08	-57	-15	43	9.15	L Precentral Gyrus
Subject 11	-50	-20	23	5.69	L Postcentral Gyrus
Subject 14	-47	-22	23	7.33	L Postcentral Gyrus
Subject 15	-55	-17	53	7.42	L BA3
Subject 16	-62	-17	20	6.7	L Postcentral Gyrus
Subject 20					
Subject 22	-62	-25	23	8.96	L Supramarginal Gyrus
Subject 25	-60	-20	48	6.3	L Postcentral Gyrus
Subject 27	-42	-20	65	13.84	L BA6
Subject 29	-52	-22	60	4.31	L BA3
Subject 30	-45	-27	23	5.96	L Inferior Parietal Lobule
Subject 33	-57	-22	18	5.75	L Supramarginal Gyrus
Subject 34	-57	-17	48	8.37	L Postcentral Gyrus
Subject 41	-55	-17	55	7.16	L BA3
Subject 42					
Subject 45	-65	-20	28	10.37	L BA1
Subject 47	-52	-17	15	7.71	L BA43
Subject 48					
Subject 50	-47	-27	65	5.24	L Postcentral Gyrus

Table 3.1: Single subject peak MNI coordinates ($P_{unc} < .0001$)

3.2 fMRI Results: Group (second-level analysis)

3.2.1 Main effect of velocity

The t-contrast results from one sided main effects for 5cm/s, 25cm/s, and 65cm/s can be inserted in a one-way ANOVA within-subjects analysis to evaluate the group main effect of various velocity stimuli with significance level set to $P_{unc} < .0001$. The result of the BOLD response of the main effect was used to identify the S1, S2 and the somatosensory areas. Fig. 3.2 shows the BOLD response of the main effect of velocity in both overall cortical activation and its coronal view. The MNI coordinates and F-values of the main effect of the velocity are listed in Table 3.2. The result from the one-way ANOVA within-subjects showed contralateral and ipsilateral BOLD responses in not only cerebral sensorimotor area (S1, S2, primary motor cortex (M1), supplementary motor cortex (SMA), insula and postcentral gyrus), but also cerebellum. The peak level of contralateral BOLD response was found in Brodmann area (BA) 3b [MNI (mm) = -47, -20, 58; F = 56.18], followed by postcentral gyrus [MNI (mm) = -62, -17, 35; F = 28.21]. The highest level of ipsilateral BOLD response was found in the precentral gyrus [MNI (mm) = 51, 1, 50; F = 28.99] followed by cerebellum near the dentate nucleus [MNI (mm) = 26, -55, -23; F = 26.97]. The cerebral responses in S1 and PPC are generally consistent with the findings from our previous MEG studies using the first and second generation of TAC-Cells (19.3 mm ID, and 6 mm ID, respectively) developed in our laboratory (Venkatesan et al., 2010; A. Popescu et al., 2013; Venkatesan et al., 2014).

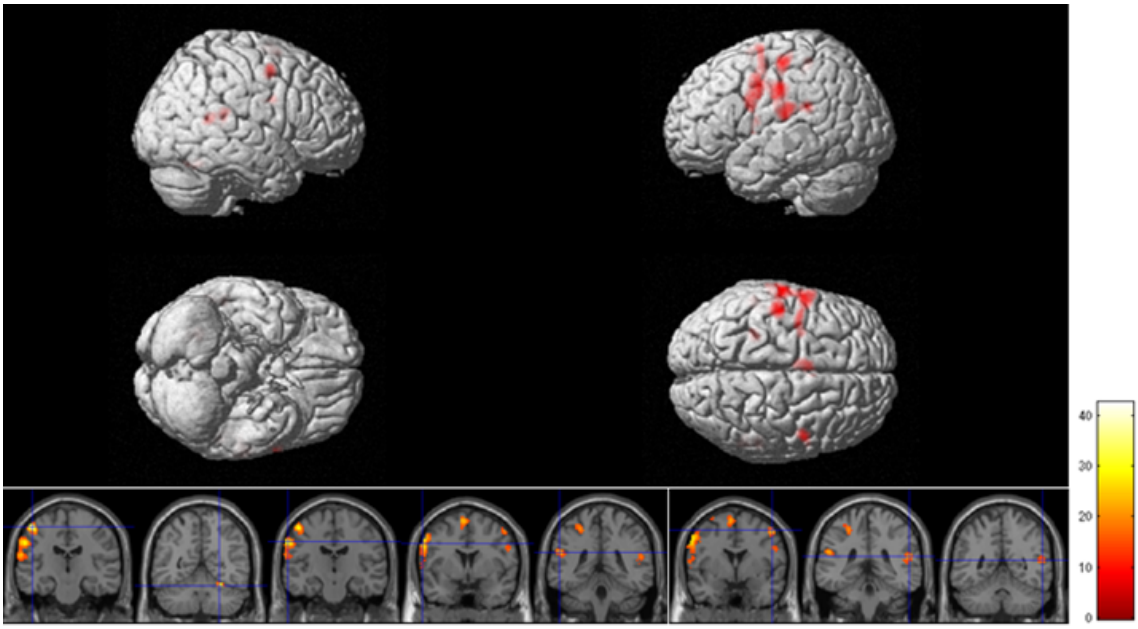

Figure 3.2: Main effect of velocity from 20 neurotypical subjects combining 3 different velocities stimulus (5 cm/s, 25 cm/s, and 65 cm/s). Color-coded evoked BOLD responses at the bottom indicate brain regions (coronal slice) with high F-values

MNI Coordinates				
x	y	z	F-value	Region
-47	-20	58	56.18	L BA3b
51	1	50	28.99	R Precentral Gyrus
-62	-17	35	28.21	L BA1
26	-55	-23	26.97	R Cerebellum
-60	3	35	26.78	L Precentral Gyrus
-45	-5	53	26.11	L Precentral Gyrus
5	1	65	25.01	R BA6
-27	-35	48	23.29	L BA3a
-55	-2	43	20.07	L Precentral Gyrus
-35	-35	43	15.61	L BA3a
-30	-40	58	15.46	L BA2
-50	-37	23	15.40	L Superior Temporal Gyrus
56	-35	20	14.99	R Superior Temporal Gyrus

Table 3.2: Main effect of the velocity MNI coordinates ($P_{unc} < .0001$)

3.2.2 BOLD signal changes in BA 3b

The MNI coordinate of BA 3b on the left somatosensory cortex [-54, -20 40] was selected by using the Anatomy toolbox v2.2b, which estimated that the MNI coordinate could be assigned to BA 3b with 82% probability. Fig. 3.3 shows the BOLD signal changes for each of the 5 conditions compared to zero in BA 3b (estimate the mean of percentage BOLD signal changes across the 20 seconds stimulus block, $P_{unc} < .0001$). The peak BOLD signal changes were found in 5 cm/s contrast, while the BOLD signal changes decreased with increasing stimulus velocity. The average BOLD signal change attenuated significantly from 25 cm/s to 65 cm/s. Similar BOLD signal changes were found between the highest velocity (65 cm/s) and All TAC-Cells ON condition. Only negative small BOLD signal changes were observed for the All TAC-Cells OFF condition.

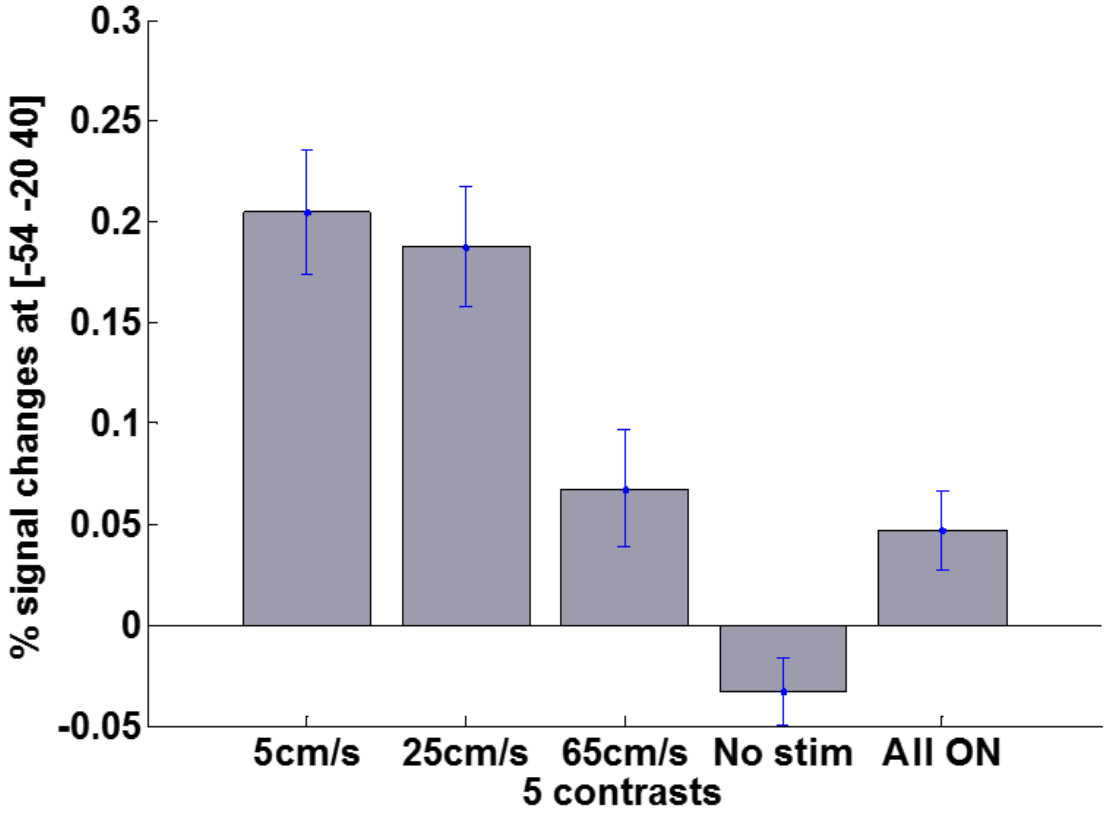

Figure 3.3: The bar graph show the BOLD signal changes of 5 contrasts compared to zero in BA 3b with SEM (estimate the mean of percentage BOLD signal changes across the 20 seconds stimulus block, $P_{unc} < .0001$)

3.2.3 One sample t-test (Velocities > All-OFF)

The results from one sample t-test in the second-level analysis showed a group result of one-sided individual velocities compared to the two control conditions (All TAC-Cells OFF and On). When the individual velocities were compared to the All TAC-Cells OFF condition (No stimulus) in Fig. 3.4, 3.5, 3.6 (the contrasts: 5 cm/s > All TAC-Cells OFF, 25 cm/s > All TAC-Cells OFF, and 65 cm/s > All TAC-Cells OFF), the contralateral BOLD activations in sensorimotor cortex were found consistently across most subjects, with the largest spatial extent of the evoked BOLD response at '25cm/s > All TAC-Cells OFF'. MNI coordinates, t-value, and brain regions are listed in Table 3.3. Contralateral BOLD responses in mostly sensorimotor cortex (BA1, 2, and pre- and postcentral gyrus) were found in both '5 cm/s > No stimulus' and '65 cm/s > No stimulus' contrasts, whereas '25 cm/s > No stimulus' contrast evoked BOLD responses in BA1, BA43 (parts of the S2 which is located at the posterior end of the lateral fissure of Sylvius) and postcentral gyrus. The ipsilateral BOLD responses were found in the inferior parietal lobule (IPL) only at '25 cm/s > No stimulus' [MNI (mm) = 53, -27, 23; t = 8.22]. The one sample t-test results (5 cm/s, 25 cm/, and 65 cm/s > No stimulus) on the rendered brain cortical surface using bspmview toolbox are shown in Fig. 3.7.

Fig. 3.8 shows the time courses of BOLD responses at BA 3b coordinates [-54, -20, 40] on the left, averaged from 15 out of 20 subjects. Five subjects were excluded due to no voxel survived at BA 3b with $P_{unc} < .0001$. The contrasts of BOLD responses time courses: '5 cm/s > No stimulus', '25 cm/s > No stimulus', and '65 cm/s > No stimulus'. The peak BOLD responses for each of the three contrasts were found 5 seconds after stimulus onset with the '25 cm/s > No stimulus' contrast showing the greatest BOLD response.

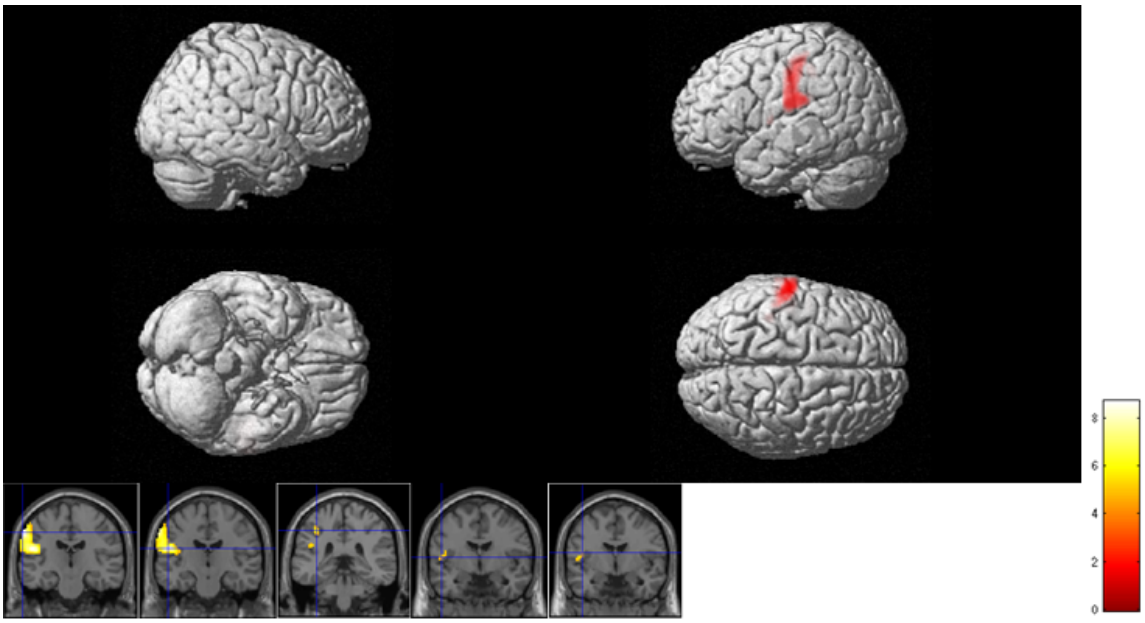

Figure 3.4: One sample t-test result (5cm/s > No stimulus, $P_{unc} < .0001$)

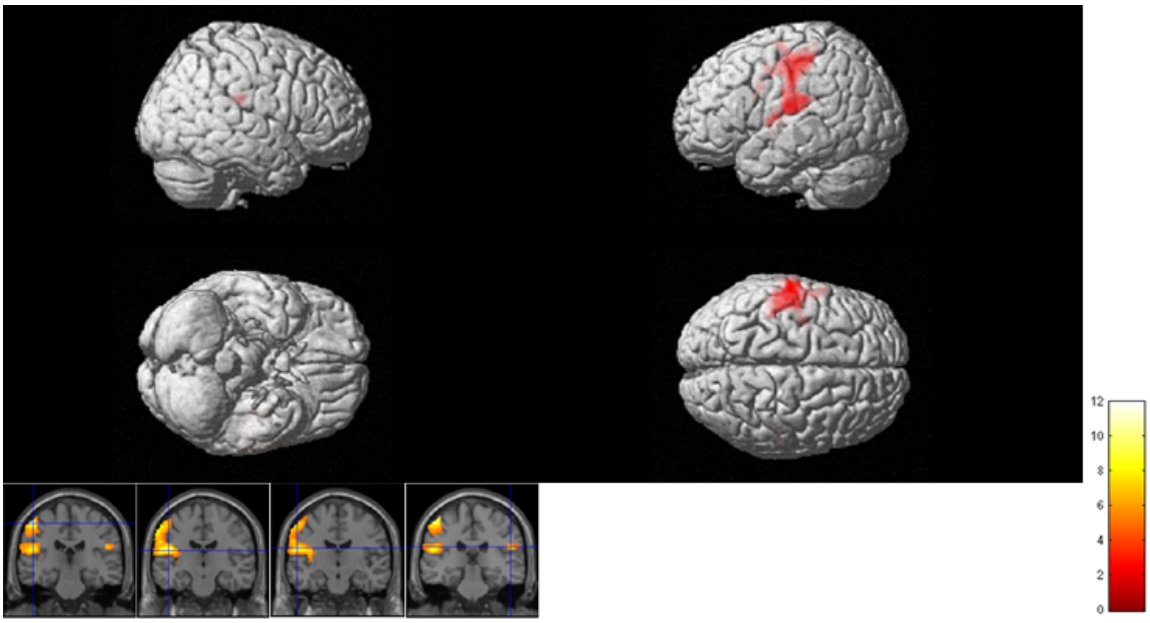

Figure 3.5: One sample t-test result (25cm/s > No stimulus, $P_{unc} < .0001$)

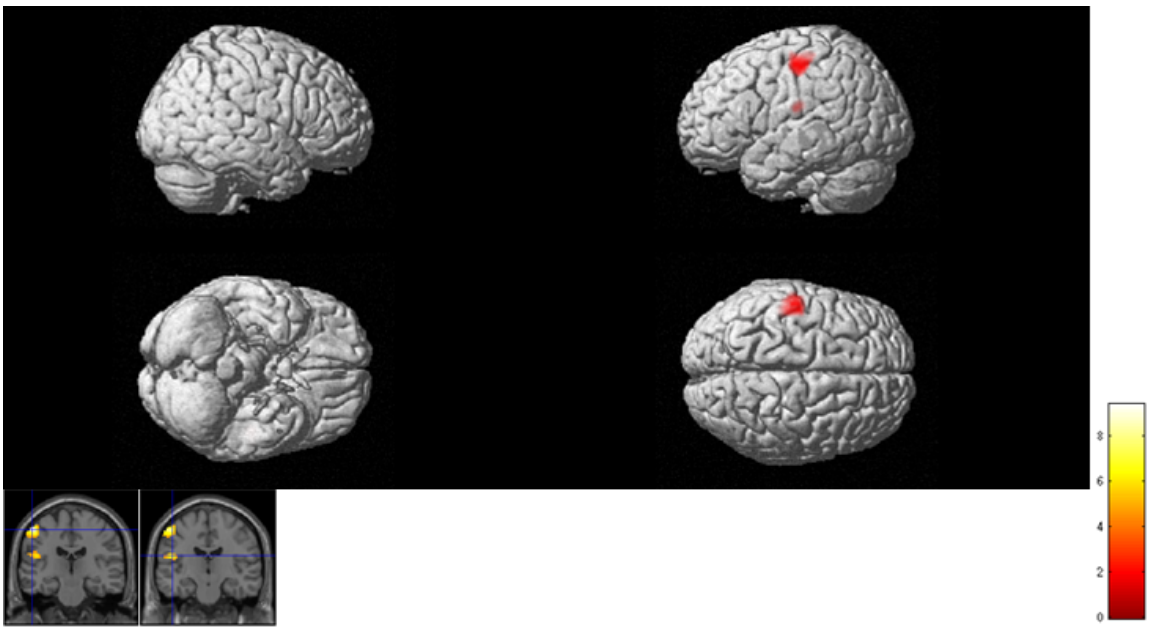

Figure 3.6: One sample t-test result (65cm/s > No stimulus, $P_{unc} < .0001$)

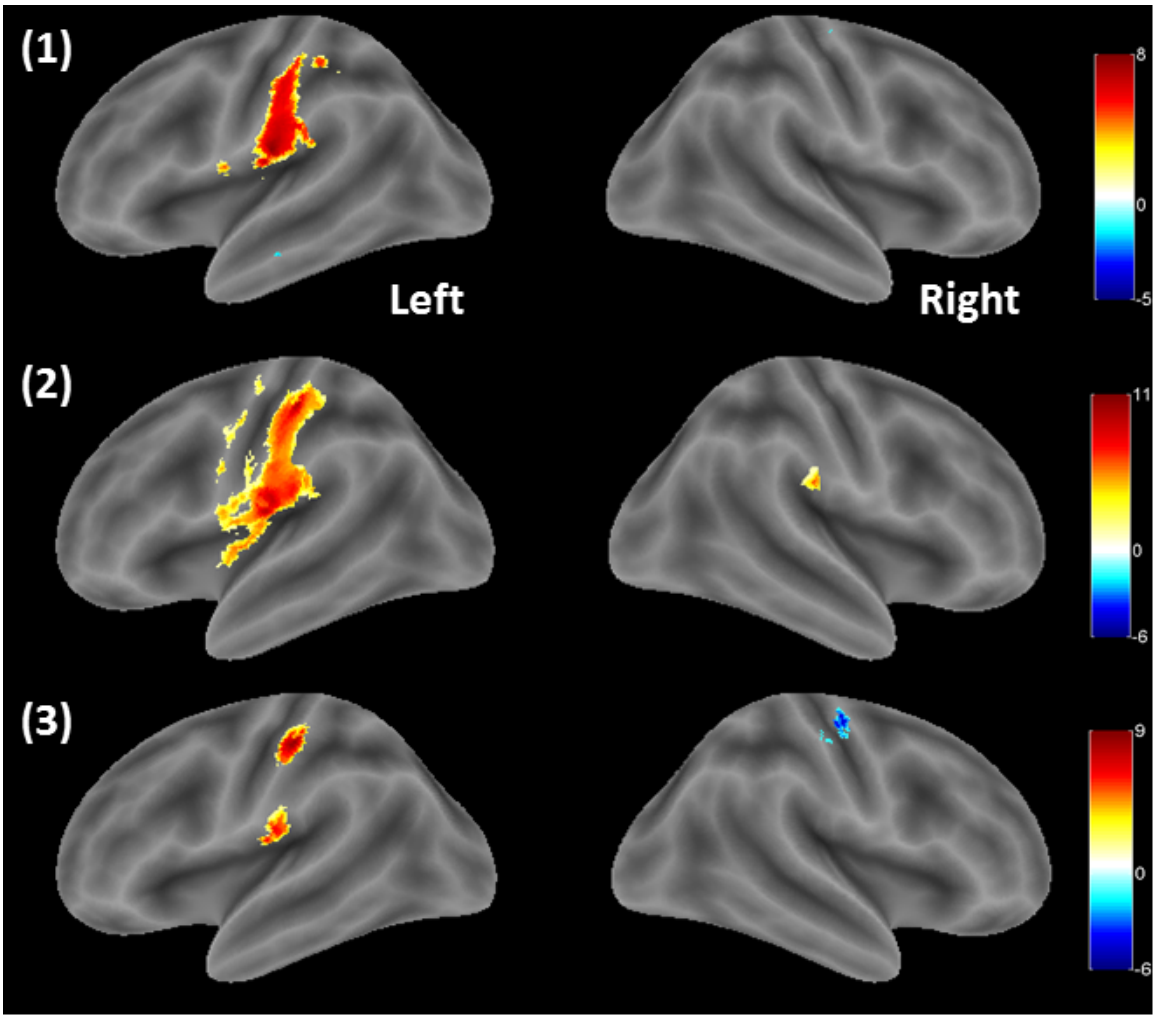

Figure 3.7: One sample t-test result on the normalized rendered brain cortical surface using bspmview (`http://www.bobspunt.com/bspmview/`) [from the top: (1) 5 cm/s, (2) 25 cm/s, and (3) 65 cm/s > No stimulus, $P_{unc} < .0001$]

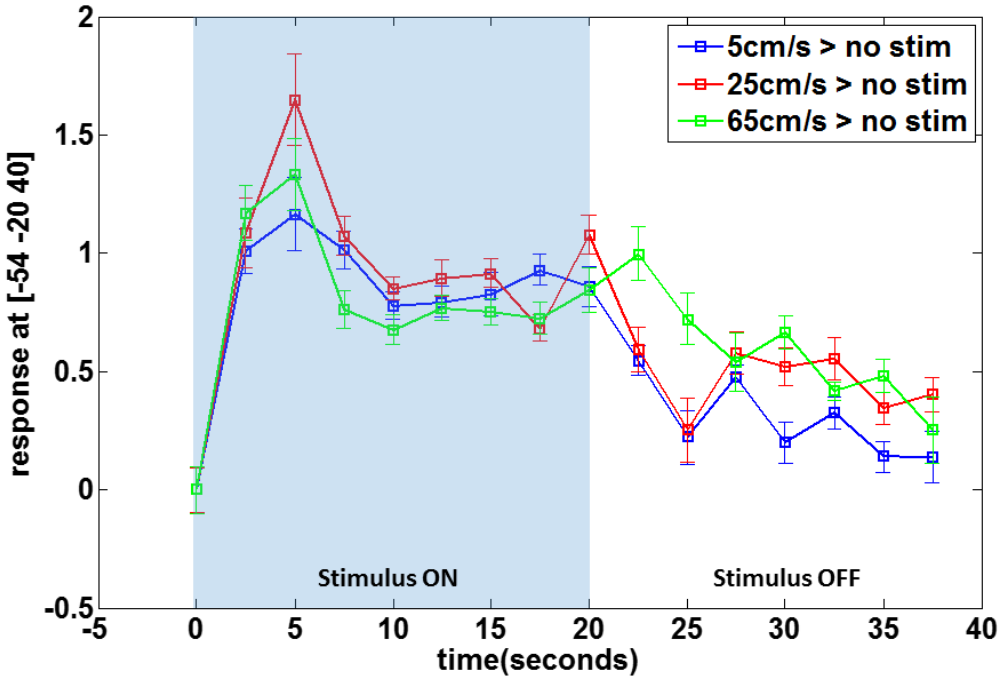

Figure 3.8: BOLD response time courses in BA 3b (estimated as the average BOLD responses across the 15 subjects during the 40 seconds block including stimulus ON and OFF, Blue = 5 cm/s > No stimulus, Red = 25 cm/s > No stimulus, Green = 65 cm/s > No stimulus)

	MNI Coordinates				
	x	y	z	t-value	Region
5cm/s > No stimulus	-65	-20	43	8.70	L BA1
	-52	-17	20	8.64	L Postcentral Gyrus
	-57	-22	50	6.80	L BA1
	-37	-35	45	5.89	L BA2
	-50	-5	8	5.66	L Precentral Gyrus
	-45	-5	15	5.04	L Rolandic Operculum
25cm/s > No stimulus	-50	-25	55	11.92	L BA1
	-47	-17	18	10.83	L BA43
	-55	-15	20	10.31	L Postcentral Gyrus
	53	-27	23	8.22	R Inferior Parietal Lobule
65cm/s > No stimulus	-52	-22	55	9.40	L BA1
	-47	-17	20	6.98	L Rolandic Operculum (OP3)

Table 3.3: One sample t-test results. Velocities > No stimulus ($P_{unc} < .0001$)

3.2.4 One sample t-test (Velocities > All-ON)

The individual velocities were compared to the All TAC-Cells ON condition as shown in Fig. 3.9, 3.10, and 3.11. Fig. 3.12 displays the one sample t-test results (5 cm/s, 25 cm/, and 65 cm/s > All-TAC-Cells ON) on the rendered brain cortical surface using bspmview toolbox. The contralateral BOLD responses in sensorimotor cortex (BA3, BA6 and pre- and postcentral gyrus) were found at the three contrasts: '5 cm/s > All-TAC-Cells ON', '25 cm/s > All-TAC-Cells ON', and '65 cm/s > All-TAC-Cells ON', whereas the ipsilateral BOLD activations in subgyral were seen only at '5 cm/s > All-TAC-Cells ON' [MNI (mm) = 33, -37, 45; t = 6.35]. As shown in Table 3.4, the peak t-value was observed at '5 cm/s > All-TAC-Cells ON' (t = 9.18) while small BOLD responses were found at the highest velocity condition (65 cm/s > All-TAC-Cells ON). The spatial extent of BOLD responses at '5 cm/s > All-TAC-Cells ON' and '25 cm/s > All-TAC-Cells ON' were larger than the highest velocity contrast.

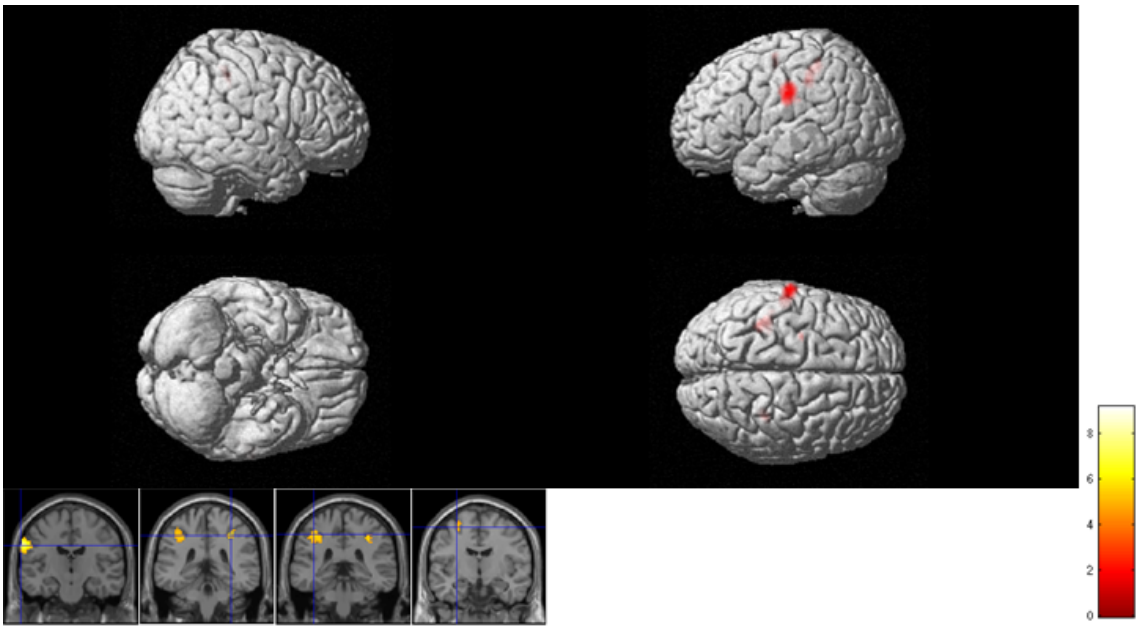

Figure 3.9: One sample t-test result (5cm/s > All-ON, $P_{unc} < .0001$)

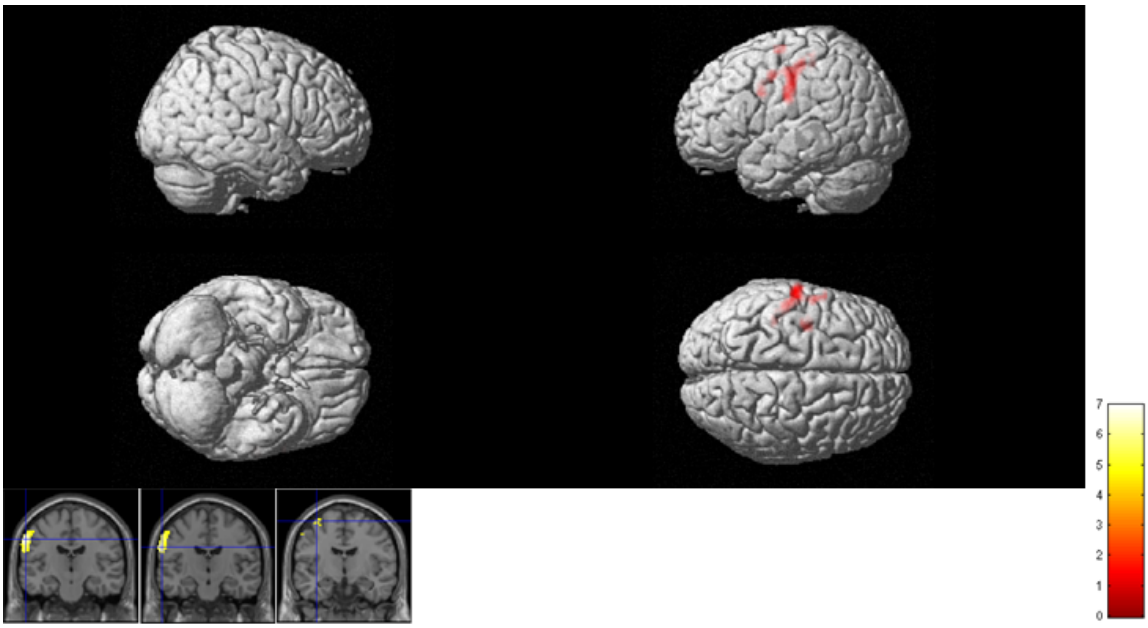

Figure 3.10: One sample t-test result (25cm/s > All-ON, $P_{unc} < .0001$)

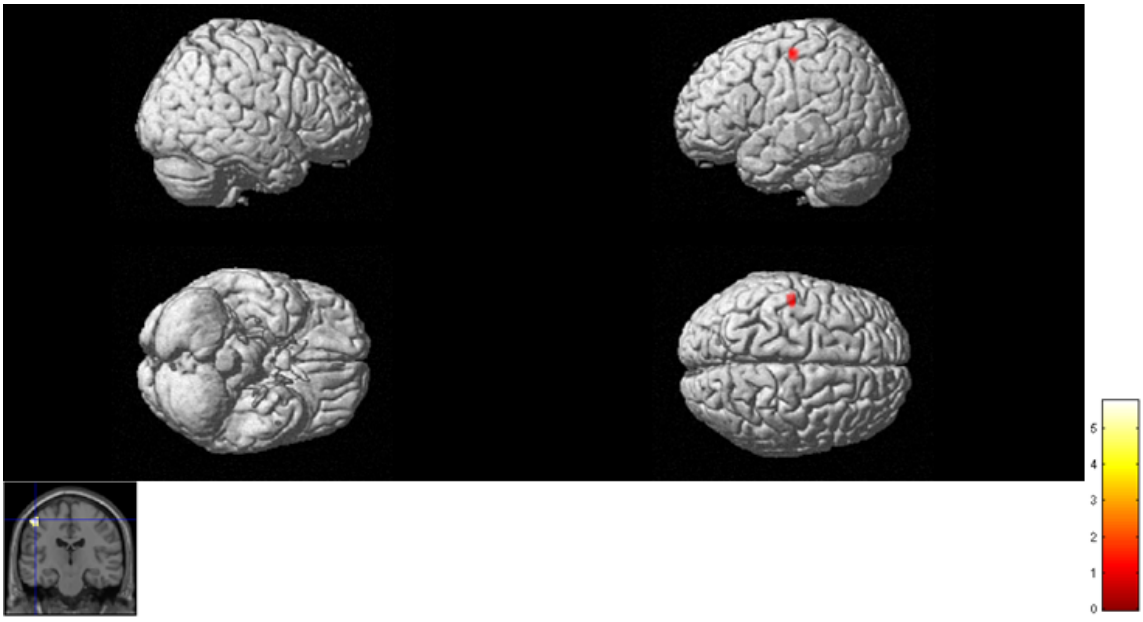

Figure 3.11: One sample t-test result (65cm/s > All-ON, $P_{unc} < .0001$)

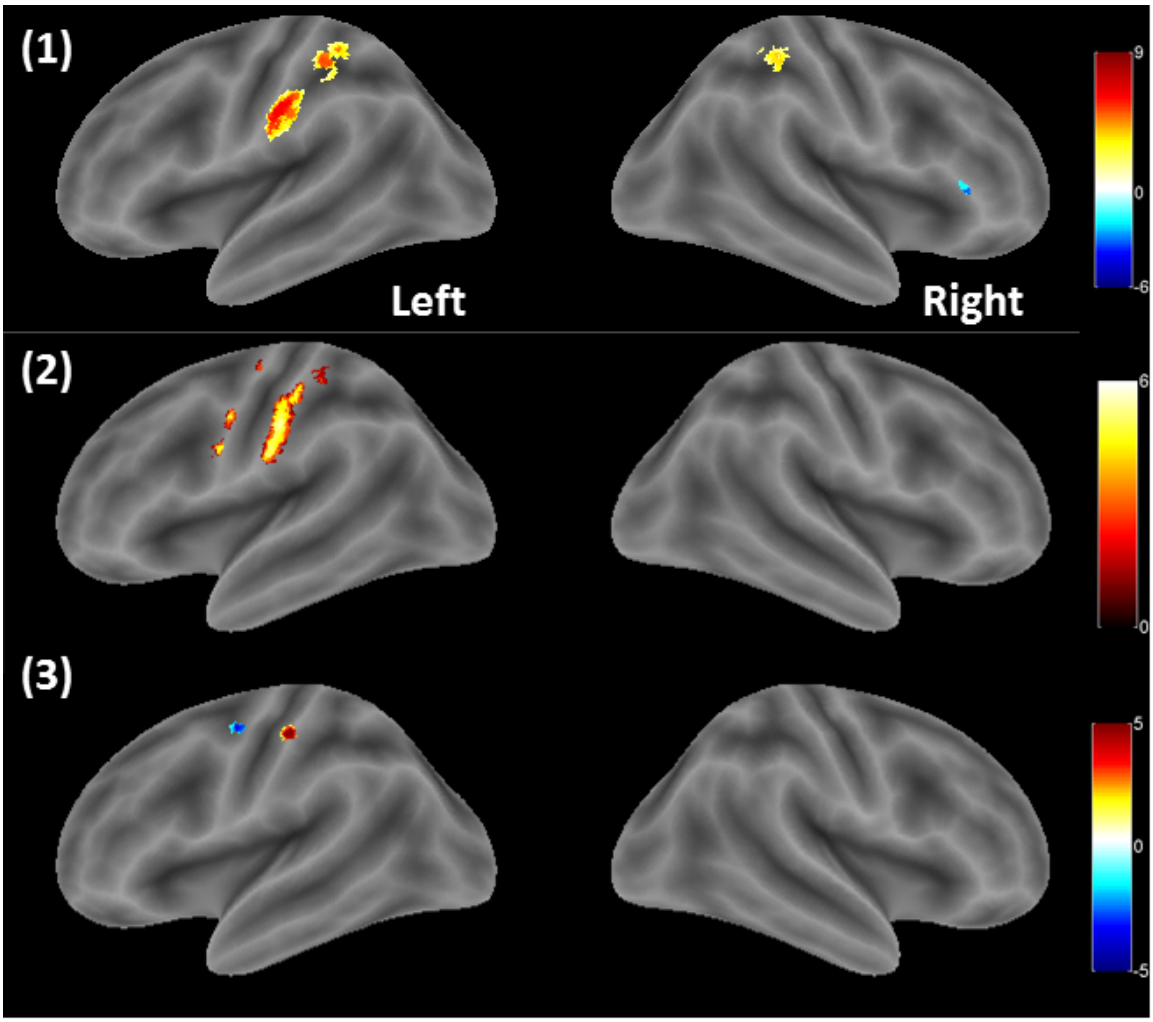

Figure 3.12: One sample t-test result on the rendered brain cortical surface using bspmview (`http://www.bobspunt.com/bspmview/`) [from the top: (1) 5 cm/s, (2) 25 cm/s, and (3) 65 cm/s > All-ON, $P_{unc} < .0001$]

	MNI Coordinates				
	x	y	z	t-value	Region
5cm/s > All-ON	-67	-17	33	9.18	L Superior Temporal Gyrus
	33	-37	45	6.35	R BA2
	-40	-35	48	5.68	L BA2
	-32	-32	45	5.57	L BA3a
	-30	-10	58	4.99	L BA6
	-25	-7	50	4.71	L BA6
25cm/s > All-ON	-60	-17	40	6.96	L BA1
	-57	-2	45	6.66	L BA6
	-62	-15	30	6.23	L BA1
	-37	-10	65	5.26	L Precentral Gyrus
65cm/s > All-ON	-47	-20	58	5.75	L BA3b

Table 3.4: One sample t-test results. Velocities > All-ON ($P_{unc} < .0001$)

Chapter 4

Discussion

4.1 Overview of this study

In this study, we used a new saltatory pneumotactile stimulus modality programmed at 3 different velocities on the glabrous hand to map the evoked hemodynamic BOLD response in cortical and subcortical somatosensory areas using fMRI methods. We found that the BOLD main effect for saltatory pneumotactile velocity was localized to several loci involving contralateral and bilateral cerebral cortex, and ipsilateral cerebellum. This elaborate network extends previous observations of pneumotactile encoding of single channel pulse train inputs (non-saltatory) in both contralateral and bilateral cerebral sensorimotor cortex, which is consistent with previous fMRI and MEG studies that cortical evoked neural activity was found in both contralateral and bilateral somatosensory and somatosensory association areas (Brodoehl et al., 2013; A. Popescu et al., 2013). We also found considerable ipsilateral BOLD responses in the deep cerebellum which were reported in the previous fMRI and PET studies using the foam-tipped motor to create the movement of the tactile stimulus (tickling) on the palm (Blakemore et al., 1999, 2001). Moreover, pneumotactile stimulation on the glabrous hand produced the largest spatial extent of the evoked BOLD responses at '25 cm/s ¿ No stimulus', which corresponds well to enhanced perceptual capacity revealed by human skin psychophysical studies employing a brush traversing across an

aperture on the skin, and the identification of an optimal stimulus velocity (between 5 and 30 cm/s on glabrous skin) revealed by single unit recordings in non-human primate somatosensory cortex during continuous skin brushing (Whitsel et al., 1978, 1986).

4.2 Finding of the BOLD localization

Hypothesis 1.

Hypothesis $\mathbf{H}_0$: There will be a significant difference pattern of BOLD response regarding to the main effect of velocity across the different areas of the cortical and subcortical somatosensory cortex.

Hypothesis $\mathbf{H}_A$: The alternative hypothesis suggests that there will be no significant difference pattern of BOLD response regarding to the main effect of velocity across the different areas of the cortical and subcortical somatosensory areas will not have different pattern of BOLD activation.

We have demonstrated regional neural activation using pneumotactile stimulation via TAC-Cells in both contralateral (20/20) and ipsilateral somatosensory cortex (6/20) in order to understand how various saltatory pneumotactile velocity profiles influence the spatial extent of brain networks in neurotypical adults. Our results showed that the contralateral BOLD responses were found at sensoritmotor cortex (S1, S2, M1, SMA, pre- and postcentral gyrus) across the most subjects (19 out of 20 subjects), whereas the ipsilateral BOLD activations were limited to S1, S2, and deep cerebellum in 6 out of 20 subjects. The robust BOLD response in contralateral sensorimotor cortex is consistent with human fMRI studies using electrical and laser stimulation (Backes et al., 2000; Bornhövd et al., 2002). In addition, our finding of a significant ipsilateral

BOLD response in the cerebellum is consistent with known somatosensory anatomical projections via the spinocerebellar tract and a previous human PET study using finger movements to create tactile stimulation which demonstrated increased ipsilateral cerebellar blood-flow responses (Fox et al., 1985). Our findings also provide evidence that moving pneumotactile stimulation evokes neural activity in both somatosensory and motor cortices.

4.3 The BOLD response of individual velocities

Hypothesis 2.

Hypothesis $\mathbf{H}_0$: There will be a significant difference pattern of BOLD response regarding to the individual velocities (5 cm/s, 25 cm/s, and 65 cm/s) among the cortical and subcortical somatosensory areas.

Hypothesis $\mathbf{H}_A$: The alternative hypothesis suggests that there will be no significant difference pattern of BOLD response regarding to the individual velocities (5 cm/s, 25 cm/s, and 65 cm/s) among the cortical and subcortical somatosensory areas.

Our results show that the spatial extent of BOLD responses increases dramatically when stimulus velocity is increased from 5 cm/s to 25 cm/s, and decrease or funnel as velocity is further increased to 65 cm/s. The effective nature of saltatory pneumotactile inputs on the glabrous hand at from the 5 cm/s to 25 cm/s velocities is generally consistent with psychophysical studies using continuous brush stimulation applied to the glabrous skin in both animals and humans and is regarded as an important feature of somatosensory processing (C. Lee & Whitsel, 1992; McGlone et al., 2012). The BOLD response time courses, especially in BA 3b, in this study increase as a function of increasing velocity which is consistent with previous fMRI studies using tactile

and nonpainful electrical median nerve stimulation (Kampe et al., 2000; Ferretti et al., 2007; Hlushchuk et al., 2015). These characteristics of moving tactile stimulation suggest that the fast-adapting (FA) mechanoreceptors which are heavily concentrated in the glabrous hand are sensitive to tactile stimulation velocity (Essick & Edin, 1995). Further, we discovered the ipsilateral BOLD signal in the IPL at 25 cm/s > No stimulus contrast. The IPL has been hypothesized to play a role in sensorimotor integration (Kitada et al., 2003; Caspers et al., 2013). Additionally, the significant BOLD response in deep cerebellum at 25 cm/sec is consistent with its presumed role in sensory information processing for monitoring and optimizing movement using somatosensory proprioceptive feedback information (Gazzola & Keysers, 2009).

4.4 Pneumotactile stimulus system

The TAC-Cells developed in our laboratory are safe, non-invasive, simple and rapid application, 100% compatible with MRI/MEG, no stimulus artifact, achieve normal physiologic recruitment order of primary mechanosensitive afferents, avoid the potential risks associated with direct-current stimulation methods, are well tolerated by participants across the lifespan, from infancy through adulthood. Most previous studies were limited to study of the median nerve using electrical current stimulation, which noted increasing somatosensory thresholds during the stimulation in healthy human participants (Dean et al., 2006). The TAC-Cells provide natural stimulation via a small pneumatically charged capsule, which can be placed on virtually any skin surface of the body, including the glabrous hand and face. Our multi-channel pneumotactile stimulus array control system (GALILEO) can be programmed to control pulse duration, relative timing between cells to create velocity trajectories over the skin, stimulus block design (continuous, random, random-balanced), and various triggering modes which are essential for task- or stimulus-related fMRI experiments.

4.5 Study limitations and future directions

Results of this study have generated new information on the spatiotemporal features of saltatory tactile velocity encoding in cerebral and deep cerebellar somatosensory representations in neurotypical adults. Moreover, this work is expected to inform future investigations whose goal is to develop new approaches to motor rehabilitation through somatosensory neurotherapeutics to improve sensorimotor function in individuals who have sustained cerebrovascular stroke or traumatic brain injury.

Although the current generation of fMRI scanners provides relatively high spatial resolution ($\sim$ 2 mm), the temporal resolution is limited (seconds) due to intrinsic properties of the hemodynamic response (Kim et al., 1997). The use of multiband echoplanar sequence can reduce the TR from 2.5 seconds to 1.0 second (Xu et al., 2013; Auerbach et al., 2013). The multiband EPI sequence would provide the better temporal resolution and maintain high spatial resolution which are useful for the BOLD response time courses analysis. Multimodal recordings of fMRI and EEG, or coregistration studies using SQUID-based superconducting MEG, or the rapidly evolving technology known as atomic (AM) or optically-pumped magnetometers (OPM) may yield the best available spatial and temporal resolution to reveal the dynamics of the human somatosensory brain. Moreover, the BOLD response time courses in other sensorimotor areas (e.g. BA 1, 2, 4, and cerebellum) could be employed to develop an enhanced model of functional brain connectivity and stimulus feature processing as a function of saltatory pneumotactile velocity.

Chapter 5

Conclusion

The principal aim of this study was to map the relation between a dynamic saltatory pneumatic stimulus array located on the glabrous hand programmed from velocity and the evoked BOLD response in the human brain. Saltatory pneumatic pulses (60 ms) arranged in a 7-channel TAC-Cell array was used to deliver traverse velocities at 5, 25, and 65 cm/s on the glabrous hand spanning D1 (thumb), D2 (index finger), and D3 (middle finger). An anatomical (MPRAGE) and 3 functional scans (BOLD) were completed in 20 healthy right-handed adults using 3T magnetic resonance imaging (MRI). Results from each subject were inserted to the one-way ANOVA within-subjects and one sample t-test to evaluate the group main effect of various velocity stimuli and individual velocities, respectively.

In summary, we found that the TAC-Cell pneumotactile stimulus array delivered at 3 different velocities on the glabrous hand was highly effective for evoking BOLD responses in primary and secondary sensorimotor cortices and deep cerebellum. The spatial extent of BOLD responses was dependent on the velocity of tactile stimuli.

Appendix A

Reference

References

Ackerley, R., Hassan, E., Curran, A., Wessberg, J., Olausson, H., & McGlone, F. (2014). An fMRI study on cortical responses during active self-touch and passive touch from others. *Frontier in Behavioral Neuroscience*, *6*(51).

Adrian. (1940). Double representation of the feet in the sensory cortex of the cat. *J. Physiol.(Lond.)*, *98*, 16–18.

Adrian. (1941). Afferent discharges to the cerebral cortex from peripheral sense organs. *The Journal of Physiology*, *100*(2), 159–191.

Akatsuka, K., Noguchi, Y., Harada, T., Sadato, N., & Kakigi, R. (2008). Neural codes for somatosensory two-point discrimination in inferior parietal lobule: an fMRI study. *NeuroImage*, *40*(2), 852–858.

Almeida, K., Brucki, S., Duarte, M., Pasqualucci, C., Rosemberg, S., & Nitrini, R. (2012). Basal ganglia lesions in subacute sclerosing panencephalitis. *Dement Neuropsychol*, *6*(4), 286-289.

Amaro, E., & Barker, G. (2006). Study design in fMRI: basic principles. *Brain and Cognition*, *60*(3), 220–232.

Andersen, R., & Gnadt, J. (1989). Posterior parietal cortex. *Rev. Oculomot. Res*, *3*, 315–335.

Aoki, T., Tsuda, H., Takasawa, M., Osaki, Y., Oku, N., Hatazawa, J., & Kinoshita, H. (2005). The effect of tapping finger and mode differences on cortical and subcortical activities: a PET study. *Experimental Brain Research*, *160*(3), 375–383.

Aronoff, R., Matyas, F., Mateo, C., Ciron, C., Schneider, B., & Petersen, C. (2010). Long-range connectivity of mouse primary somatosensory barrel cortex. *European Journal of Neuroscience*, *31*(12), 2221–2233.

Ashburner, J., & Friston, K. (2000). Voxel-based morphometry - the methods. *NeuroImage*, *11*(6), 805–821.

Ashburner, J., & Friston, K. (2005). Unified segmentation. *NeuroImage*, *26*(3), 839–851.

Auerbach, E., Xu, J., Yacoub, E., Moeller, S., & Uğurbil, K. (2013). Multiband accelerated spin-echo echo planar imaging with reduced peak RF power using time-shifted RF pulses. *Magnetic Resonance in Medicine*, *69*(5), 1261–1267.

Backes, W., Mess, W., van Kranen-Mastenbroek, V., & Reulen, J. (2000). Somatosensory cortex responses to median nerve stimulation: fMRI effects of current amplitude and selective attention. *Clinical Neurophysiology*, *111*(10), 1738–1744.

Barlow, S. (1987). Mechanical frequency detection thresholds in the human face. *Experimental Neurology*, *96*(2), 253–261.

Barlow, S., Finan, D., Lee, J., & Chu, S. (2008). Synthetic orocutaneous stimulation entrains preterm infants with feeding difficulties to suck. *Journal of Perinatology*, *28*(8), 541–548.

Barlow, S., & Rosner, A. O. (2015). Oral sensorimotor development. *Routledge Handbook of Communication Disorders*, 103.

Berne, R., Koeppen, B., & Stanton, B. (2008). *Berne & Levy Physiology* (No. p. 578).

Mosby/Elsevier.

Bertolasi, L., Priori, A., Tinazzi, M., Bertasi, V., & Rothwell, J. (1998). Inhibitory action of forearm flexor muscle afferents on corticospinal outputs to antagonist muscles in humans. *The Journal of Physiology*, *511*(3), 947–956.

Biswas, A., Manivannan, M., & Srinivasan, M. (2015). Vibrotactile sensitivity threshold: Nonlinear stochastic mechanotransduction model of the Pacinian corpuscle. *IEEE Transactions on Haptics*, *8*(1), 102–113.

Björnsdotter, M., & Olausson, H. (2011). Vicarious responses to social touch in posterior insular cortex are tuned to pleasant caressing speeds. *The Journal of Neuroscience*, *31*(26), 9554–9562.

Blakemore, S., Frith, C., & Wolpert, D. (2001). The cerebellum is involved in predicting the sensory consequences of action. *NeuroReport*, *12*(9), 1879–1884.

Blakemore, S., & Sirigu, A. (2003). Action prediction in the cerebellum and in the parietal lobe. *Experimental Brain Research*, *153*(2), 239–245.

Blakemore, S., Wolpert, D., & Frith, C. (1999). The cerebellum contributes to somatosensory cortical activity during self-produced tactile stimulation. *NeuroImage*, *10*(4), 448–459.

Bornhövd, K., Quante, M., Glauche, V., Bromm, B., Weiller, C., & Büchel, C. (2002). Painful stimuli evoke different stimulus–response functions in the amygdala, prefrontal, insula and somatosensory cortex: a single-trial fMRI study. *Brain*, *125*(6), 1326–1336.

Brett, M., Anton, J., Valabregue, R., & Poline, J. (2002). Region of interest analysis using the MarsBaR toolbox for SPM 99. *NeuroImage*, *16*(2), S497.

Brodmann, K. (1909). Vergleichende lokalisationslehre der groshirnrinde. *Leipzig: Barth*.

Brodoehl, S., Klingner, C., Stieglitz, K., & Witte, O. (2013). Age-related changes in

the somatosensory processing of tactile stimulation: An fMRI study. *Behavioural Brain Research*, *238*, 259–264.

Buneo, C., & Andersen, R. (2006). The posterior parietal cortex: sensorimotor interface for the planning and online control of visually guided movements. *Neuropsychologia*, *44*(13), 2594–2606.

Buonomano, D., & Merzenich, M. (1998). Cortical plasticity: from synapses to maps. *Annual Review of Neuroscience*, *21*(1), 149–186.

Bursztyn, L., Ganesh, G., Imamizu, H., Kawato, M., & Flanagan, J. (2006). Neural correlates of internal-model loading. *Current Biology*, *16*(24), 2440–2445.

Burton, H., Abend, N., MacLeod, A., Sinclair, R., Snyder, A., & Raichle, M. (1999). Tactile attention tasks enhance activation in somatosensory regions of parietal cortex: a positron emission tomography study. *Cerebral Cortex*, *9*(7), 662–674.

Bystritsky, A., & Korb, A. (2015). A Review of Low-Intensity Transcranial Focused Ultrasound for Clinical Applications. *Current Behavioral Neuroscience Reports*, *2*(2), 60–66.

Casey, K., Morrow, T., Lorenz, J., & Minoshima, S. (2001). Temporal and spatial dynamics of human forebrain activity during heat pain: analysis by positron emission tomography. *Journal of Neurophysiology*, *85*(2), 951–959.

Caspers, S., Schleicher, A., Bacha-Trams, M., Palomero-Gallagher, N., Amunts, K., & Zilles, K. (2013). Organization of the human inferior parietal lobule based on receptor architectonics. *Cerebral Cortex*, *23*(3), 615–628.

Cauna, N., & Ross, L. (1960). The fine structure of Meissner's touch corpuscles of human fingers. *The Journal of Biophysical and Biochemical Cytology*, *8*(2), 467–482.

Chavhan, G., Babyn, P., Thomas, B., Shroff, M., & Haacke, M. (2009). Principles, techniques, and applications of T2*-based MR imaging and its special

applications 1. *Radiographics*, *29*(5), 1433–1449.

Chee, M., Venkatraman, V., Westphal, C., & Siong, S. (2003). Comparison of block and event-related fMRI designs in evaluating the word-frequency effect. *Human Brain Mapping*, *18*(3), 186–193.

Chen, J., & Pike, G. (2009). Origins of the BOLD post-stimulus undershoot. *NeuroImage*, *46*(3), 559–568.

Chen, T., Babiloni, C., Ferretti, A., Perrucci, M., Romani, G., Rossini, P., ... Del Gratta, C. (2008). Human secondary somatosensory cortex is involved in the processing of somatosensory rare stimuli: an fMRI study. *NeuroImage*, *40*(4), 1765–1771.

Cho, K., Kim, J., Kwon, S., Cho, A., & Kang, D. (2005). Significance of susceptibility vessel sign on T2*-weighted gradient echo imaging for identification of stroke subtypes. *Stroke*, *36*(11), 2379–2383.

Cho, Z., Son, Y., Kim, H., Kim, K., Oh, S., Han, J., ... Kim, Y. (2007). A hybrid PET-MRI: An integrated molecular-genetic imaging system with HRRT-PET and 7.0T MRI. *International Journal of Imaging Systems and Technology*, *17*(4), 252–265.

Cho, Z., Son, Y., Kim, H., Kim, K., Oh, S., Han, J., ... Kim, Y. (2008). A fusion PET-MRI system with a high-resolution research tomograph-PET and ultra-high field 7.0T MRI for the molecular-genetic imaging of the brain. *Proteomics*, *8*(6), 1302–1323.

Cocosco, C., Kollokian, V., Kwan, R., Pike, G., & Evans, A. (1997). Brainweb: Online interface to a 3D MRI Simulated Brain Database. In *NeuroImage* (Vol. 5, p. 425).

Constantinidis, C., Bucci, D., & Rugg, M. (2013). Cognitive functions of the posterior parietal cortex. *Frontiers in Integrative Neuroscience*, *7*, 35.

Cooper, D. (2008). *Introduction to Neuroscience I.* CU Neuroscience Series. Retrieved from `https://books.google.com/books?id=jXnkai44PxYC`

Coulter, J. (1974). Sensory transmission through lemniscal pathway during voluntary movement in the cat. *Journal of Neurophysiology*, *37*(5), 831–845.

Dale, A., & Buckner, R. (1997). Selective averaging of rapidly presented individual trials using fMRI. *Human Brain Mapping*, *5*(5), 329–340.

Dallmann, C., Ernst, M., & Moscatelli, A. (2015). The role of vibration in tactile speed perception. *Journal of Neurophysiology*, *114*(6), 3131–3139.

Daum, D., & Hynynen, K. (1999). A 256-element ultrasonic phased array system for the treatment of large volumes of deep seated tissue. *Ultrasonics, Ferroelectrics, and Frequency Control, IEEE Transactions on*, *46*(5), 1254–1268.

Dean, J., Bowsher, D., & Johnson, M. (2006). The effects of unilateral transcutaneous electrical nerve stimulation of the median nerve on bilateral somatosensory thresholds. *Clinical Physiology and Functional Imaging*, *26*(5), 314–318.

Del Gratta, C., Della Penna, S., Ferretti, A., Franciotti, R., Pizzella, V., Tartaro, A., ... Rossini, P. (2002). Topographic organization of the human primary and secondary somatosensory cortices: comparison of fMRI and MEG findings. *NeuroImage*, *17*(3), 1373–1383.

Desmurget, M., Reilly, K., Richard, N., Szathmari, A., Mottolese, C., & Sirigu, A. (2009). Movement intention after parietal cortex stimulation in humans. *Science*, *324*(5928), 811–813.

Devlin, J., Russell, R., Davis, M., Price, C., Wilson, J., Moss, H., ... Tyler, L. (2000). Susceptibility-induced loss of signal: comparing PET and fMRI on a semantic task. *NeuroImage*, *11*(6), 589–600.

DeYoe, E., Carman, G., Bandettini, P., Glickman, S., Wieser, J., Cox, R., ... Neitz, J. (1996). Mapping striate and extrastriate visual areas in human cerebral cortex.

Proceedings of the National Academy of Sciences, *93*(6), 2382–2386.

Dreyer, D., Hollins, M., & Whitsel, B. (1978). Factors influencing cutaneous directional sensitivity. *Sensory Processes*, *2*(2), 71–79.

Eickhoff, S., Heim, S., Zilles, K., & Amunts, K. (2006). Testing anatomically specified hypotheses in functional imaging using cytoarchitectonic maps. *NeuroImage*, *32*(2), 570–582.

Eickhoff, S., Paus, T., Caspers, S., Grosbras, M., Evans, A., Zilles, K., & Amunts, K. (2007). Assignment of functional activations to probabilistic cytoarchitectonic areas revisited. *NeuroImage*, *36*(3), 511–521.

Eickhoff, S., Stephan, K., Mohlberg, H., Grefkes, C., Fink, G., Amunts, K., & Zilles, K. (2005). A new SPM toolbox for combining probabilistic cytoarchitectonic maps and functional imaging data. *NeuroImage*, *25*(4), 1325–1335.

Elias, J., Huss, D., Voss, T., Loomba, J., Khaled, M., Zadicario, E., ... others (2013). A pilot study of focused ultrasound thalamotomy for essential tremor. *New England Journal of Medicine*, *369*(7), 640–648.

Ernst, R., & Anderson, W. (1966). Application of fourier transform spectroscopy to magnetic resonance. *Review of Scientific Instruments*, *37*(1), 93–102.

Essick, G., & Edin, B. (1995). Receptor encoding of moving tactile stimuli in humans. II. The mean response of individual low-threshold mechanoreceptors to motion across the receptive field. *The Journal of Neuroscience*, *15*(1), 848–864.

Evans, A., Collins, L., Mills, S., Brown, E., Kelly, R., & Peters, T. (1993). 3D statistical neuroanatomical models from 305 MRI volumes. In *Nuclear science symposium and medical imaging conference, 1993* (pp. 1813–1817).

Ferretti, A., Babiloni, C., Arienzo, D., Del Gratta, C., Rossini, P. M., Tartaro, A., & Romani, G. L. (2007). Cortical brain responses during passive nonpainful median nerve stimulation at low frequencies (0.5–4 Hz): an fMRI study. *Human*

Brain Mapping, *28*(7), 645–653.

Fox, P., Burton, H., & Raichle, M. (1987). Mapping human somatosensory cortex with positron emission tomography. *Journal of Neurosurgery*, *67*(1), 34–43.

Fox, P., Raichle, M., & Thach, T. (1985). Functional mapping of the human cerebellum with positron emission tomography. *Proceedings of the National Academy of Sciences*, *82*(21), 7462–7466.

Foxe, J., Wylie, G., Martinez, A., Schroeder, C., Javitt, D., Guilfoyle, D., ... Murray, M. (2002). Auditory-somatosensory multisensory processing in auditory association cortex: an fMRI study. *Journal of Neurophysiology*, *88*(1), 540–543.

Francis, S., Kelly, E., Bowtell, R., Dunseath, W., Folger, S., & McGlone, F. (2000). fMRI of the responses to vibratory stimulation of digit tips. *NeuroImage*, *11*(3), 188–202.

Fredericks, C. (1996). Disorders of the cerebellum and its connections. *Pathophysiology of the Motor Systems: Principles and Clinical Presentations.*, 445–466.

Friston, K., Ashburner, J., Kiebel, S., Nichols, T., & Penny, W. (Eds.). (2007). *Statistical Parametric Mapping: The Analysis of Functional Brain Images*. Academic Press.

Friston, K., Fletcher, P., Josephs, O., Holmes, A., Rugg, M., & Turner, R. (1998). Event-related fMRI: characterizing differential responses. *NeuroImage*, *7*(1), 30–40.

Friston, K., Holmes, A., Worsley, K., Poline, J., Frith, C., Frackowiak, R., et al. (1994). Statistical parametric maps in functional imaging: a general linear approach. *Human Brain Mapping*, *2*(4), 189–210.

Friston, K., Stephan, K., Lund, T., Morcom, A., & Kiebel, S. (2005). Mixed-effects and fMRI studies. *NeuroImage*, *24*(1), 244–252.

Friston, K., Zarahn, E., Josephs, O., Henson, R., & Dale, A. (1999). Stochastic

designs in event-related fMRI. *NeuroImage*, *10*(5), 607–619.

Gazzola, V., & Keysers, C. (2009). The observation and execution of actions share motor and somatosensory voxels in all tested subjects: single-subject analyses of unsmoothed fMRI data. *Cerebral Cortex*, *19*(6), 1239–1255.

Geyer, S., Schleicher, A., & Zilles, K. (1999). Areas 3a, 3b, and 1 of human primary somatosensory cortex: 1. microstructural organization and interindividual variability. *NeuroImage*, *10*(1), 63–83.

Girouard, H., & Iadecola, C. (2006). Neurovascular coupling in the normal brain and in hypertension, stroke, and Alzheimer disease. *Journal of Applied Physiology*, *100*(1), 328–335.

Gleeson, B., Horschel, S., & Provancher, W. (2010). Perception of direction for applied tangential skin displacement: Effects of speed, displacement, and repetition. *Haptics, IEEE Transactions on*, *3*(3), 177–188.

Glover, G. (2011). Overview of functional magnetic resonance imaging. *Neurosurgery Clinics of North America*, *22*(2), 133–139.

Goldstein, E., & Thomson, L. (2007). *Sensation and perception*. Thomson Wadsworth.

Haase, A., Frahm, J., Matthaei, D., Hänicke, W., & Merboldt, K. (1986). FLASH imaging: rapid NMR imaging using low flip-angle pulses. *Journal of Magnetic Resonance*, *213*(2), 533–541.

Hämäläinen, H., Hiltunen, J., & Titievskaja, I. (2002). Activation of somatosensory cortical areas varies with attentional state: an fMRI study. *Behavioural Brain Research*, *135*(1), 159–165.

Hamann, W., & Iggo, A. (1988). Ruffini corpuscle–a stretch receptor in the connective tissue of the skin and locomotion apparatus. *Transduction and Cellular Mechanisms in Sensory Receptors*, *74*, 221.

Hamdy, S., Rothwell, J., Aziz, Q., Singh, K., & Thompson, D. (1998). Long-term

reorganization of human motor cortex driven by short-term sensory stimulation. *Nature Neuroscience*, *1*(1), 64–68.

Hare, R., Smith, A., Forster, B., MacKay, A., Whittall, K., Kiehl, K., & Liddle, P. (1998). Functional magnetic resonance imaging: the basics of blood-oxygen-level dependent (BOLD) imaging. *Canadian Association of Radiologists Journal*, *49*(5), 320.

Heeger, D., & Ress, D. (2002). What does fMRI tell us about neuronal activity? *Nature Reviews Neuroscience*, *3*(2), 142–151.

Herculano-Houzel, S. (2009). The human brain in numbers: a linearly scaled-up primate brain. *Frontiers in Human Neuroscience*, *3*(31).

Hernandez-Garcia, L., & Jahanian, H. (2014). Perfusion based functional MRI.

Hlushchuk, Y., Simões-Franklin, C., Nangini, C., & Hari, R. (2015). Stimulus-Rate Sensitivity Discerns Area 3b of the Human Primary Somatosensory Cortex. *PLOS one*, *10*(5), e0128462.

Hsiao, S. (2008). Central mechanisms of tactile shape perception. *Current Opinion in Neurobiology*, *18*(4), 418–424.

Huang, R., & Sereno, M. (2007). Dodecapus: An MR-compatible system for somatosensory stimulation. *NeuroImage*, *34*(3), 1060–1073.

Hynynen, K., Clement, G., McDannold, N., Vykhodtseva, N., King, R., White, J., ... Jolesz, F. (2004). 500-element ultrasound phased array system for noninvasive focal surgery of the brain: A preliminary rabbit study with ex vivo human skulls. *Magnetic Resonance in Medicine*, *52*(1), 100–107.

Iggo, A. (2012). *Somatosensory System*. Springer Berlin Heidelberg.

Jo, H., Lee, J., Kim, J., Shin, Y., Kim, I., Kwon, J., & Kim, S. (2007). Spatial accuracy of fMRI activation influenced by volume-and surface-based spatial smoothing techniques. *NeuroImage*, *34*(2), 550–564.

Johansson, R. (1978). Tactile sensibility in the human hand: receptive field characteristics of mechanoreceptive units in the glabrous skin area. *The Journal of Physiology*, *281*(1), 101–125.

Johansson, R., & Flanagan, R. (2009). Coding and use of tactile signals from the fingertips in object manipulation tasks. *Nature Reviews Neuroscience*, *10*(5), 345–359.

Johansson, R., & Vallbo, B. (1979). Tactile sensibility in the human hand: relative and absolute densities of four types of mechanoreceptive units in glabrous skin. *The Journal of Physiology*, *286*(1), 283–300.

Jones, E., & Powell, T. (1969). The cortical projection of the ventroposterior nucleus of the thalamus in the cat. *Brain Research*, *13*(2), 298–318.

Jueptner, M., & Weiller, C. (1998). A review of differences between basal ganglia and cerebellar control of movements as revealed by functional imaging studies. *Brain*, *121*(8), 1437–1449.

Kaas, J. (1993). The functional organization of somatosensory cortex in primates. *Annals of Anatomy-Anatomischer Anzeiger*, *175*(6), 509–518.

Kampe, K., Jones, R., & Auer, D. (2000). Frequency dependence of the functional MRI response after electrical median nerve stimulation. *Human Brain Mapping*, *9*(2), 106–114.

Karkhanis, A., Heider, B., Silva, F., & Siegel, R. (2014). Spatial effects of shifting prisms on properties of posterior parietal cortex neurons. *The Journal of Physiology*, *592*(16), 3625–3646.

Kawato, M., Kuroda, T., Imamizu, H., Nakano, E., Miyauchi, S., & Yoshioka, T. (2003). Internal forward models in the cerebellum: fMRI study on grip force and load force coupling. *Progress in Brain Research*, *142*, 171–188.

Kay, K., David, S., Prenger, R., Hansen, K., & Gallant, J. (2008). Modeling low-

frequency fluctuation and hemodynamic response timecourse in event-related fMRI. *Human Brain Mapping*, *29*(2), 142–156.

Keyson, D., & Houtsma, A. (1995). Directional sensitivity to a tactile point stimulus moving across the fingerpad. *Perception & Psychophysics*, *57*(5), 738–744.

Khaslavskaia, S., Ladouceur, M., & Sinkjaer, T. (2002). Increase in tibialis anterior motor cortex excitability following repetitive electrical stimulation of the common peroneal nerve. *Experimental Brain Research*, *145*(3), 309–315.

Kim, S., Richter, W., & Uurbil, K. (1997). Limitations of temporal resolution in functional MRI. *Magnetic Resonance in Medicine*, *37*(4), 631–636.

Kim, S., & Uĝurbil, K. (1997). Comparison of blood oxygenation and cerebral blood flow effect in fMRI: Estimation of relative oxygen consumption change. *Magnetic Resonance in Medicine*, *38*(1), 59–65.

Kitada, R., Kochiyama, T., Hashimoto, T., Naito, E., & Matsumura, M. (2003). Moving tactile stimuli of fingers are integrated in the intraparietal and inferior parietal cortices. *Neuroreport*, *14*(5), 719–724.

Kurth, R., Villringer, K., Curio, G., Wolf, K., Krause, T., Repenthin, J., ... Villringer, A. (2000). fMRI shows multiple somatotopic digit representations in human primary somatosensory cortex. *NeuroReport*, *11*(7), 1487–1491.

Kurth, R., Villringer, K., Mackert, B., Schwiemann, J., Braun, J., Curio, G., ... Wolf, K. (1998). fMRI assessment of somatotopy in human Brodmann area 3b by electrical finger stimulation. *Neuroreport*, *9*(2), 207–209.

Kwong, K., Belliveau, J., Chesler, D., Goldberg, I., Weisskoff, R., Poncelet, B., ... Turner, R. (1992). Dynamic magnetic resonance imaging of human brain activity during primary sensory stimulation. *Proceedings of the National Academy of Sciences*, *89*(12), 5675–5679.

Laird, A., Robinson, J., McMillan, K., Tordesillas-Gutiérrez, D., Moran, S., Gonzales,

S., ... others (2010). Comparison of the disparity between Talairach and MNI coordinates in functional neuroimaging data: validation of the lancaster transform. *NeuroImage*, *51*(2), 677–683.

Lancaster, J., Tordesillas-Gutiérrez, D., Martinez, M., Salinas, F., Evans, A., Zilles, K., ... Fox, P. (2007). Bias between MNI and Talairach coordinates analyzed using the ICBM-152 brain template. *Human Brain Mapping*, *28*(11), 1194–1205.

Lee, C., & Whitsel, L. (1992). Mechanisms underlying somatosensory cortical dynamics: I. In vivo studies. *Cerebral Cortex*, *2*(2), 81–106.

Lee, W., Kim, H., Jung, Y., Song, I., Chung, Y., & Yoo, S. (2015). Image-guided transcranial focused ultrasound stimulates human primary somatosensory cortex. *Scientific Reports*, *5*.

Legon, W., Sato, T., Opitz, A., Mueller, J., Barbour, A., Williams, A., & Tyler, W. (2014). Transcranial focused ultrasound modulates the activity of primary somatosensory cortex in humans. *Nature Neuroscience*, *17*(2), 322–329.

Logothetis, N. (2008). What we can do and what we cannot do with fMRI. *Nature*, *453*(7197), 869–878.

Lomber, S., Yi, S., & Woller, E. (2006). Relocation of specific visual functions following damage of mature posterior parietal cortex. *Progress in Brain Research*, *157*, 157–172.

Lu, H., Golay, X., Pekar, J., & Van Zijl, P. (2004). Sustained poststimulus elevation in cerebral oxygen utilization after vascular recovery. *Journal of Cerebral Blood Flow & Metabolism*, *24*(7), 764–770.

Maldjian, J., Gottschalk, A., Patel, R., Detre, J., & Alsop, D. (1999). The sensory somatotopic map of the human hand demonstrated at 4 Tesla. *NeuroImage*, *10*(1), 55–62.

Malonek, D., & Grinvald, A. (1996). Interactions between electrical activity and

cortical microcirculation revealed by imaging spectroscopy: implications for functional brain mapping. *Science*, *272*(5261), 551.

Mansfield, P. (1977). Multi-planar image formation using NMR spin echoes. *Journal of Physics C: Solid State Physics*, *10*(3), L55.

Maricich, S., Wellnitz, S., Nelson, A., Lesniak, D., Gerling, G., Lumpkin, E., & Zoghbi, H. (2009). Merkel cells are essential for light-touch responses. *Science*, *324*(5934), 1580–1582.

Martuzzi, R., Zwaag, W., Farthouat, J., Gruetter, R., & Blanke, O. (2014). Human finger somatotopy in areas 3b, 1, and 2: A 7T fMRI study using a natural stimulus. *Human Brain Mapping*, *35*(1), 213–226.

Matthews, P., & Jezzard, P. (2004). Functional magnetic resonance imaging. *Journal of Neurology, Neurosurgery & Psychiatry*, *75*(1), 6–12.

McGlone, F., Olausson, H., Boyle, J., Jones-Gotman, M., Dancer, C., Guest, S., & Essick, G. (2012). Touching and feeling: differences in pleasant touch processing between glabrous and hairy skin in humans. *European Journal of Neuroscience*, *35*(11), 1782–1788.

Melzack, R., & Katz, J. (2007). McGill Pain Questionnaire. In *Encyclopedia of Pain* (pp. 1102–1104). Springer.

Miezin, F., Maccotta, L., Ollinger, J., Petersen, S., & Buckner, R. (2000). Characterizing the hemodynamic response: effects of presentation rate, sampling procedure, and the possibility of ordering brain activity based on relative timing. *NeuroImage*, *11*(6), 735–759.

Milner, T., Franklin, D., Imamizu, H., & Kawato, M. (2007). Central control of grasp: manipulation of objects with complex and simple dynamics. *NeuroImage*, *36*(2), 388–395.

Mugler III, J. (2006). Basic principles. *Clinical Magnetic Resonance Imaging. 3rd ed.*

Philadelphia, Pa: Saunders Elsevier, 23–57.

Mumford, J., & Nichols, T. (2009). Simple group fMRI modeling and inference. *NeuroImage*, *47*(4), 1469–1475.

Nakamura, A., Yamada, T., Goto, A., Kato, T., Ito, K., Abe, Y., ... Kakigi, R. (1998). Somatosensory homunculus as drawn by MEG. *NeuroImage*, *7*(4), 377–386.

Narsude, M., Gallichan, D., Van Der Zwaag, W., Gruetter, R., & Marques, J. (2015). Three-dimensional echo planar imaging with controlled aliasing: A sequence for high temporal resolution functional MRI. *Magnetic Resonance in Medicine*.

Nasrallah, I., & Dubroff, J. (2013). An overview of PET neuroimaging. In *Seminars in Nuclear Medicine* (Vol. 43, pp. 449–461).

Ng, B., Abugharbieh, R., Huang, X., & McKeown, M. (2006). Characterizing fMRI activations within regions of interest (ROIs) using 3d moment invariants. In *Computer Vision and Pattern Recognition Workshop, 2006. CVPRW'06. Conference on* (pp. 63–63). IEEE.

Nieto-Castanon, A., Ghosh, S., Tourville, J., & Guenther, F. (2003). Region of interest based analysis of functional imaging data. *NeuroImage*, *19*(4), 1303–1316.

Nii, Y., Uematsu, S., Lesser, R., & Gordon, B. (1996). Does the central sulcus divide motor and sensory functions? Cortical mapping of human hand areas as revealed by electrical stimulation through subdural grid electrodes. *Neurology*, *46*(2), 360–367.

Nitsche, M., & Paulus, W. (2000). Excitability changes induced in the human motor cortex by weak transcranial direct current stimulation. *The Journal of Physiology*, *527*(3), 633–639.

Nolte, J. (2010). *Essentials of the Human Brain*. Philadelphia, Mosby/Elsevier.

Nordin, M., & Hagbarth, K. (1989). Mechanoreceptive units in the human infra-orbital nerve. *Acta Physiologica Scandinavica*, *135*(2), 149–161.

Ogawa, S., Lee, T., Kay, A., & Tank, D. (1990). Brain magnetic resonance imaging with contrast dependent on blood oxygenation. *Proceedings of the National Academy of Sciences*, *87*(24), 9868–9872.

Olausson, H., Lamarre, Y., Backlund, H., Morin, C., Wallin, B., Starck, G., ... others (2002). Unmyelinated tactile afferents signal touch and project to insular cortex. *Nature Neuroscience*, *5*(9), 900–904.

Olausson, H., & Norrsell, U. (1993). Observations on human tactile directional sensibility. *The Journal of Physiology*, *464*(1), 545–559.

Panczykowski, D., Monaco III, E., & Friedlander, R. (2014). Transcranial Focused Ultrasound Modulates the Activity of Primary Somatosensory Cortex in Humans. *Neurosurgery*, *74*(6), N8–N9.

Pasalar, S., Ro, T., & Beauchamp, M. (2010). TMS of posterior parietal cortex disrupts visual tactile multisensory integration. *European Journal of Neuroscience*, *31*(10), 1783–1790.

Pauling, L., & Coryell, C. (1936). The magnetic properties and structure of hemoglobin, oxyhemoglobin and carbonmonoxyhemoglobin. *Proceedings of the National Academy of Sciences of the United States of America*, *22*(4), 210.

Pei, Y., & Bensmaia, S. (2014). The neural basis of tactile motion perception. *Journal of Neurophysiology*, *112*(12), 3023–3032.

Penfield, W., Boldrey, E., et al. (1937). Somatic motor and sensory representation in the cerebral cortex of man as studied by electrical stimulation. *Brain*, *60*(4), 389–443.

Penfield, W., & Jasper, H. (1954). Epilepsy and the functional anatomy of the human brain. Little, Brown & Company, Boston. Chap. XI.

Penfield, W., & Rasmussen, T. (1950). The cerebral cortex of man; a clinical study of localization of function. New York: Macmillam.

Ploner, M., Schmitz, F., Freund, H., & Schnitzler, A. (1999). Parallel activation of primary and secondary somatosensory cortices in human pain processing. *Journal of Neurophysiology*, *81*(6), 3100–3104.

Poldrack, R. (2007). Region of interest analysis for fMRI. *Social Cognitive and Affective Neuroscience*, *2*(1), 67–70.

Popescu, A., Barlow, S., Venkatesan, L., Wang, J., & Popescu, M. (2013). Adaptive changes in the neuromagnetic response of the primary and association somatosensory areas following repetitive tactile hand stimulation in humans. *Human Brain Mapping*, *34*(6), 1415–1426.

Popescu, M., Barlow, S., Popescu, A., Estep, M., Venkatesan, L., Auer, E., & Brooks, W. (2010). Cutaneous stimulation of the digits and lips evokes responses with different adaptation patterns in primary somatosensory cortex. *NeuroImage*, *52*(4), 1477–1486.

Portas, C., Krakow, K., Allen, P., Josephs, O., Armony, J., & Frith, C. (2000). Auditory processing across the sleep-wake cycle: simultaneous EEG and fMRI monitoring in humans. *Neuron*, *28*(3), 991–999.

Pouget, A., & Snyder, L. (2000). Computational approaches to sensorimotor transformations. *Nature Neuroscience*, *3*, 1192–1198.

Poustchi-Amin, M., Mirowitz, S., Brown, J., McKinstry, R., & Li, T. (2001). Principles and Applications of Echo-planar imaging: A Review for the General Radiologist 1. *Radiographics*, *21*(3), 767–779.

Powell, T., & Mountcastle, V. (1959). Some aspects of the functional organization of the cortex of the postcentral gyrus of the monkey: a correlation of findings obtained in a single unit analysis with cytoarchitecture. *Bull Johns Hopkins Hosp*, *105*(133-62).

Price, D. (2000). Psychological and neural mechanisms of the affective dimension of

pain. *Science*, *288*(5472), 1769–1772.

Pujol, J., López-Solà, M., Ortiz, H., Vilanova, J. C., Harrison, B., Yücel, M., ... Deus, J. (2009). Mapping brain response to pain in fibromyalgia patients using temporal analysis of fMRI. *PLoS One*, *4*(4), e5224.

Raichle, M., & Mintun, M. (2006). Brain work and brain imaging. *Annu. Rev. Neurosci.*, *29*, 449–476.

Ridding, M., Brouwer, B., Miles, T., Pitcher, J., & Thompson, P. (2000). Changes in muscle responses to stimulation of the motor cortex induced by peripheral nerve stimulation in human subjects. *Experimental Brain Research*, *131*(1), 135–143.

Ridley, R., & Ettlinger, G. (1976). Impaired tactile learning and retention after removals of the second somatic sensory projection cortex (SII) in the monkey. *Brain Research*, *109*(3), 656–660.

Rozzi, S., Calzavara, R., Belmalih, A., Borra, E., Gregoriou, G. G., Matelli, M., & Luppino, G. (2006). Cortical connections of the inferior parietal cortical convexity of the macaque monkey. *Cerebral Cortex*, *16*(10), 1389–1417.

Ruben, J., Schwiemann, J., Deuchert, M., Meyer, R., Krause, T., Curio, G., ... Villringer, A. (2001). Somatotopic organization of human secondary somatosensory cortex. *Cerebral Cortex*, *11*(5), 463–473.

Rushworth, M., Nixon, P., Renowden, S., Wade, D., & Passingham, R. (1997). The left parietal cortex and motor attention. *Neuropsychologia*, *35*(9), 1261–1273.

Sanchez-Panchuelo, M., Francis, S., Bowtell, R., & Schluppeck, D. (2010). Mapping human somatosensory cortex in individual subjects with 7T functional MRI. *Journal of Neurophysiology*, *103*(5), 2544–2556.

Scheffe, H. (1999). *The analysis of variance* (Vol. 72). John Wiley & Sons.

Scheibert, J., Leurent, S., Prevost, A., & Debrégeas, G. (2009). The role of fingerprints in the coding of tactile information probed with a biomimetic sensor. *Science*,

323(5920), 1503–1506.

Schweisfurth, M., Frahm, J., & Schweizer, R. (2014). Individual fMRI maps of all phalanges and digit bases of all fingers in human primary somatosensory cortex. *Frontiers in Human Neuroscience*, *8*(658).

Silva, A., Lee, S., Iadecola, C., & Kim, S. (2000). Early temporal characteristics of cerebral blood flow and deoxyhemoglobin changes during somatosensory stimulation. *Journal of Cerebral Blood Flow & Metabolism*, *20*(1), 201–206.

Small, S., Hlustik, P., Noll, D., Genovese, C., & Solodkin, A. (2002). Cerebellar hemispheric activation ipsilateral to the paretic hand correlates with functional recovery after stroke. *Brain*, *125*(7), 1544–1557.

Steinbrink, J., Villringer, A., Kempf, F., Haux, D., Boden, S., & Obrig, H. (2006). Illuminating the bold signal: combined fMRI–fNIRS studies. *Magnetic Resonance Imaging*, *24*(4), 495–505.

Stippich, C., Hofmann, R., Kapfer, D., Hempel, E., Heiland, S., Jansen, O., & Sartor, K. (1999). Somatotopic mapping of the human primary somatosensory cortex by fully automated tactile stimulation using functional magnetic resonance imaging. *Neuroscience Letters*, *277*(1), 25–28.

Stoodley, C., Valera, E., & Schmahmann, J. (2012). Functional topography of the cerebellum for motor and cognitive tasks: an fMRI study. *NeuroImage*, *59*(2), 1560–1570.

Talairach, J., & Szikla, G. (1967). *Atlas of stereotaxic anatomy of the telencephalon.* Masson.

Talairach, J., & Tournoux, P. (1988). *Co-planar stereotaxic atlas of the human brain: 3-dimensional proportional system: an approach to cerebral imaging.* Stuttgart, New York.

Thickbroom, G., Byrnes, M., & Mastaglia, F. (2003). Dual representation of the

hand in the cerebellum: activation with voluntary and passive finger movement. *NeuroImage*, *18*(3), 670–674.

Tokuda, O., Harada, Y., Shiraishi, G., Motomura, T., Fukuda, K., Kimura, M., & Matsunaga, N. (2014). MRI of the anatomical structures of the knee: the proton density-weighted fast spin-echo sequence vs the proton density-weighted fast-recovery fast spin-echo sequence. *The British Journal of Radiology*.

Tommerdahl, M., Simons, S., Chiu, J., Favorov, O., & Whitsel, B. (2006). Ipsilateral input modifies the primary somatosensory cortex response to contralateral skin flutter. *The Journal of Neuroscience*, *26*(22), 5970–5977.

Tseng, Y., Diedrichsen, J., Krakauer, J., Shadmehr, R., & Bastian, A. (2007). Sensory prediction errors drive cerebellum-dependent adaptation of reaching. *Journal of Neurophysiology*, *98*(1), 54–62.

Uludağ, K., Dubowitz, D., Yoder, E., Restom, K., Liu, T., & Buxton, R. (2004). Coupling of cerebral blood flow and oxygen consumption during physiological activation and deactivation measured with fMRI. *NeuroImage*, *23*(1), 148–155.

van Zijl, P., Hua, J., & Lu, H. (2012). The bold post-stimulus undershoot, one of the most debated issues in fMRI. *NeuroImage*, *62*(2), 1092–1102.

Venkatesan, L., Barlow, S., Popescu, M., & Popescu, A. (2014). Integrated approach for studying adaptation mechanisms in the human somatosensory cortical network. *Experimental Brain Research*, *232*(11), 3545–3554.

Venkatesan, L., Barlow, S., Popescu, M., Popescu, A., & Auer, E. (2010). Tac-cell inputs to human hand and lip induce short-term adaptation of the primary somatosensory cortex. *Brain Research*, *1348*, 63–70.

Verrillo, R., & Bolanowski, S. (1986). The effects of skin temperature on the psychophysical responses to vibration on glabrous and hairy skin. *The Journal of the Acoustical Society of America*, *80*(2), 528–532.

Wansapura, J., Holland, S., Dunn, S., & Ball, W. (1999). NMR relaxation times in the human brain at 3.0 Tesla. *Journal of Magnetic Resonance Imaging*, *9*(4), 531–538.

Weibull, A., Björkman, A., Hall, H., Rosén, B., Lundborg, G., & Svensson, J. (2008). Optimizing the mapping of finger areas in primary somatosensory cortex using functional MRI. *Magnetic Resonance Imaging*, *26*(10), 1342–1351.

Whitsel, B., Dreyer, D., & Hollins, M. (1978). Representation of moving stimuli by somatosensory neurons. *Federation Proceedings*, *37*(9), 2223–2227.

Whitsel, B., Franzen, O., Dreyer, D., Hollins, M., Young, M., Essick, G., & Wong, C. (1986). Dependence of subjective traverse length on velocity of moving tactile stimuli. *Somatosensory & Motor Research*, *3*(3), 185–196.

Wienbruch, C., Candia, V., Svensson, J., Kleiser, R., & Kollias, S. S. (2006). A portable and low-cost fMRI compatible pneumatic system for the investigation of the somatosensensory system in clinical and research environments. *Neuroscience Letters*, *398*(3), 183–188.

Wolf, U., Rapoport, M., & Schweizer, T. (2009). Evaluating the affective component of the cerebellar cognitive affective syndrome. *The Journal of Neuropsychiatry and Clinical Neurosciences*, *21*, 3.

Woolsey, C., Erickson, T., & Gilson, W. (1979). Localization in somatic sensory and motor areas of human cerebral cortex as determined by direct recording of evoked potentials and electrical stimulation. *Journal of Neurosurgery*, *51*(4), 476–506.

Xerri, C., Coq, J., Merzenich, M., & Jenkins, W. (1996). Experience-induced plasticity of cutaneous maps in the primary somatosensory cortex of adult monkeys and rats. *Journal of Physiology-Paris*, *90*(3), 277–287.

Xing, J., Andersen, R., et al. (2000). Models of the posterior parietal cortex which

perform multimodal integration and represent space in several coordinate frames. *Journal of Cognitive Neuroscience*, *12*(4), 601–614.

Xu, J., Moeller, S., Auerbach, E., Strupp, J., Smith, S., Feinberg, D., ... Uğurbil, K. (2013). Evaluation of slice accelerations using multiband echo planar imaging at 3T. *NeuroImage*, *83*, 991–1001.

Appendix B

Pairwise Comparisons of BOLD signal changes (%)

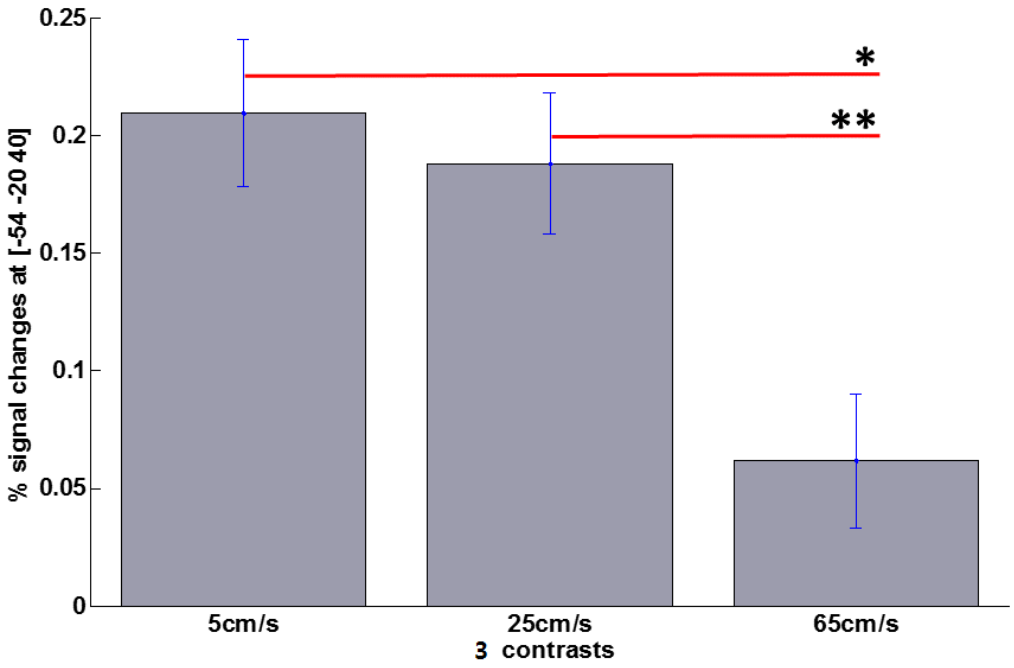

Figure B.1: Pairwise comparisons of 3 BOLD signal changes (%). *: $p < .002$, **: $p < .009$

Difference of Levels	Difference of Means	SE of Difference	95% CI	t-value	Adjusted p-value
2 - 1	-0.0216	0.0421	(-0.1210, 0.0778)	-0.51	0.865
3 - 1	-0.1477	0.0421	(-0.2471, -0.0483)	-3.51	0.002
3 - 2	-0.1261	0.0421	(-0.2255, -0.0267)	-3.00	0.009

Table B.1: Tukey pairwise comparions. 1 = 5cm/s, 2 = 25cm/s, 3 = 65 cm/s

Appendix C

Galileo stimulation Xml script file

```
<Series>
  <Date>7/23/2015 4:45 PM</Date>
  <File>D:\USERS\Taek\fMRI_sequence\HAND_09 velocity.xml</File>
  <Description>Velocity Set</Description>
  <Continuous>False</Continuous>
  <Sequence Num="1">
    <On>True</On>
    <Runs>4</Runs>
    <CycleTime>5000</CycleTime>
    <Description>All 60ms pulses 5 cm/sec</Description>
    <Channel Num="1">
      <OnTime>0</OnTime>
      <OffTime>60</OffTime>
    </Channel>
    <Channel Num="2">
      <OnTime>500</OnTime>
      <OffTime>560</OffTime>
    </Channel>
    <Channel Num="3">
      <OnTime>1400</OnTime>
      <OffTime>1460</OffTime>
    </Channel>
    <Channel Num="4">
      <OnTime>2700</OnTime>
      <OffTime>2760</OffTime>
    </Channel>
    <Channel Num="5">
      <OnTime>4100</OnTime>
      <OffTime>4160</OffTime>
    </Channel>
    <Channel Num="6">
      <OnTime>0</OnTime>
      <OffTime>0</OffTime>
    </Channel>
```

```
    <Channel Num="7">
      <OnTime>0</OnTime>
      <OffTime>0</OffTime>
    </Channel>
    <Channel Num="8">
      <OnTime>0</OnTime>
      <OffTime>0</OffTime>
    </Channel>
  </Sequence>
  <Sequence Num="2">
    <On>True</On>
    <Runs>20</Runs>
    <CycleTime>1000</CycleTime>
    <Description>All 60ms pulses, 25 cm/sec</Description>
    <Channel Num="1">
      <OnTime>0</OnTime>
      <OffTime>60</OffTime>
    </Channel>
    <Channel Num="2">
      <OnTime>100</OnTime>
      <OffTime>160</OffTime>
    </Channel>
    <Channel Num="3">
      <OnTime>280</OnTime>
      <OffTime>340</OffTime>
    </Channel>
    <Channel Num="4">
      <OnTime>540</OnTime>
      <OffTime>600</OffTime>
    </Channel>
    <Channel Num="5">
      <OnTime>820</OnTime>
      <OffTime>880</OffTime>
    </Channel>
    <Channel Num="6">
      <OnTime>0</OnTime>
      <OffTime>0</OffTime>
    </Channel>
    <Channel Num="7">
      <OnTime>0</OnTime>
      <OffTime>0</OffTime>
    </Channel>
    <Channel Num="8">
      <OnTime>0</OnTime>
      <OffTime>0</OffTime>
    </Channel>
  </Sequence>
  <Sequence Num="3">
```

```
    <On>True</On>
    <Runs>50</Runs>
    <CycleTime>400</CycleTime>
    <Description>All 60ms pulses, 65 cm/sec</Description>
    <Channel Num="1">
      <OnTime>0</OnTime>
      <OffTime>60</OffTime>
    </Channel>
    <Channel Num="2">
      <OnTime>38</OnTime>
      <OffTime>98</OffTime>
    </Channel>
    <Channel Num="3">
      <OnTime>107</OnTime>
      <OffTime>167</OffTime>
    </Channel>
    <Channel Num="4">
      <OnTime>207</OnTime>
      <OffTime>267</OffTime>
    </Channel>
    <Channel Num="5">
      <OnTime>315</OnTime>
      <OffTime>375</OffTime>
    </Channel>
    <Channel Num="6">
      <OnTime>0</OnTime>
      <OffTime>0</OffTime>
    </Channel>
    <Channel Num="7">
      <OnTime>0</OnTime>
      <OffTime>0</OffTime>
    </Channel>
    <Channel Num="8">
      <OnTime>0</OnTime>
      <OffTime>0</OffTime>
    </Channel>
  </Sequence>
  <Sequence Num="4">
    <On>True</On>
    <Runs>20</Runs>
    <CycleTime>1000</CycleTime>
    <Description>All 60ms pulses, non-stim</Description>
    <Channel Num="1">
      <OnTime>0</OnTime>
      <OffTime>0</OffTime>
    </Channel>
    <Channel Num="2">
      <OnTime>0</OnTime>
```

```
        <OffTime>0</OffTime>
      </Channel>
      <Channel Num="3">
        <OnTime>0</OnTime>
        <OffTime>0</OffTime>
      </Channel>
      <Channel Num="4">
        <OnTime>0</OnTime>
        <OffTime>0</OffTime>
      </Channel>
      <Channel Num="5">
        <OnTime>0</OnTime>
        <OffTime>0</OffTime>
      </Channel>
      <Channel Num="6">
        <OnTime>0</OnTime>
        <OffTime>0</OffTime>
      </Channel>
      <Channel Num="7">
        <OnTime>0</OnTime>
        <OffTime>0</OffTime>
      </Channel>
      <Channel Num="8">
        <OnTime>0</OnTime>
        <OffTime>0</OffTime>
      </Channel>
    </Sequence>
  <Sequence Num="5">
      <On>True</On>
      <Runs>20</Runs>
      <CycleTime>1000</CycleTime>
      <Description>All 60ms pulses, same OnTime</Description>
      <Channel Num="1">
        <OnTime>0</OnTime>
        <OffTime>60</OffTime>
      </Channel>
      <Channel Num="2">
        <OnTime>0</OnTime>
        <OffTime>60</OffTime>
      </Channel>
      <Channel Num="3">
        <OnTime>0</OnTime>
        <OffTime>60</OffTime>
      </Channel>
      <Channel Num="4">
        <OnTime>0</OnTime>
        <OffTime>60</OffTime>
      </Channel>
```

```
      <Channel Num="5">
        <OnTime>0</OnTime>
        <OffTime>60</OffTime>
      </Channel>
      <Channel Num="6">
        <OnTime>0</OnTime>
        <OffTime>0</OffTime>
      </Channel>
      <Channel Num="7">
        <OnTime>0</OnTime>
        <OffTime>0</OffTime>
      </Channel>
      <Channel Num="8">
        <OnTime>0</OnTime>
        <OffTime>0</OffTime>
      </Channel>
    </Sequence>
</Series>
```

Appendix D

Galileo stimulation output file

```
Series - START
Date:7/23/2015 4:43:31 PM
File:D:\USERS\Taek\fMRI_sequence\LastDownloadedSeries.xml
Description:Velocity Set
Continuous:False
HardwareTrigger:2
Runs:1
CBRuns:4
RandomRuns:1

_____

SEQ:1 True
Runs:4
CycleTime:5000
Description:All 60ms pulses 5 cm/sec
VALID:True
1: 0-60
2: 500-560
3: 1400-1460
4: 2700-2760
5: 4100-4160

_____

SEQ:2 True
Runs:20
CycleTime:1000
Description:All 60ms pulses, 25 cm/sec
VALID:True
1: 0-60
2: 100-160
3: 280-340
4: 540-600
5: 820-880
```

```
_____
SEQ:3 True
Runs:50
CycleTime:400
Description:All 60ms pulses, 65 cm/sec
VALID:True
1: 0-60
2: 38-98
3: 107-167
4: 207-267
5: 315-375

_____
SEQ:4 True
Runs:20
CycleTime:1000
Description:All 60ms pulses, non-stim
VALID:True

_____
SEQ:5 True
Runs:20
CycleTime:1000
Description:All 60ms pulses, same OnTime
VALID:True
1: 0-60
2: 0-60
3: 0-60
4: 0-60
5: 0-60

SEQ:6 OFF
SEQ:7 OFF
SEQ:8 OFF
SEQ:9 OFF
SEQ:10 OFF
SEQ:11 OFF
SEQ:12 OFF
SEQ:13 OFF
SEQ:14 OFF
SEQ:15 OFF
SEQ:16 OFF
SEQ:17 OFF
SEQ:18 OFF
SEQ:19 OFF
SEQ:20 OFF
SEQ:21 OFF
SEQ:22 OFF
```

```
SEQ:23 OFF
SEQ:24 OFF
SEQ:25 OFF
Series - END


OPENED:7/23/2015 4:58:23 PM
DESCRIPTION:User entered data here!
RANDOM BALANCED
-------------------------------------------------------------

Seq, Repeat
1, 1
1, 1
1, 2
1, 3
1, 4
1, 1
1, 2
1, 3
1, 4
3, 1
3, 2
3, 3
3, 4
3, 5
3, 6
3, 7
3, 8
3, 9
3, 10
3, 11
3, 12
3, 13
3, 14
3, 15
3, 16
3, 17
3, 18
3, 19
3, 20
3, 21
3, 22
3, 23
3, 24
3, 25
3, 26
3, 27
3, 28
```

3, 29
3, 30
3, 31
3, 32
3, 33
3, 34
3, 35
3, 36
3, 37
3, 38
3, 39
3, 40
3, 41
3, 42
3, 43
3, 44
3, 45
3, 46
3, 47
3, 48
3, 49
3, 50
3, 1
3, 2
3, 3
3, 4
3, 5
3, 6
3, 7
3, 8
3, 9
3, 10
3, 11
3, 12
3, 13
3, 14
3, 15
3, 16
3, 17
3, 18
3, 19
3, 20
3, 21
3, 22
3, 23
3, 24
3, 25
3, 26

3, 27
3, 28
3, 29
3, 30
3, 31
3, 32
3, 33
3, 34
3, 35
3, 36
3, 37
3, 38
3, 39
3, 40
3, 41
3, 42
3, 43
3, 44
3, 45
3, 46
3, 47
3, 48
3, 49
3, 50
5, 1
5, 2
5, 3
5, 4
5, 5
5, 6
5, 7
5, 8
5, 9
5, 10
5, 11
5, 12
5, 13
5, 14
5, 15
5, 16
5, 17
5, 18
5, 19
5, 20
4, 1
4, 2
4, 3
4, 4

4, 5
4, 6
4, 7
4, 8
4, 9
4, 10
4, 11
4, 12
4, 13
4, 14
4, 15
4, 16
4, 17
4, 18
4, 19
4, 20
2, 1
2, 2
2, 3
2, 4
2, 5
2, 6
2, 7
2, 8
2, 9
2, 10
2, 11
2, 12
2, 13
2, 14
2, 15
2, 16
2, 17
2, 18
2, 19
2, 20
3, 1
3, 2
3, 3
3, 4
3, 5
3, 6
3, 7
3, 8
3, 9
3, 10
3, 11
3, 12

3, 13
3, 14
3, 15
3, 16
3, 17
3, 18
3, 19
3, 20
3, 21
3, 22
3, 23
3, 24
3, 25
3, 26
3, 27
3, 28
3, 29
3, 30
3, 31
3, 32
3, 33
3, 34
3, 35
3, 36
3, 37
3, 38
3, 39
3, 40
3, 41
3, 42
3, 43
3, 44
3, 45
3, 46
3, 47
3, 48
3, 49
3, 50
5, 1
5, 2
5, 3
5, 4
5, 5
5, 6
5, 7
5, 8
5, 9
5, 10

5, 11
5, 12
5, 13
5, 14
5, 15
5, 16
5, 17
5, 18
5, 19
5, 20
4, 1
4, 2
4, 3
4, 4
4, 5
4, 6
4, 7
4, 8
4, 9
4, 10
4, 11
4, 12
4, 13
4, 14
4, 15
4, 16
4, 17
4, 18
4, 19
4, 20
5, 1
5, 2
5, 3
5, 4
5, 5
5, 6
5, 7
5, 8
5, 9
5, 10
5, 11
5, 12
5, 13
5, 14
5, 15
5, 16
5, 17
5, 18

5, 19
5, 20
5, 1
5, 2
5, 3
5, 4
5, 5
5, 6
5, 7
5, 8
5, 9
5, 10
5, 11
5, 12
5, 13
5, 14
5, 15
5, 16
5, 17
5, 18
5, 19
5, 20
3, 1
3, 2
3, 3
3, 4
3, 5
3, 6
3, 7
3, 8
3, 9
3, 10
3, 11
3, 12
3, 13
3, 14
3, 15
3, 16
3, 17
3, 18
3, 19
3, 20
3, 21
3, 22
3, 23
3, 24
3, 25
3, 26

3, 27
3, 28
3, 29
3, 30
3, 31
3, 32
3, 33
3, 34
3, 35
3, 36
3, 37
3, 38
3, 39
3, 40
3, 41
3, 42
3, 43
3, 44
3, 45
3, 46
3, 47
3, 48
3, 49
3, 50
2, 1
2, 2
2, 3
2, 4
2, 5
2, 6
2, 7
2, 8
2, 9
2, 10
2, 11
2, 12
2, 13
2, 14
2, 15
2, 16
2, 17
2, 18
2, 19
2, 20
4, 1
4, 2
4, 3
4, 4

4, 5
4, 6
4, 7
4, 8
4, 9
4, 10
4, 11
4, 12
4, 13
4, 14
4, 15
4, 16
4, 17
4, 18
4, 19
4, 20
1, 1
1, 2
1, 3
1, 4
4, 1
4, 2
4, 3
4, 4
4, 5
4, 6
4, 7
4, 8
4, 9
4, 10
4, 11
4, 12
4, 13
4, 14
4, 15
4, 16
4, 17
4, 18
4, 19
4, 20
1, 1
1, 2
1, 3
1, 4
2, 1
2, 2
2, 3
2, 4

2, 5
2, 6
2, 7
2, 8
2, 9
2, 10
2, 11
2, 12
2, 13
2, 14
2, 15
2, 16
2, 17
2, 18
2, 19
2, 20
2, 1
2, 2
2, 3
2, 4
2, 5
2, 6
2, 7
2, 8
2, 9
2, 10
2, 11
2, 12
2, 13
2, 14
2, 15
2, 16
2, 17
2, 18
2, 19
2, 20

CLOSED:7/23/2015 5:12:46 PM